Western Norway University of Applied Sciences

NUMERICAL ANALYSIS OF FIRE-DRIVEN SMOKE PLUMES IN THE ATMOSPHERE

Master Thesis in Fire Safety

Author:	Author sign.
Ruben Dobler Strand	RUBEN DOBLER STRAND

Selected:	Open assignment
Fall 2016	

Supervisors:

Øyvind Økland
David René Ursin Johansen

Keywords:	Pages: + Annex:
Fire plume, plume rise, atmosphere, simulation, LES, CFD, plume lapse rates Røyksøyle, atmosfæren, simulering, LES, CFD	Haugesund, 01. June, 2017 Place/Date/Year

This work is part of the master's program in Fire safety at Western Norway University of Applied Sciences. The student(s) is responsible for the applied methods, results, conclusions and assessments of this work.

Preface

Thanks to my supervisors David René Ursin Johansen and Øyvind Økland for the help during this work.

A special thanks, after five years;

David René Ursin Johansen

Bjarne Christian Hagen

Summary

Plumes originating from fires may serve as a risk for people and environmental safety. Depending on what fuels a fire the content of the plume will vary [1]. From simple carbonaceous soot particulates, known to cause thousands of premature deaths [2], to radioactivity and embers. They could all be a part of a rising plume. Knowledge on plume rise therefore becomes essential when impact of fire plumes shall be assessed.

Theory suggest that a rising stack plume cools adiabatically [3]. However, a fire is somewhat different from a stack plume. Fire plumes are highly buoyant and can have significant vertical momentum over a greater vertical length scale [4].If a fire plume has regions of adiabatic rise then it could serve as means for simplified calculations. However, the meteorological conditions are highly influential on a rising plume and needs to be considered. By expressing the atmospheric conditions through lapse rates of temperature, that is, the change of temperature with height. Then, such lapse rates could be compared to theoretical plume lapse rate of temperature. Together they could form a new method for assessing plume rise.

This thesis investigated fire plume lapse rates in an environment of synthetic turbulence. It was found that certain regions of plume rise cools adiabatically. It could serve as a simplified approach if the *height of adiabatic cooling* was known. This height refers to the height at which cooling by expansion overcomes cooling by entrainment. The adiabatic cooling appears to be the case for neutral and near neutral conditions which is consistent with theory. Further, importance of stabilities was found to decrease with increasing winds. This is caused by the effective reduction in final rise heights for increased wind velocities. Results suggest this to be related to a critical velocity. A velocity for which effects of increased winds appear with less impact on the final rise height. Plume rise calculations may become simpler during such conditions as the height may solely rely on wind speeds. However, for calm winds, stability is of major importance.

For a rising plume in calm conditions small increases in the wind velocities are seen to reduce the final rise height by roughly 50 %. Clearly, during such conditions any minor changes in atmospheric winds could significantly alter the situation.

The contribution of this study has been to partly break down the complex development of the plume lapse rates. More manageable areas concerning the development of the lapse rates have been pointed out. If these areas are well understood it is believed that the final rise height of a fire plume or other buoyant plumes could be assessed through plume lapse rates.

Sammendrag (NORWEGIAN)

Røyksøyler fra branner kan utgjøre en fare for mennesker og miljø. Avhengig av brensel vil innholdet i røyksøylen kunne variere [1]. Alt fra lettere karbonpartikler som sot til tyngre og farligere stoffer som glør og radioaktivitet. Sot er kjent for å forårsake premature dødsfall [1]. Kunnskap om røyksøyler er derfor avgjørende for at effekten av dem skal kunne anslås.

Litteratur tilsier at røyksøyler fra piper, til eksempel kjøletårn, avkjøles adiabatisk når den stiger. Røyksøyler fra branner er annerledes, de inneholder en betydelig oppdrift og vertikal bevegelsesmengde over en lengre vertikal avstand. Dersom en røyksøyle fra en brann har områder hvor den kjøles adiabatisk, så kan dette muligens benyttes til forenklede beregninger. Røyksøylens stigning er videre påvirket av forholdene i atmosfæren. Disse forholdene kan uttrykkes ved bruk av endringsrater for temperatur med høyde. Dersom det var mulig å beskrive endringsraten for temperatur med høyde i en røyksøyle, så kunne denne vært benyttet sammen med den atmosfæriske raten til å fastslå røyksøylens stigning.

Denne oppgaven har undersøkt endringsrate for temperatur i røyksøyler i syntetisk turbulente omgivelser. Det ble funnet at deler av stigningen til røyksøyler, fra brann, kjøles adiabatisk. Det er muligheter for at dette kan være en forenklet fremgangsmåte dersom høyden hvor adiabatisk stigning begynner er kjent. Denne høyden refererer til høyden hvor kjøling grunnet trykkforandringer overgår kjøling ved innblanding. Den adiabatiske kjølingen er tilsynelatende tilfellet ved nøytrale og tilnærmet nøytrale atmosfæreforhold. Det ble videre funnet at betydningen av stabiliteten avtar ved økte vindhastigheter. Dette skyldes reduksjonen i maksimal høyde på røyksøylen når vinden øker. Resultat antyder at dette er relatert tile en kritisk hastighet. En hastighet hvor videre økning i vindhastighet ikke påvirker den endelige høyden til røyksøylen nevneverdig. Beregninger av røyksøylens maksimale stigning kan tenkes å forenkles under slike omstendigheter. Dette gitt, at atmosfæriske forhold utelukkende kan representeres gjennom den kritiske vindhastigheten.

For en stigende røyksøyle i en rolig atmosfære vil små forandringer i vindhastighet kunne medføre betydelige endringer. Enkle beregninger viser en reduksjon i maksimal stigning for røyksøylen på 50 %. Under slike forhold vil små forandringer i vindhastighet betydelig kunne endre situasjonen.

Bidraget fra denne oppgaven har vært å bryte ned endringsraten for temperatur i en røyksøyle til mindre områder. Dersom mer kunnskap blir tilgjengelig på disse områdene, så er det mulig å beskrive endringsraten til en røyksøyle fra en brann eller andre søyler med oppdrift. Dermed kan røyksøyler vurderes basert på endringsrater for temperatur av røyksøylen og atmosfæren.

Content

Nomenclature

$\boldsymbol{F}_{S_b}, \boldsymbol{F}_t$	-	Forces on a cubed parcel of air [N]
p	-	Pressure or power law wind profile exponent
S_b, S_t	-	Refers to bottom and top surfaces, respectively, of cubed parcel of air in the atmosphere. The surface being point of reference.
∇	-	Del operator
ρ	-	Fluid density
Γ_e	-	Environmental lapse rate
Γ_d	-	Dry adiabatic lapse rate
Γ_m	-	Moist adiabatic lapse rate
c_p	-	Specific heat at constant pressure
g	-	Gravitational acceleration
m_s	-	Saturated mixing ratio, temperature dependent
L	-	Latent heat of vaporization of water
u, v, w	-	Velocity in u, v and w direction
θ_v	-	Virtual potential temperature
N	-	Brunt Väisälä frequency, commonly presented through a squared value, N^2, or number of samples in an interval
σ^2	-	Variance
i	-	The i'th datapoint in a sample of N points
t	-	Time, time period
u_*	-	Friction velocity
τ_s	-	Surface stress, wall shear stress
z	-	Height above surface
z_i	-	Height from surface to capping inversion
w_*	-	Deardoff velocity scale
q	-	Specific humidity
V	-	Wind vector or wind speed
SH^2	-	Magnitude of wind shear vector
R_i	-	Richardson number
L	-	Monin-Obukhov length scale
Re	-	Reynolds number
ν	-	Kinematic viscosity

l	-	Characteristic velocity, for example boundary layer height
U	-	Fluid velocity
κ	-	Von Karman constant
z_0	-	Aerodynamic roughness length
z_r	-	Reference height used in power law wind functions, meteorological standard equals 10 meters
V_r	-	Reference wind speed
$(z_1 z_2)^{0.5}$	-	Geometric mean height used for calculation of exponent p
δ_v	-	Viscous length scale
y^+	-	Distance from wall in wall units

Superscripts and subscipts

d	-	Dry conditions
m	-	Moist conditions
$'$	-	Deviation from reference or mean
0	-	Environmental reference state, ambient consitions

1 INTRODUCTION

Plumes are present on a wide range of scales rising from heated electrical components and cigarettes to massive fires and volcanoes. They arise due to density differences [5]. Depending on their nature and content plumes may pose a risk to the surroundings. Carrying pollutants, toxics and for the extreme cases even radioactivity up in the atmosphere [6] [7]. At higher altitudes, horizontal spread allow potentially hazardous materials to be transported distances away from the source [8] [9]. Thus, concerning both environmental and people safety on a local and global scale [2] [8].

Plumes originating from fires contain a variety of chemical species, like soot [10] [1]. These species may serve as a risk to people safety. Each year thousands of people die prematurely due to inhalation of these particulates, though not necessarily originating from a fire [2]. The chemical species contained within the plume depends on what fuels the fire [1]. Fire plumes are not restricted to the transport of chemical species. Lofting of embers through the buoyant plume can result in fire spread distances away from the source, referred to as spot fires [11] [4].

With regards to people and environmental safety, knowledge on plume rise has many areas of application. Whenever the impact of a fire plume is to be considered with regards to buildings, fire spread, local and global concentration of species and the atmosphere, information on the plume trajectory is needed. Clearly, such information is important both to support decision making in the field, as well as to provide larger transport models with required input [10].

The study of rising plumes has been ongoing since the introduction of the *classical plume theory* over 60 years ago. Among the founding fathers were Morton, Taylor and Turner [12]. Even though classical plume theory applies many different assumptions, it is a powerful and simple approach to a complicated phenomenon [5]. Today different approaches in assessing plume properties exist. A common problem however, is the vast amount of available information. Simple empirical and

analytical equations differ by a factor ten and more, a known problem for those concerned with plume rise [7]. Such plume rise equations, appear inadequate and problems should be investigated.

According to Briggs [13] the potential temperature for most stack plumes can be assumed constant, corresponding to adiabatic rise. By stack plumes is meant a plume rising from a stack, such as power plant cooling towers. The underlying assumption is that fine scale mixing is the only significant heat transfer taking place. The adiabatic rise corresponds to the plume cooling as a result of pressure changes with altitude in the atmosphere. Fire plumes are different in nature than many stack plumes, high temperatures and low initial momentum [4]. Mixing of ambient air into such buoyant plumes is the foundation of classical plume theory as proposed by Taylor [14]. However, the mixing of the plume with surrounding atmosphere is not consistent with adiabatic cooling. At least not for all the different atmospheric stabilities that rising plumes might encounter [15] [7]. A rising plume heavily rely on buoyancy and meteorological conditions [16] [17] [4].

If a rising plume experiences regions of adiabatic changes. Then, such changes might be used for easy assessment of plume temperatures with altitude. Meteorologist refers to the decrease of an atmospheric variable with height as a *lapse rate*, most commonly temperature. If such lapse rates were known for fire plumes, and with relatively good accuracy could be predicted. Then, combining such information with meteorological data could result in a general friendly approach to plume rise assessment.

A problem for modellers has been the lack of systematic measuring techniques and definitions when assessing plume trajectories, which is essential for development and evaluation of models [7] [8]. Three basic techniques have been photographing, sampling by aircraft and remote sensors like LIDAR [8]. Performing full scale experiments as part of an analysis can therefore become expensive. Clearly, assessment by photographs is inconsistent and would allow for subjective interpretations. Small scale experiments could serve as an alternative. However, though being a real flow, it does not necessarily duplicate many features of the atmospheric boundary layer. Hoult and Weil [18] points at the effect of turbulence in the crossflow as the possibly greatest uncertainty related to the application of laboratory experiments to large scale flows. Further, small scale experiments require test locations and equipment.

A tool that has been growing for the last 50 years, and which has become important in the prediction of fluid flow is Computational Fluid Dynamics, CFD [5]. The obvious advantage of CFD is its availability. The requirements for performing CFD analysis is a computer with sufficient computing power. Open source software is easy accessible.

1.1 Objectives

Much research has been performed on plume rise, plume trajectory and dispersion of pollutants. The reporting and study of plume lapse rates however appears scarce, if any. This thesis serves as an introductory study on gross features of plume temperature lapse rates during different atmospheric stabilities and wind conditions. That is, the changes of the average plume temperature with altitude.

The ability to predict plume temperature lapse rates would give the possibility of assessing height of neutral buoyancy. Such data could be used for estimation of plume momentum which causes overshoot of final rise height. Further, it could become a part of local and global dispersion models through assigning injection heights as well as a tool in assessing deposition of pollutants with regards to people and environmental safety.

Main objectives:

Through numerical analysis,

- Find suited method for estimation of fire plume temperature
- Investigate fire plume temperature lapse rates and final rise height
- Compare fire plume temperature lapse rates with theoretical adiabatic lapse rate
- Perform sensitivity study on fire plume lapse rates and assess synthetic eddy modelling
- Compare simulation results with common plume rise equations
- Contribute to future work on estimating final rise heights, injection heights and injection quantities such as mass.

2 ATMOSPHERIC BOUNDARY LAYER AND FIRE PLUMES

Chapter 2.1 serve the purpose of introducing relevant physics within the atmospheric boundary layer, ABL. Initially, the vertical structure of the ABL is described before advancing on to stability and turbulence within. This should provide with enough information as to understand how a rising plume could be affected by atmospheric conditions. Chapter 2.2 presents theory on fire plumes. The chapter starts at the source of the fire and describes the fire and buoyant plume throughout the atmospheric boundary layer. Chapter 2.3 serve the purpose of explaining different approaches in estimating plume rise and trajectory, with focus in CFD. Relatively simple explanations will be given in all chapters. The purpose is to gain simple understanding of the principle dynamics governing atmospheric fire plumes.

2.1 Physics of the Atmospheric Boundary Layer, ABL

2.1.1 Atmospheric Boundary Layer

To understand how a smoke plume is affected as it rises through the lower region of the atmosphere it is necessary to understand parts of the physics taking place in this region. The region of interest is called the atmospheric boundary layer, and is the part of the troposphere that is in contact with earth's surface. This chapter will give a short introduction to this boundary layer, how its stability and depth may vary during day and night, and how turbulence is generated within.

2.1.1.1 Boundary Layer Structure

The atmospheric boundary layer can be subdivided into different regions, a lower- middle and top region [20] [21]. The physics within these regions, to different degrees, change in a diurnal cycle as it is governed by the solar input. The daily cycle becomes more prominent during fair weather due to the large differences in incoming solar radiation during day and night [22] [21]. The below example, given in figure 1, on the development of the atmospheric boundary layer is based on days of fair weather.

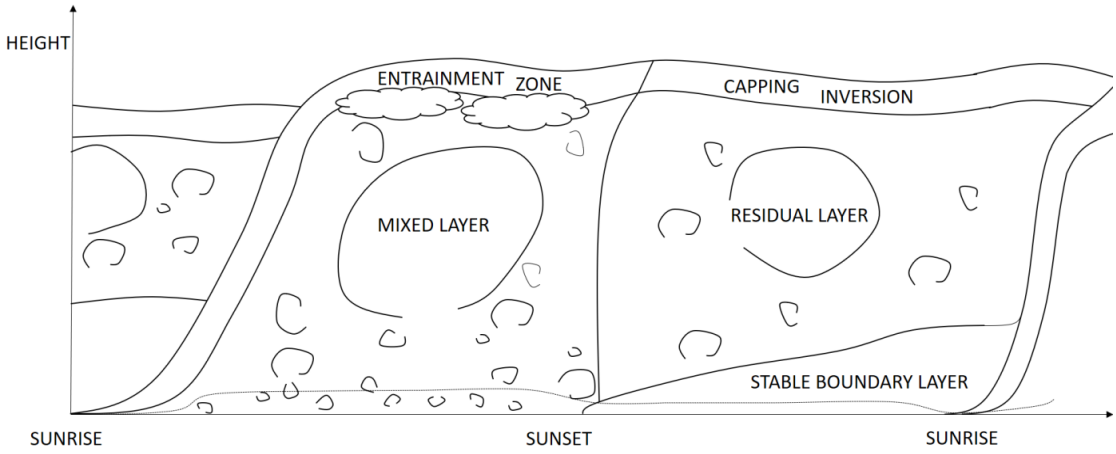

Figure 1 - Vertical cross section of the ABL showing the occurrence of various layers depending on hour of the day.

The surface layer is the bottom 5-10 percent of the atmospheric boundary layer. It is defined as a region where vertical heat and momentum fluxes vary with less than 10 percent, nearly constant [21] [23] [24]. At the bottom of the surface layer, earth's surface receives shortwave radiation from the sun as well as longwave radiation from the atmosphere [21]. The surface will absorb and reflect incoming radiation depending on the surface structure and emissivity, as well as the angle of the incoming radiation [1]. The ground temperature rises as radiation is absorbed and conducted into the ground. This cause for the ground to heat the adjacent layer of air which in turn rises due to the force of buoyancy. Plumes often forms as sheets of rising air, updrafts, intersects close to the ground. The rising plumes and updraft sheets merge higher up in the atmosphere to form larger thermals of about a kilometre in diameter. This layer of the atmospheric boundary layer is known as the mixed layer and is highly turbulent due to the vigorous up- and downdrafts [21].

Above the mixed layer lays a capping inversion which separates the turbulent mixed layer from the free atmosphere. The capping inversion is a strong stable top layer through which entrainment of free atmosphere air into the mixed layer takes place. Hence, it is called the entrainment zone [21].

The boundary layer thickness varies significantly. Its vertical extent can range from tens of meters to 4 kilometres or more [21] [25]. Its depth is ultimately determined by the temperature profile [22] [21]. The highest altitudes are reached during the presence of the mixed layer. Thermals and turbulent eddies from within this layer penetrates through the capping inversion. This results in pressure gradients that cause wisps of air from the free atmosphere to be drawn through the entrainment zone and down into the mixed layer, where it is immediately mixed. The air that penetrates through the capping inversion however, returns to the mixed layer as it has a lower potential temperature than the surrounding air in the free atmosphere [21]. This process causes the mixed layer to grow during the day.

When the sun sets the ground cools and the continuous destabilization of the air caused by the surface heat flux comes to an end [26] [21]. Turbulence within the mixed layer starts to decay, as thermals cease, and the layer is now called the residual layer. During the night, the layer becomes a nearly neutral layer. The colder surface continues to cool the adjacent air and the bottom of the residual layer is transformed into a stably stratified boundary layer, called the nocturnal boundary layer. This layer increase in depth during the night and when the sun rises, the cycle repeats [21].

Neutral boundary layers or neutral stratification occurs during overcast and windy conditions [22]. It is conditions for which the surface heat flux is weak [20] [21].

2.1.2 Atmospheric Scales

There are many different scales, average size, of motions within atmospheric flow. The largest becoming greater than 20 000 km, known as planetary-scales, comparable to the circumference of earth [21]. For such sizes, the scales are bound to be horizontal. On the other end of the spectrum are the smallest of the micro-scales, where most of the turbulent kinetic energy are dissipated [15]. Separating these outer edges are a spectrum of different sized scales of motion, synoptic scales, meso scales and the micro scales. The micro scales are the range of boundary layer turbulence, ranging from larger than 200 metres to the smallest of the micro scales [21].

For convective boundary layer conditions the largest vertical scales extend from the Earth's surface to the capping inversion [15].

2.1.3 Pressure Gradient Force

The pressure gradient force is the force arising when there is a difference in pressure across a surface. The air mass in the atmosphere is densest near the ground and becomes less dense with increasing altitudes [27]. Imagine a cubed parcel of air with lengths δx, δy, δz and density ρ. The pressure in the parcel centre is p. Considering the vertical direction, the parcel is exposed to a pressure at surface S_b in the bottom, S_t at the top and and the action of gravity on the parcels mass, see figure 2.

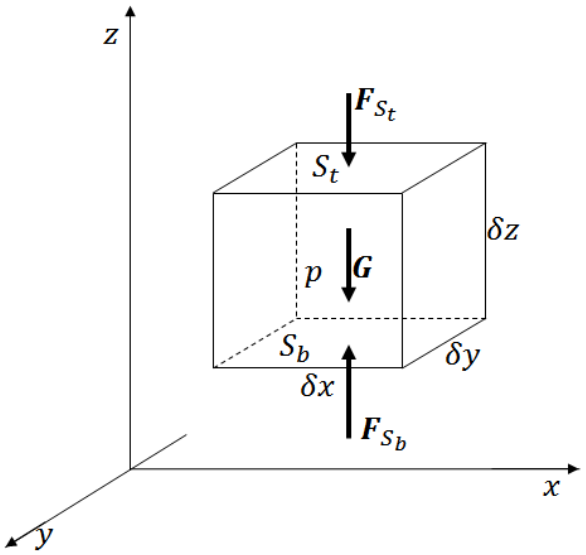

Figure 2 - Imagined cubed parcel showing body and surface forces in the vertical. Horizontal pressure forces are assumed to balance

Defining the positive direction as upwards the surface forces in the vertical can be expressed by,

$$\boldsymbol{F}_{S_b} = \left(p + \frac{\partial p}{\partial z}\frac{\delta z}{2}\right)\delta x \delta y \tag{2.1}$$

$$\boldsymbol{F}_{S_t} = -\left(p - \frac{\partial p}{\partial z}\frac{\delta z}{2}\right)\delta x \delta y \tag{2.2}$$

and body forces due to gravitational acceleration,

$$\boldsymbol{F}_B = -\rho g \delta x \delta y \delta z \tag{2.3}$$

Summing these vertical forces and setting the sum equal to zero results in the general hydrostatic equation [28] [17] [27],

$$\frac{\partial p}{\partial z} = -\rho g \tag{2.4}$$

where ρ is the density of air, p is pressure, g is gravitational acceleration and z is height.

Notice that the above expression is negative. This is the usual representation of the pressure gradient force and indicates that direction of pressure increase is opposite of resulting force. Hence, air is moving from high to low pressure.

In the case of a *hydrostatic balance*, the pressure gradient force is balanced by the force of gravity and there is an absence of vertical flow. Usually these forces are in a state of balance to within 1 % [23].

2.1.4 Lapse Rates

A lapse rate is the decrease of an atmospheric variable with height, most commonly temperature [29]. Three common temperature lapse rates are the environmental, dry adiabatic and moist adiabatic lapse rate. In this report, if nothing else is specified, a lapse rate is always a temperature lapse rate.

The environmental lapse rate, Γ_e, represents the temperature of the surrounding environment. It is found by measuring the temperature at different heights in the atmosphere [30] [31]. In general, the environmental lapse rate decreases with height [31] [32]. A *normal lapse rate* is defined as an average value of the environmental lapse rate, which is $-0.649℃/100\,m$ [32] [17]. The actual environmental lapse rate is a result of the decreasing heat absorption capacity with height, caused by the decrease in density [27]. Consequently, it varies with location and heat flux.

The *adiabatic lapse rate* is a constant, it explains the change of temperature for an ascending or descending air parcel that do not interact with its surroundings [30]. The change in temperature are adiabatic and is a result of change in pressure with altitude [17] [30] [31].

Applying the adiabatic assumption on a vertically displaced parcel of air, the first law of thermodynamics becomes,

$$0 = c_p dT - \frac{1}{\rho} dp \tag{2.5}$$

Here, for air; c_p is specific heat at constant pressure, T is temperature in kelvin, ρ is density and p is pressure. The last term in equation 2.5 can be substituted from the hydrostatic equation, equation 2.4, [17] [27]

$$\left(\frac{dT}{dz}\right)_d = -\frac{g}{c_p} = \frac{0.98\ ℃}{100m} = \Gamma_d \tag{2.6}$$

where g is gravitational acceleration. Equation 2.6 is the formula for the dry adiabatic temperature gradient, Γ_d, equal to 0.98 ℃ drop in temperature per 100-meter elevation, $-0.98\ ℃\ /100\ m$ [31] [17]. A parcel lifted dry adiabatically will cool according to this rate as shown in figure 3.

The moist adiabatic lapse rate, Γ_m, is the change of temperature with altitude for a saturated air parcel. It is given by [17],

$$\left(\frac{dT}{dz}\right)_m = -\frac{g}{c_p} - \frac{L\ dm_s}{c_p dz} \tag{2.7}$$

Where m_s is the temperature dependent saturated mixing ratio, mass of water vapor per mass of air at saturation, and L is the latent heat of vaporization for water. This lapse rate are dependent on temperature. It ranges from about $-0.9\ ℃\ /100\ m$ to $-0.4\ ℃\ /100\ m$ typically for cold polar climates and warm tropical climates respectively [17]. The moist adiabatic lapse rate is less than the dry rate due to release of latent heat of condensation as a saturated parcel of air rises above its condensation level, LCL [21] [31], see figure 3.

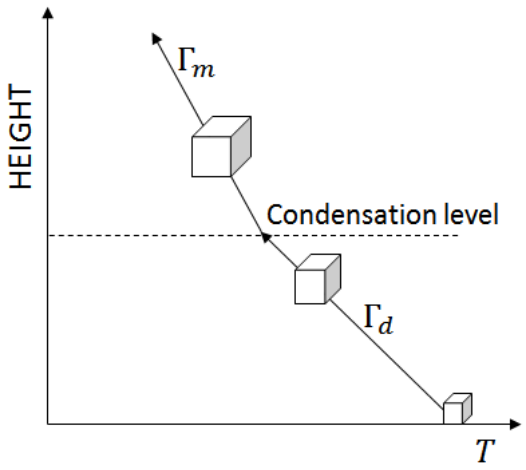

Figure 3 - Presenting the dry and moist adiabatic lapse rates. If a parcel is lifted adiabatically it cools according to the dry rate until it reaches the LCL. At this height, release of latent heat causes the change in temperature to decrease, corresponding to the moist adiabatic lapse rate.

The adiabatic process is a simplification of the actual processes causing change in temperature for an ascending or descending parcel of air. It does not account for the atmospheric mixing that continuously takes place within the atmosphere [31].

An important parameter when considering adiabatic rise is the potential temperature. It is the temperature of a parcel of air if brought adiabatically to a reference pressure. The reference pressure is set to 1000 hPa, approximately sea level pressure [3]. The potential temperature allows for direct comparison of fluid parcels at different elevations. It can be found by integrating equation 2.5 from sea level pressure to the pressure at a given level, and takes the form [7],

$$\theta \approx T + \frac{g}{c_p} z \tag{2.8}$$

Here, height z is height above mean sea level, c_p is specific heat of air and T is temperature in Kelvin [17]. The potential temperature typically increases with height in the troposphere. Another potential temperature is the virtual potential temperature, θ_v. This is the potential temperature for dry air at which the density would be the same as moist air [33]. For a dry adiabatic displacement, the virtual potential temperature is conserved [26]. As water vapour is less dense than dry air, dry air has a lower θ_v. The equivalent potential temperature, θ_e, is the conserved quantity in a humid atmosphere. It exceeds θ with a humidity dependent amount [26] [34].

2.1.5 Static Stability and Vertical Motions

Static stability can be understood as atmospheric resistance to vertical motion [31]. More precisely, it expresses fluid vertical motion depending on the vertical stratification of potential temperature or density [26]. A detailed description on this topic is beyond the scope of this text. However, it is necessary to understand the fundamentals of static stability and how it can be expressed.

Temperature lapse rates can be used to determine the stability of the atmosphere [30]. This method, referred to as *the parcel method*, considers a hypothetical air parcel, like in figure 4, lifted along the dry, Γ_d, or moist, Γ_m, adiabatic lapse rates. The parcel's characteristics are then compared to its surroundings, represented through the environmental lapse rate, Γ_e [30] [26]. If the environmental lapse rate is less than the adiabatic rate then a rising air parcel will find itself in warmer surroundings. Hence, the air parcel would fall back to initial position and the atmosphere is termed stable [27]. In the case of environmental lapse rates greater than the dry adiabatic rate conditions are unstable. During such conditions a rising parcel finds itself in cooler environments and continues to rise, (b). When the environmental lapse rate equals the adiabatic lapse rate conditions are termed neutral.

Such conditions are consistent with the parcel experiencing no acceleration at all, (c) [26] [30] [27] [21].

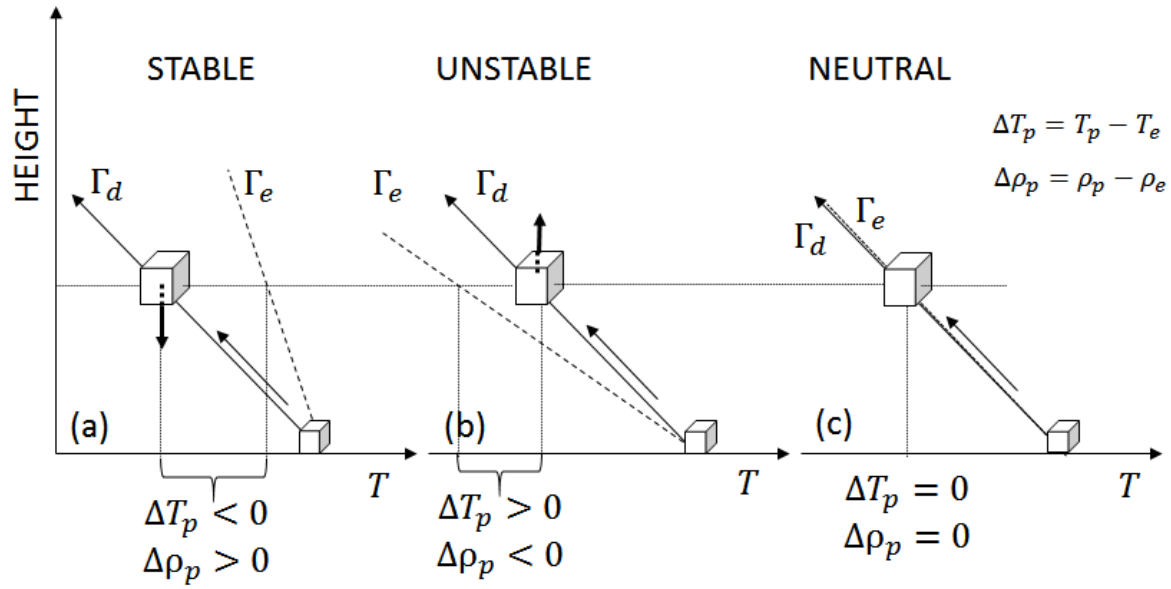

Figure 4 - Presenting the three cases of stability. The parcels can only move along the dry adiabatic, solid line, as this is the adiabatic assumption. Figure (a) shows a stable atmosphere where the fluid parcel is moved along the dry adiabatic line and surrounding temperatures become warmer. Surrounding temperatures are represented by the dotted line. The fluids acceleration is down towards initial position. Figure (b) show a similar displacement. Here the parcel is situated in colder and denser environment. It accelerates upwards. Figure (c) shows coinciding environmental and adiabatic lapse rates. Fluid parcel has no acceleration.

When considering stability through lapse rates, the nonlocal influence of stratification needs to be accounted for [21] [30]. Small vertical displacements are the key assumption in the parcel method, but could render an analysis with inappropriate stabilities. Hence, what is shown here is a simple introduction.

The slightest hydrostatic imbalance will cause for acceleration of a displaced parcel. Such imbalance between the pressure gradient force and the gravity force is often driven by buoyancy [26]. A way to characterize the static stability of the atmosphere is by use of the squared Brunt-Väisälä frequency, This frequency, N, is a frequency of oscillation for a vertically displaced parcel of air in a statically stable atmosphere [7]. The squared frequency takes the form [26],

$$N^2 = \left(\frac{g}{\theta_{v0}}\right)\left(\frac{\partial \theta_{v0}}{\partial z}\right) \tag{2.9}$$

where θ_{v0} is the virtual potential temperature and zero indicates an environmental reference state, g is gravitational acceleration and z is height. The squared frequency is given here for a stable system, where it is set to equal the restoring force per displacement. Pressure effects are ignored.

For the case of negative rate of change of θ_{v0} with height conditions are said to be unstable. The buoyancy frequency is then given by $N^2 = -|N^2|$. For positive values of the frequency the conditions are stable. For neutral conditions $N^2 = 0$ [26]. Notice that the squared frequency is defined through the virtual potential temperature. Hence, it accounts for density differences due to moisture in the air and consequently it is somewhat more accurate than the lapse rates from figure 4.

The stability, squared Brunt-Väisälä frequency and atmospheric effects are related as follows [26] [30] [27] [21];

STABLE	$N^2 > 0$	Vertical flow is reduced as displaced parcels are forced back to initial position. Depending on degree of stability, high stability equals high N^2 values, displaced parcels will oscillate with different vertical displacements and time periods.
NEUTRAL	$N^2 = 0$	Displacements have no restoring force.
UNSTABLE	$N^2 = -\|N^2\|$	Rising air will continue to rise and updrafts and downdrafts occur.

2.1.6 Turbulence

Turbulence is found in most natural and industrial flows, however, a precise definition seems difficult. Instead, turbulence could be described through some of its many characteristics.

Turbulent flow is irregular, rotational and three dimensional. It causes increased transport of momentum, mass and energy through stirring and mixing, a process known as turbulent diffusion [35] [36]. Turbulence is a response to instabilities which it tends to reduce. Hence, turbulence needs continuous destabilization or supply of energy to sustain [21]. If the supply fails, the turbulent kinetic energy is dissipated into internal energy by the deformation work of the viscous stresses [35] [36]. This is known as turbulent dissipation and all turbulent flows are inherently dissipative.

Whether a flow is laminar or turbulent depends on the inertial and viscous forces. If inertial forces dominate, the flow is turbulent. If viscous forces dominate, they suppress the inertial perturbations in the flow, and the flow is laminar. Ratio of these forces are expressed through the Reynolds number, which can be quantitatively used to define the transition between the flow regimes [37]. The critical Reynolds value is not a constant but varies with the flow configuration. It is given as,

$$Re = \frac{Ul}{\nu} \tag{2.10}$$

Where Re is the Reynolds number, U is fluid velocity, l is some characteristic length such as pipe diameter or boundary layer thickness and ν is the kinematic viscosity of the fluid.

A way to look upon turbulence is through the concept of it being a set of different sized eddies, rotating three dimensional structures. The eddies exist in the flow with different length scales l and belonging velocities, $u(l)$, and timescales $\tau(l) \equiv l/u(l)$. For increasing Reynolds numbers, the ratio of integral to small scale structures increases. As the integral scale, largest structures, are bounded by the flow domain the increased ratio implies that the small-scale structures becomes smaller with increasing Reynolds numbers [37].

2.1.6.1 Generation of Turbulence

Generation of turbulence can take place thermally, mechanically or inertially [26] [21]. Thermal or convective turbulence occurs under unstable conditions as the previously described rising thermals. Mechanical generation of turbulence, *forced convection*, is the main contributor to turbulence in neutral stratified layers [22]. It occurs when there is a shear in the mean wind. Such as shear caused by viscosity and velocity gradients, due to *frictional drag* [20] [21]. It can also be caused by wind swirling behind obstacles, such as large buildings or trees, *wake turbulence*, or just away from any solid object as *free shear*. Inertial generation is a form of shear turbulence and is caused by larger eddies accelerating nearby fluid [21].

Whatever cause for turbulence generation, static stability matters. For convective turbulence to occur it requires a negative rate of change in vertical potential temperature with increased heights [26]. Corresponding to a negative value for the squared Brunt-Väisälä frequency. If the frequency is positive however, statically stable, it inhibits shear induced turbulence. The shear turbulence may be visualized as fluid layers of different velocities, that interfere with one another and may mix through

Kelvin-Helmholtz instability pattern [26] [21]. Such mixing or displacements in the vertical would be opposed by the restoring forces of the static stability. A measure of the opposing shear instability and stratification is represented through the Richardson number,

$$Ri = \frac{N^2}{SH^2} \tag{2.11}$$

Here, SH^2 is the wind shear vector magnitude $\partial \boldsymbol{V}/\partial z$. A critical Richardson number exist, based on observations, it is equal to $1/4$. For Ri values above this critical number stability dominates shear growth and disturbances in the flow becomes stable oscillations. For the case of values below this limit, perturbations may develop into turbulence. The limit is far from finite, if turbulence is present increasing the Ri number to values above the limit, may not suppress turbulence. Turbulence can exist in the flow for values as high as 1, but becomes laminar at larger values [21]. Shear turbulence intensity within a non-neutral surface layer is greatest beneath the Monin-Obukhov length, L [26] [21].

2.1.6.2 Statistical Approach

Prediction of large scale motions and smaller turbulent scales by use of simulations are only possible for short durations of time. Large thermals in the atmosphere can be predicted to about 15 to 30 minutes [21], which would be adequate for many atmospheric fire scenarios. Small-scale turbulence however, important in molecular mixing, can only be predicted for a few seconds. It is simply too computational expensive. The inability to predict turbulence for practically useful periods of time is due to the highly non-linear nature of turbulent flow [21].

An approach to the problem is a statistical description of the net effects of many eddies, rather than individual turbulent structures. Turbulence is said to be quasi-random, as there for a given period, can be found well defined mean velocities and temperatures [21]. As the fluctuations are bounded statistically robust calculations of the standard deviation can be calculated. This however, would vary with the problem in question and how quickly things change within the system.

Consider a point in space; it might be a point in a rising smoke plume or just some point within the boundary layer. For a time period with duration t, the velocity component in the u direction is measured N times at regular time intervals, Δt, such that $t = N \times \Delta t$. The mean velocity $\bar{u}$ is thus [21],

$$\bar{u} = \frac{1}{N}\sum_{i=1}^{N} u_i \tag{2.12}$$

Subtracting the mean velocity from an instantaneous value of u, results in a fluctuating velocity component [21].

$$u_i' = u_i - \bar{u} \tag{2.13}$$

The prime indicates the fluctuating velocity, which varies rapidly with time. This fluctuating velocity can be used to find the turbulence intensity in the u direction.

$$\sigma_u^2 = \frac{1}{N-1}\sum_{i=1}^{N} (u_i')^2 \tag{2.14}$$

The turbulence intensity is given by the variance, σ_u^2, here by the unbiased variance. A flow is said to be homogenous if the variance is relatively uniform in space, and stationary if the variance is relatively constant in time [21]. Isotropic turbulence or isotropic flow is also related to the variance. If the turbulence intensity is the same in all directions the flow and turbulence is isotropic, $\sigma_u^2 = \sigma_v^2 = \sigma_w^2$, as opposed to anisotropic turbulence $\sigma_u^2 \neq \sigma_v^2 \neq \sigma_w^2$.

The velocity variance is more than just turbulence intensity, it represents the turbulent kinetic energy, TKE. For all directions in space [15] [38];

$$TKE = \frac{1}{2}\left(\overline{u'^2} + \overline{v'^2} + \overline{w'^2}\right) \tag{2.15}$$

and represented by the variance,

$$TKE = (\sigma_u^2 + \sigma_v^2 + \sigma_w^2) \tag{2.16}$$

2.1.6.3 Anisotropic and Isotropic Turbulence a Function of Stability

The static stability modulates the shape of turbulent eddies. Large eddies are strongly anisotropic during unstable conditions with the vertical motion component having a greater turbulent energy than horizontal components. Under such conditions a smoke plume would spread more rapidly in the vertical, and could be seen to loop up and down. Nearly isotropic turbulence is encountered during neutral conditions [21]. Smoke plumes in such an environment would spread equally in the horizontal and vertical direction [39]. During statically stable but dynamically unstable conditions buoyant consumption results in anisotropic turbulence with little energy in the vertical component but moderate TKE in the horizontal component. Buoyant consumption is referred to as the process

where rising air attains negative buoyancy and sinking air positive buoyancy, which would suppress the vertical component of turbulence [21]. Turbulence could be almost completely suppressed under extreme static stabilities [26]. During such conditions, a plume would blow downwind with almost no dispersion. However, it would oscillate up and down as a laminar wave [7].

2.1.6.4 Friction Velocity

The friction velocity, u_*, is a velocity scale useful for characterizing turbulent mixing. It is most applicable within the surface layer for statically neutral conditions, where mechanical generation of turbulence dominates. It is given by [23] [40],

$$u_* = \left(\overline{u'w'}^2 + \overline{v'w'}^2\right)^{1/4} = \left|\frac{\tau_s}{\rho}\right|^{1/2} \tag{2.17}$$

The covariance's are the vertical fluxes of horizontal momentum, kinematic momentum fluxes, τ_s is surface stress and ρ the density of air. It is used for calculating the Monin Obukhov length, boundary layer height and turbulence intensity [21] [22] [23].

2.1.7 Vertical Structure

Quantities such as temperature, humidity, potential temperature and wind velocities all takes on different vertical profiles within the boundary layer. How they distribute with height depends on several variables, best summarized through vertical turbulent transport.

Typical vertical profiles are shown in figure 5. The profiles are day and night conditions over land.

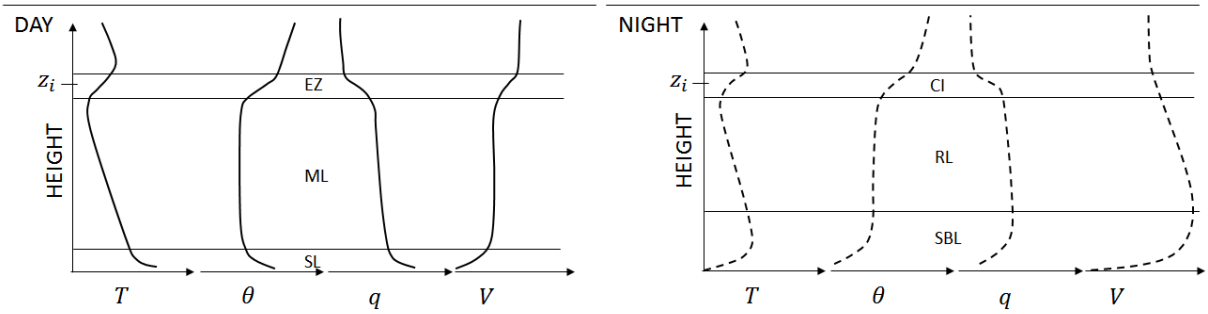

Figure 5 - Typical vertical profiles for day and night conditions. Showing temperature T, potential temperature θ, specific humidity q and wind speed V. Surface layer is SL, mixed layer ML, entrainment zone EZ, stable boundary layer SBL, residual layer, RL and capping inversion, CI. Figure based on [21]

The boundary layer depth is ultimately determined by the temperature profile. Through buoyant consumption or production of temperature turbulent mixing is either supressed or enhanced. Turbulence mixes low potential temperature air near the ground with higher potential temperature air from aloft. The result is a relatively uniform profile with height, as can be seen in figure 4. This mixing in the lower troposphere creates a potential temperature jump, which corresponds to the capping inversion. Within the surface layer at daytimes the temperature gradient is super adiabatic, consistent with the positive heat flux in this region.

At night, the stable nocturnal boundary layer forms near ground, the turbulence here is weak and sporadic due to consumption of TKE. The resulting temperature profiles are seen to increase with height, as they are cooled from below. The temperature gradient further decreases as turbulence no longer cause extensive mixing. At the top of the boundary layer, the capping inversion still exist as a stable top layer and profiles look the same. Between the bottom and top layer is the residual layer, with decaying turbulence and residual, moisture, heat and pollutants from the previous day. This layer appears equal to the mixed layer, but may have a shorter vertical extent as the nocturnal boundary layer grows during night. [21]. The average surface temperature at sea level is 15 degrees Celsius [27].

The extent of moisture in an air parcel could be expressed as absolute or relative humidity. The absolute humidity refers to grams of water per kilogram or cubic meter of air, when on a mass basis it is often referred to as specific humidity. Relative humidity is the ratio of the amount of water present at a particular temperature to the maximum amount of water it can hold [27].

The specific humidity within the surface layer decreases with height as evaporation from the surface takes place. The mixed layer becomes more humid than the free atmosphere resulting in a humidity jump at the capping inversion. At night time the humidity could be reduced in the bottom regions due to dew or frost formation, if neither present, the specific humidity profile stays relatively the same [21].

2.1.7.1 Wind Characterization

The most important forces determining atmospheric motions at higher altitudes are the pressure gradient force and the Coriolis force. When these two forces are in balance they give rise to geostrophic conditions and the belonging geostrophic winds [23]. These winds occur above the capping inversion, in laminar regions of the free atmosphere [21]. In fact, the ABL height is often defined as the region where turbulence disappears [22], meaning that geostrophic winds quickly recover their potential above the inversion. It is the high static stability within the capping inversion

that traps turbulence below and prevents further vertical communication of the surface drag [21]. Within the ABL winds are sub geostrophic. Depending on the static stability the vertical communication of surface drag varies, and hence so do the wind profiles. Winds within this layer are affected by pressure, Coriolis and friction forces [22]. This causes wind speed and direction to change throughout the layer. Within the surface layer however, Coriolis forces are negligible and the turning of the wind with height becomes unimportant. Here it is the orography, vegetation and buildings that influence the wind [23].

The wind profiles that can be seen in figure 6, show vertical profiles of wind speed for different values of the Brunt-Väisälä frequency, static stabilities. The wind profile for negative B-V frequencies, can be seen to increase rapidly. This is due to the vigorous turbulence that do well in communicating momentum downward. The communication of surface drag also results in homogenized wind speeds during daytime. The opposite is true for positive values of the B-V frequency. The wind speed increases less rapidly due to static stability causing less momentum to be mixed downward [21], reduced vertical momentum flux. For the neutral profile, convective turbulence is negligible compared to the mechanical generation. Occurring wind speeds can be high, and the wind profile near ground is seen to increase fast [23].

For near ground wind the speed is reduced as momentum is absorbed through vegetation and obstacles [41]. This cause the wind to be quite variable with height. Measurements and predictions of the winds are normally at a height of 10 meters, meteorological standards [42]

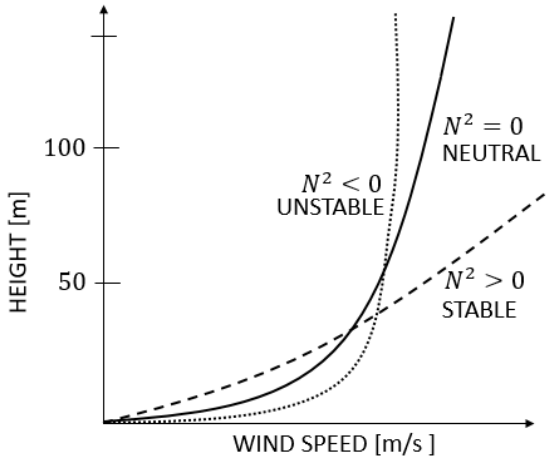

Figure 6 - Typical wind speeds and variation with height, within the surface layer, for different stabilities. Figure based on [21]

2.1.7.2 Wind Profiles

Different mathematical expressions exist to describe the wind profile throughout the ABL [24] [40]. Probably the two most well-known profiles are the logarithmic and the power law. As already mentioned, depending on location within the ABL the wind is affected differently. Within the surface layer frictional drag is great and Coriolis effect is negligible, while higher up it is the opposite [40]. Within the surface layer the wind exhibits a nearly logarithmic profile due to the drag and the hence the logarithmic wind profile is a good approximation. The surface layer depth will vary, but is typically about 10 percent of the ABL depth [21]. The logarithmic profile therefore is a good representation within heights to about 200 metres, corresponding to the surface layer for typical ABL depths. The power law expression is better over moderate height range of 20 -300 metres [4].

The logarithmic wind profile for neutral conditions,

$$u(z) = \frac{u_*}{\kappa} ln\left(\frac{z}{z_0}\right) \tag{2.18}$$

can be derived at when combining wind profile expressions for the core of the ABL and the surface layer. Here, $u(z)$ is the wind speed at the height z, u_* is the friction velocity, κ the von Karman constant and z_0 the aerodynamic roughness length. The friction velocity is the characteristic velocity scale for the inner layer, it is given by $u_* = \sqrt{\tau_s/\rho}$ [37] and is further presented in the chapter on *wall flow*. The von Karman constant is an experimental factor whose value has led to discussions [43] [44], a value of 0.4 is widely accepted [44] [20] [45] [46].

The above expression introduced a parameter known as the aerodynamic roughness length z_0, not to be confused with the sand-grain roughness height [46]. The roughness length constitutes what is referred to as the laminar bottom layer [20]. It is a measure of the ability for the surface non-homogeneity to drag momentum from the wind, and is not to be interpreted as the length of typical roughness elements at the surface [23]. By definition, it is the height of zero wind speed as extrapolated down from heights of known wind speed [21]. The roughness length influences the boundary layer depth. For the same atmospheric conditions a higher z_0 would give a deeper ABL compared to a smoother surface [45].

The power law velocity profile gives a better representation of the entire ABL depth than the logarithmic profile [47] [4] :

$$V(z) = V_r \left(\frac{z}{z_r}\right)^p \tag{2.19}$$

Here, $V(z)$ is the wind speed at height z, V_r is a known reference wind speed at height z_r and p is the power law exponent, $0 < p < 1$ [24] [47]. The power law wind profile is an empirical relation and the exponent must be determined so that the profile fits the mean wind observations. The exponent depends on atmospheric stability, height range over which its fitted, surface roughness, upstream topography and vertical momentum flux, some of which is correlated [47] [24].

An expression estimating the exponent p could be derived at by combining the power law with the logarithmic law [24],

$$p = \frac{1}{ln\left(\frac{(z_1 z_2)^{0.5}}{z_0}\right)} \tag{2.20}$$

Where $(z_1 z_2)^{0.5}$ is known as the geometric mean height. z_1 and z_2 can be understood as the outer limits of the range in which the profile shall fit. The sublayer between z_1 and z_2 can be represented by the exponent p calculated at a height z given that $z = (z_1 z_2)^{0.5},\ z_1 \geq 10\ m$ [47]. Equation 2.20 can be seen to include height and surface roughness and so it does not include all the dependent variables of the exponent. A way to assure further consistency could be to evaluate the wind profile expressed through the calculated exponent with regards to stability and upstream topography. Several expressions exist to retrieve at a value of the exponent, the expression used here was chosen for its simplicity [47].

2.1.7.3 Wall Flow

An assumption of Kolmogorov's theory is the existence of a substantial inertial range between the largest and smallest eddies of the flow [37]. The range is known to decay at a slope of -5/3 and is present in a wide range of high Reynolds number flow, such as free shear flow away from any solid surface [15]. For such flows, the largest eddies are determined by the size of the physical domain,

and is independent of viscosity or Reynolds numbers. Such a flow is consistent with atmospheric flows at a certain distance above the earth's surface. The region is referred to as the outer region, see figure 7. However, this assumption of Kolmogorov is not valid for flows over rigid walls. For a thin region near the wall, the behaviour of turbulence is determined by viscosity and the wall shear stress, τ_w. The largest eddies, regardless of the Reynolds number, are always dependent on the viscosity [37]. The region is known as the inner region and for ABL flows it corresponds to a layer near the ground, see figure 7.

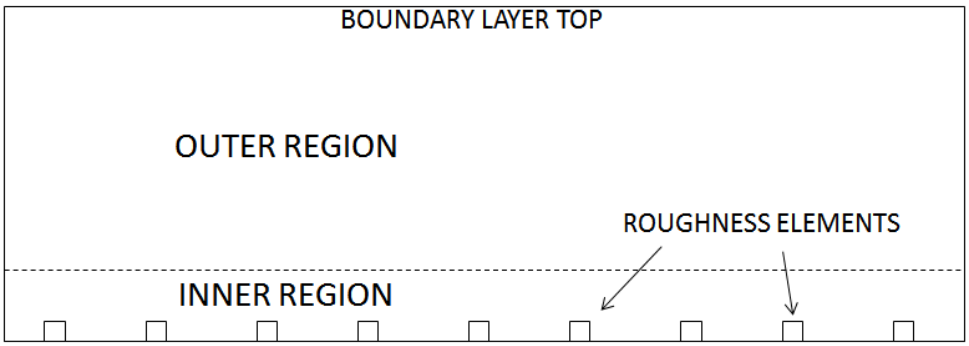

Figure 7 - Illustration of inner and outer region.

From dimensional analysis, a characteristic velocity scale and length scale for the inner layer are given as,

$$u_* = \sqrt{\frac{\tau_s}{\rho}}\,, \qquad \delta_v = \frac{v}{u_*} \tag{2.21}$$

Here u_* is known as the friction velocity, ρ is fluid density, δ_v is the viscous length scale and v is the kinematic viscosity [37] [15]. Quantities normalized by the friction velocity or the viscous length scale are referred to as being expressed in *wall units.* When considering wall flows different regions from the wall are expressed in *wall units* of $y^+ = y/\delta_v$. y^+ is similar to a local Reynolds number and determines the relative importance of inertial and viscous effects [37]. The inner region is divided into different layers. The *viscous layer* is closest to the surface, within, inertial effects can be neglected compared to viscous effects. Further out, there is layer in which the length scale is proportional to the distance to the wall, called *the log layer*. Beyond the log layer the size of the

largest eddies scale with the physical boundaries of the system [15] [37]. A buffer layer exist between the viscous sublayer and the log layer [15]. See figure 8.

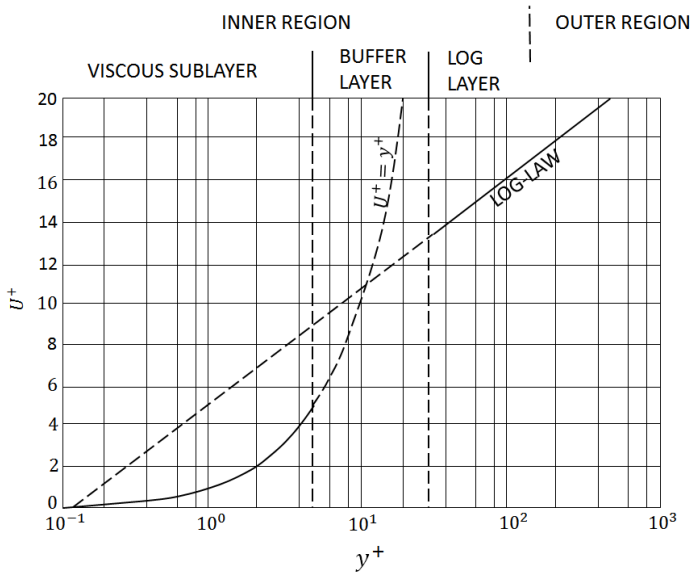

Figure 8 - Logarithmic representation of the *law of the wall* and *log law* approach to wall flows in the inner region

2.2 Fire and Plume Dynamics

2.2.1 General introduction to fire and plumes

For a fire to take place, combustible gases need to be mixed molecularly with oxygen. If the mixture is within the limits of flammability an ignition source could initiate a series of chemical exothermic reactions. If the heat produced from the fire is sufficient for continuous supply of fuel to the regions of combustion, then the reactions could continue. The amount of heat needed to sustain combustion is fuel dependent, as the amount of heat needed to produce combustible vapours varies between different solids and liquids. For a liquid fuel a general expression for the mass loss rate of volatiles per surface area is [1] [48],

$$\dot{m}'' = \frac{\dot{Q}_F'' - \dot{Q}_L''}{L_v} \tag{2.22}$$

here, $\dot{m}''$ is mass loss per unit fire area and time, $\dot{Q}_F''$ is incoming heat flux from the flame, $\dot{Q}_L''$ is heat flux loss from the fuel surface and L_v is latent heat of evaporation [1]. The latter represents the fuel specific amount of energy required per mass volatiles produced. If the equation instead was to represent the melting of a solid fuel, the denominator would have been replaced by the latent heat of gasification [49] [48].

The amount of heat released from a fire is given by [50] [1],

$$\dot{Q}'' = \chi\, \dot{m}'' \Delta H_c \tag{2.23}$$

Where, $\dot{Q}''$ is heat release rate per unit area, usually in kilowatts, $\dot{m}''$ is the mass loss rate of fuel per area, ΔH_c is heat of combustion, fuel dependent, and χ is the combustion efficiency, fuel and condition dependent. The combustion efficiency accounts for incomplete combustion [50] [1].

The heat release rate, $\dot{Q}$, is the total heat release rate from the combustion of fuel vapours. This heat will be transported away from the combustion region through radiation $\dot{Q}_r$, and convection $\dot{Q}_c$. Except from some heat that is stored in the yet unburned materials. The fraction of the radiated energy depends, among others, on soot formation, combustion efficiency and heat release rate. The radiation fraction is typically 0.3-0.4 [51] [1]. The rest of the energy is transported as hot combustion

products, gas and particles, and rises from the fire to form a buoyant smoke plume [48]. This latter flow of energy is called the convective heat release rate and equals a fraction of 0.6 – 0.7 of $\dot{Q}$ [51].

Within the flame, in regions of high temperature- and fuel concentrations carbonaceous particles are formed, which is called soot. These particles give rise to the yellow luminosity as well as being the main contributor to flame radiation. The tendency for soot production varies between fuels and fire scenario. The flame radiates in all directions, causing increased mass loss rate per unit area, as well as fire spread [1].

The fire and belonging buoyant flow is referred to as the *fire plume*. During no or low wind conditions the fire plume may be assumed axisymmetric. Such a fire plume is assumed to have a vertical axis of symmetry along the centreline [1] [48]. The fire plume is divided into three regions; *buoyant plume*, *intermittent flame* and *continuous flame.* The latter is the region in which flames are always present, hence continuous flame region [50] [1]. The intermittent region is where shape and flame height fluctuates periodically, as turbulence are shedding at the flame edge. The fluctuations occur with periodic oscillations, normally 1-3 Hz, and depends on fire diameter [48]. The mean flame height, L, of a fire occurs in this region. It is by definition the height at which flames are present 50 % of the time [51]. The buoyant plume region is the region where combustion has trailed off, and hot gases and particles rise [48].

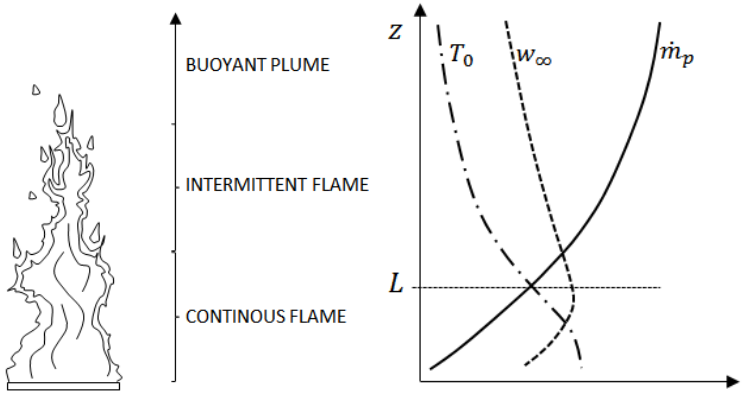

Figure 9 - On the left side is shown the different regions of a fire plume. The right-side show development of plume properties with altitude. The two figures do not correspond in the vertical scale.

The highest temperature of a fire plume is along its centreline. Within the continuous flame region, it is nearly constant with height, but it decreases sharply as combustion reactions trails off and air is

entrained along the vertical. The temperature further decreases towards the edge of the plume at regions of ambient air entrainment [51].

The velocity as well has its maximum along the centreline of the fire plume. In the continuous region, close to a buoyancy dominated source, the velocities are low. It then increases with height until about some small distance below the mean flame height, from which it decreases similarly to the temperature profile [48], as can be seen of figure 9.

The mass flow rate of the plume increases steadily with height as ambient air is continually entrained along the plume boundaries [1].

2.2.2 Buoyant Plumes

A plume occurs as buoyant fluid rises above a heat source. A distinction is made between a buoyant plume and a forced plume, as the forced plume is also under propulsion of momentum [15]. A vertical jet fire would be an example of the latter, where both momentum and buoyancy contributes the plume rise. Typically, free burning liquids or solids do not discharge substantial initial momentum.

Plumes rising from a persistent heat source depends on the characteristics of the source. The relative importance between buoyancy and momentum determines the type of fire [1] [48]. The Froude number could be used as means of classification, and is expressed as,

$$F_r = \frac{U^2}{gD} \tag{2.24}$$

Where U is the gas velocity from the source and D is a characteristic dimension, typically the fuel bed or source diameter. Jet fires with high exit velocities correspond to high Froude numbers, while natural fires would be consistent with low Froude numbers. For natural fires, like wildfires, the near-source flow is dominated by buoyancy-driven acceleration [4]. Such a source would correspond to a lazy plume, a plume with a deficit of momentum flux. While high Froude number sources would correspond to forced plumes [6].

An important relation for the square root of the Froude number is its proportionality to the dimensionless heat release rate, expressed as,

$$\dot{Q}_c^* = \frac{\dot{Q}_c}{\rho_0 c_p T_0 \sqrt{gD} D^2} \tag{2.25}$$

For most large fires the value of the dimensionless heat release rate is less than 2, and in general for most situations less than 10 [48].

While a wildfire, or other large buoyancy dominated sources, may not discharge substantial initial momentum, their buoyancy flux is significant compared to forced industrial waste plumes. Therefore, for a greater vertical length scale, the generation of vertical momentum is orders of magnitude greater than forced plumes [4]. This cause a steep near source rise and great altitudes can be reached, occasionally with stratospheric penetration [4] [8]. Off course, the extent of the fire area for a wildfire is not comparable to any industrial forced plume.

2.2.3 Plume Dynamics

2.2.3.1 Final rise height

Initially, the *smoke plume rise height* or *final rise height* of plumes can appear with somewhat different definitions in the literature [7] [8]. Consequently, it must be defined for this work. Through this thesis the final rise height is considered the greatest altitude of the considered variable. Hence, the final rise height of a plume corresponds to the maximum altitude the visible plume reaches in the atmosphere. However, in this work it will more often be associated with the thermal plume. The final rise height of the thermal plume represents the greatest altitude of positive buoyancy. This will be elaborated on in the below chapter on plumes in quiescent environments.

2.2.3.2 General Description of Plume in Quiescent Stratified Environment

A plume is a sustained turbulent fluid flow within a gravitational field, generated by a continuous release of lower density fluid into a denser environment. The potential energy of the lower density fluid drives the fluid motion. [5]

The particulate smoke rising from the combustion region consists almost entirely of solid particles. Most of which are formed due to incomplete combustion in the gas phase [1]. They rise in the buoyant plume together with heated liquid particulates and gases originating from combustion and pyrolysis [1]. As this convective column rise it expands radially as it entrains ambient fluid along its

boundaries [6]. The transport of matter at the plume boundaries are caused by turbulence. The occurring eddies are characterized by the relative velocity between the rising convective column and the ambient surrounding air [12]. At this point the content of the convective column is known as smoke, and the plume is referred to as a smoke plume [1].

The driving force of the smoke plume is its heat flux. It is the convective energy originating from the fire. Commonly, it is expressed through the buoyancy flux, F, given as [15],

$$F = \frac{\alpha g \dot{Q}_c''}{\rho_0 C_p} \tag{2.26}$$

with units of m^4/s^3. Here α is the thermal expansion coefficient of the fluid, g is gravitational acceleration, ρ_0 is the reference density of the fluid and C_p is the fluids heat capacity at constant pressure [15]. $\dot{Q}_c''$ is the previously described convective heat flux [10] [52].

Under the propulsion of the buoyancy flux the constituents rise towards higher altitudes, tending to remain within the plume envelope [10]. The amount of entrained ambient fluid determines the plume growth and dilutes buoyancy, momentum, energy and concentrations [13]. The entrainment is high in the lower regions of plume rise. Here, the relative velocities between the smoke plume and the surrounding air are at its greatest, see figure 10 [15] [12]. The entrainment causes rapid dilution of buoyancy hence increased density. And reduced vertical plume velocity. The plume radius increases as mass is entrained [48] [15]. As buoyancy is diluted velocity and entrainment decreases [12]. The rapid dilution in the lower regions trails off. At some altitude, the density of the smoke plume equal that of its surroundings. At this height, the plume still has momentum and continues to rise [15]. The velocity begins to decrease more rapidly and some distance above the height of zero buoyancy the vertical velocity vanishes. The bulk of the smoke plume will reach this latter height [12], referred to as the final rise height of the plume. As the plume then spreads sideways it descends toward the height of zero buoyancy. The mean height of the smoke plume level in between these two heights [12].It is important to remember that this is the specific case of plume rise during quiescent stratified conditions. These are the conditions for which classical plume theory are derived [48] [12].

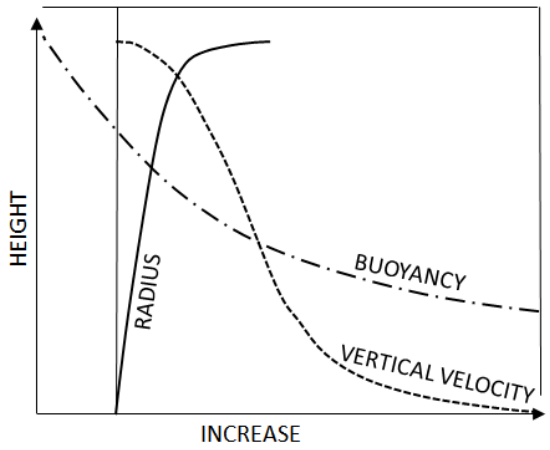

Figure 10 - The figure show the development of vertical velocity, buoyancy and plume radius as a function of height. It is given here as a general graphical explanation to the plume properties. In actuality, it is based on numerical integration of plume equations, interested reader are referred to [12] [15].

During conditions of stratified ambient, the buoyancy flux, F, is not a constant within the plume [7] [15]. This is due to the increase in potential temperature with height. The entrained air at a certain elevation will not have the same potential temperature as air aloft and the buoyancy flux reduces. This cause for a lower final rise height [10]. Intuitively, the more stable the atmosphere the lower the final rise height of the plume will become.

In addition to the cooling by entrainment, the plume further cools by expansion as it continuously rises into regions of lower ambient pressure. This can be seen from consideration of the first law of thermodynamics, equation 2.5. This additional cooling correspond to the adiabatic lapse rate of $0.98\ ℃/100\ m$. If a rising plume reaches its lifting condensation level, latent heat is released [53]. This heat increases plume buoyancy and results in increased final rise height [10]. The additional latent heat from condensation of water results in cooling according to the moist adiabatic lapse rate. Due to the condensation of water vapour clouds will form at the LCL [53]. Plumes reaching the LCL are not considered further in this report. It is more relevant when considering wildfires and their significant vertical momentum [4] [10]. For information on lapse rates see subchapter on lapse rates.

2.2.3.3 Plumes in a Turbulent Environment

For a plume in a quiescent environment ambient fluid gets mixed and entrained into the plume by the plume internal dynamics [5] [13]. However, for a turbulent environment, the process of entrainment and mixing into the plume becomes further dependent on the properties of ambient turbulence. The plume entrainment is enhanced through these external forces [5]. Compared to a

quiescent environment this additional entrainment results in additional decrease of centreline velocities and buoyancy, as well as increased mass flux [5].

The mean wind affects the plume by more than just causing transversal shear and increased entrainment [4]. Wind causes plumes and fires to bend over. Together with turbulence a smoke plume could be completely dissolved by the atmosphere before reaching any final rise height. The wind speed of the atmosphere increases with altitude causing a rising plume to continuously enter regions of higher horizontal velocities. At some altitude the mean plume momentum could become equal to the mean momentum of the wind. This height is referred to as the buoyancy length. It represents the vertical distance over which a bent-over plume will have a relatively steep trajectory [4].

The trajectory of the smoke plume is further dependent on how the windspeed increases with altitude. If near-ground winds are weak, due to low vertical momentum flux, a plume may rise and gain buoyancy generated momentum [4]. During such conditions the rising plume may penetrate to higher altitudes before becoming significantly bent over.

2.2.3.4 Neutral Conditions

In theory, a rising plume will never reach its final rise height during neutral conditions. Air entrained along the vertical rise has the same potential temperature as air aloft. This corresponds to a constant environmental potential temperature lapse rate. The buoyancy flux of the plume during such conditions are constant and the rise could continue to great heights [15]. However, neutral conditions can be highly turbulent [7]. This could cause great dilution of buoyancy and vertical momentum reducing the final rise height of the plume. Further, large scale eddies are capable of pushing segments of the plume down to the ground [3]. Plume rise in neutral conditions can therefore be limited by ambient turbulence as the plume breaks apart [17].

Plumes that undergo internal heat generation, condensation or evaporation do not have a constant buoyancy flux [13] [6].

2.2.3.5 Classical Plume Theory

Classical plume theory considers fire plumes in a quiescent stratified ambient. Such plumes are referred to as being axisymmetric. Classical plume theory and its main assumptions is a powerful simplification to a difficult and complex problem. A short review of classical plume theory assumptions and correlations will now be presented.

The classical plume theory of Morton, Taylor and Turner applied the following three main assumptions [12];

- The plume grows due to self-induced entrainment in which the velocity of the entrained air is proportional to the local gas velocity of the plume at that height.
- Profiles of temperature, velocity and buoyancy force are assumed top-hat profiles for all heights z within the plume. Top-hat profiles is consistent with considered quantities being constant for all radial distances at the considered height. Outside the plume envelope velocities are zero and temperature is ambient
- Differences in densities between the plume and the ambient surrounding air are assumed to be small, so that the plume density can be said to equal the ambient density except where they produce buoyancy forces [48]

Other common assumptions are;

- The energy released from the fire originates from a point source and is injected into the plume where it remains within the envelope throughout the rise [48]
- Gaussian distribution of temperature, velocity and buoyancy within the plume [4]
- Circular or elliptic cross section [1]
- Ambient turbulence is overcome by plume internal turbulence [54]

These assumptions are of different criticality, a discussion is beyond the scope of this text. Interested readers are referred to [14] [12] [4] [48]

Results from classical plume theory suggest that the plume mass flow increases with the energy release rate to the 1/3 power and with height to the 5/3 power. Hence, considerations of mass flow rates rely more heavily on the height of consideration than the heat released by the fire. Further, the temperature in the plume increases with the energy release rate to the 2/3 power and decreases with height to the -5/3 power. Thus, expressing a higher dependency to the height above the source than the heat release rate. Temperature is seen to depend on heat release rate to a greater extent than mass flow [48].

Zukoski and Heskestad expanded on the ideal plume equations. Zukoski tuned the equations by introducing an experimentally determined constant, while Heskestad relaxed many of the assumptions as well as examining experimental data and tuning the equations. The modified plume equations of Heskestad and Zukoski have the same dependencies to the energy release rate and height as the ideal plume equations.

2.2.4 Plume Rise Formulas

This chapter introduces a set of ordinary plume rise formulas. The formulas will be used for comparison with simulations in later chapters. A vast amount of equations is available, however, results highly depend on applied equations. Empirical and semi analytical equations can become crude assumptions outside their area of applicability [7]. Still, they should not be underestimated if correctly applied. Many equations are curve fits and applied inside their intended range, they could perform very well [4]. In general, a plume rise equation has the following structure [55];

$$\Delta z = \frac{SOURCE\ MOMENTUM,\ \ PLUME\ BUOYANCY}{WIND\ SPEED,\ \ STABILITY}$$

Below are presented 15 common plume rise formulas. Initially intended for stack plumes, but easily applicable to fires. The formulas are taken from the extensive work of James E. Carson and Harry Moses [56]. They assessed 15 plume rise equations and compared them to 711 plume rise observations. Correction factors was assigned the different equations based on observations. In the following, the 15 plume rise equations are presented without correction factors. All formulas use a consistent set of variables as presented below [56];

$\dot{Q}_{cal} = Heat\ release\ rate, \frac{Kcal}{sec}$

$V_s = Stack\ exit\ velocity, \frac{m}{s}$

$d = Stack\ diameter, m$

$U_s = Mean\ wind\ at\ top\ of\ stack, \frac{m}{s}$

$T_0 = Ambient\ air\ temperature, K$

$T_\infty = Stack\ gas\ temperature, K$

$H_s = Heigh\ of\ stack$, m

$F = buoyancy\ flux \frac{m^4}{s^3}$

$L = Horizontal\ distance\ from\ source, m$

$S = Stability\ parameter$

2.2.4.1 The Holland formula

$$\Delta z = \frac{1.5 V_s d + 0.04 \dot{Q}_{cal}}{U} \tag{2.27}$$

Empirical equation based on wind tunnel tests and stack plumes.

2.2.4.2 The Stümcke formula

$$\Delta z = \frac{1.5 \times V_s d + 65 d^{\frac{3}{2}} \times \left(\frac{T_0 - T_\infty}{T_\infty}\right)^{\frac{1}{4}}}{U} \tag{2.28}$$

Empirical modification of the Holland formula.

2.2.4.3 The CONCAWE formula

$$\Delta z = \frac{2.58 \times \dot{Q}_{cal}^{0.58}}{U^{0.7}} \tag{2.29}$$

The CONCAWE working group came up with the following formula. They used 438 plume rise observations and regression techniques to determine the constants.

2.2.4.4 The CONCAWE 2, simplified

$$\Delta z = \frac{5.53 \times \dot{Q}_{cal}^{\frac{1}{2}}}{U^{\frac{3}{4}}} \tag{2.30}$$

A simplified version of the CONCAWE formula.

2.2.4.5 The Lucas-Moore-Spurr formula (Lucas M. S.)

$$\Delta z = \frac{135 \times \dot{Q}_{cal}^{\frac{1}{4}}}{U} \tag{2.31}$$

Based on the work of Priestley [56] and stack plume observations.

2.2.4.6 The Rauch formula

$$\Delta z = \frac{47.2 \times \dot{Q}_{cal}^{\frac{1}{4}}}{U} \tag{2.32}$$

The Rauch formula has an equal form as the Lucas-Moore-Spurr formula. It is based on stack observations from two stacks.

2.2.4.7 The Stone-Clarke formula (Stone C)

$$\Delta z = \frac{(104.2 + 0.171 H_s) \times \dot{Q}_{cal}^{\frac{1}{4}}}{U} \tag{2.33}$$

A modification of the Lucas-Moore-Spurr formula. Authors argued that stack height needed to enter the equation as it was important for wind conditions.

2.2.4.8 The Carson-Moses 1967 All-Data formulas (C. M. 1967)

$$\Delta z = \frac{4.12 \times V_s d}{U} + \frac{2.92 \times \dot{Q}_{cal}^{\frac{1}{2}}}{U} \tag{2.34}$$

Based upon 752 plume rise observations and multiple regression techniques. Data from all stability classes were used.

2.2.4.9 The Carson-Moses 1967 formulas for stability classes (C. M. S. 1967)

Neutral

$$\Delta z = \frac{3.72 \times V_s d}{U} + \frac{3.15 \times \dot{Q}_{cal}^{\frac{1}{2}}}{U} \tag{2.35}$$

Stable

$$\Delta z = \frac{1.22 \times V_s d}{U} + \frac{4.9 \times \dot{Q}_{cal}^{\frac{1}{2}}}{U} \tag{2.36}$$

Carson and Moses used in the same data as in the 167 *All-data formulas*. This time separating the 752 equations into stability classes before applying regression techniques.

2.2.4.10 The Moses-Carson 1968 All-data formula (M. C. 1968)

$$\Delta z = \frac{-0.029 \times V_s d}{U} + \frac{5.35 \times \dot{Q}_{cal}^{\frac{1}{2}}}{U} \tag{2.37}$$

Gaining new data and insight Carson and Moses came up with a new All-data formula.

2.2.4.11 The Moses-Carson 1968 formulas for stability classes (M. C. S. 1968)

Neutral

$$\Delta z = \frac{0.35 \times V_s d}{U} + \frac{5.41 \times \dot{Q}_{cal}^{\frac{1}{2}}}{U} \tag{2.38}$$

Stable

$$\Delta z = \frac{-1.04 \times V_s d}{U} + \frac{4.58 \times \dot{Q}_{cal}^{\frac{1}{2}}}{U} \tag{2.39}$$

As mentioned above, new data and insight resulted in revising of the 1967 formulas.

2.2.4.12 Briggs transitional

$$\Delta z = \frac{F^{\frac{1}{3}} \times L^{\frac{2}{3}}}{U} \tag{2.40}$$

Briggs used dimensional analysis to come up with a bent over plume equation.

2.2.4.13 Briggs windy stable formula

$$\Delta z = 2.6\left(\frac{F}{UN^2}\right)^{\frac{1}{3}} \tag{2.41}$$

For a stable atmosphere Briggs included the stability parameter. The formula is based on dimensional analysis.

2.2.4.14 Briggs neutral windy

$$\Delta z = 400\frac{F}{U^3} \tag{2.42}$$

Briggs suggested this equation for neutral atmospheres. The concept is that a neutral atmosphere will never reduce buoyancy to zero.

2.2.4.15 Csanady formula

$$\Delta z = 400\frac{F}{U^3} \tag{2.43}$$

Derived by dimensional analysis and stack plume observations

2.2.5 Plume rise and dispersion

At some point the plume rise is determined by the atmospheric stability [13]. Depending on the stability the plume rises and spread may be very different. Several types of plume spread have been identified.

2.2.5.1 Fanning Plume

For the case of a highly stable stratified atmosphere, the fanning plume occurs. As the atmospheric temperature increases with height, the rising plume quickly stabilizes as it becomes surrounded by air of the same potential density. This stable atmosphere is effective at suppressing vertical motions, but horizontal winds and diffusion may spread the plume laterally. The result is a flat plume in the

vertical, but it can take on a fan-shape when viewed in the horizontal plane, hence fanning plume. The transport of smoke in these plumes can sustain significant concentrations for great downwind distances. It is typical for Pasquill stability class E or F. [39] [27] [13]

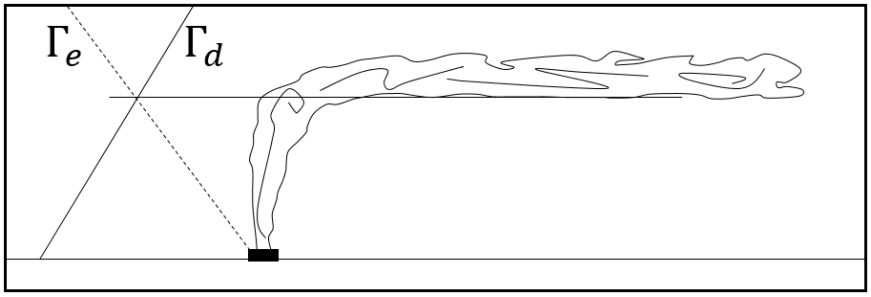

Figure 11 - Fanning plume

2.2.5.2 Fumigation Plume

A special case that could develop from fanning plumes is the fumigation plume. It occurs when the stable nocturnal boundary layer erodes as turbulence increases, typically in the morning. The stable layer that kept the smoke vertically confined now disappears from below and an unstable or neutral turbulent mixed layer is left behind [21]. The result could be rapid downward mixing of pollutants and smoke, known as *inversion breakup fumigation*. [27] [13] [39]

2.2.5.3 Lofting Plumes

The opposite case of fanning and fumigation is the lofting plume. It occurs when the plume rises above a stable layer and into a region of neutral or unstable conditions. The plume is prevented from downward transport due to the stable layer below, but is transported upwards due to turbulence [39] [27]. For such regions, the ground concentration of smoke would be low.

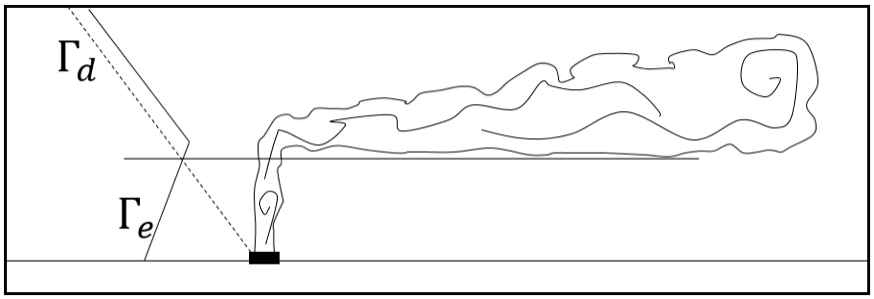

Figure 12 - Lofting plume

2.2.5.4 Coning Plume

For the case of near neutral conditions, neutral lapse rate from the ground to well above plume height, the coning plume occurs. The neutral conditions cause a well-mixed atmosphere, resulting in nearly equal plume spread in all directions, hence the cone shape. [13] [27] [39]

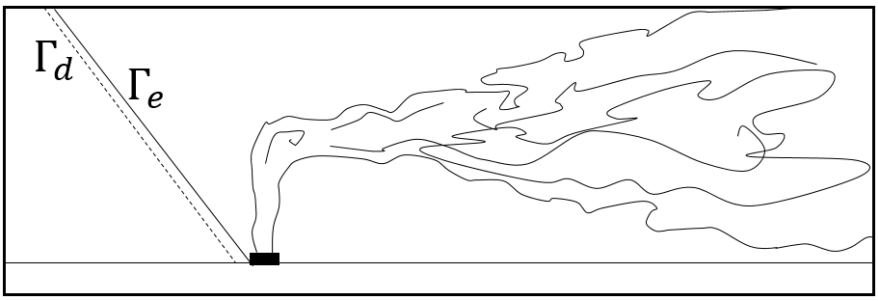

Figure 13 - Coning plume

2.2.5.5 Looping Plumes

The looping plume occurs during super-adiabatic conditions, unstable atmospheres. As the plume pass through thermals it rises and sinks rapidly. The result is a great vertical spread and smoke is quickly diluted and dispersed. It corresponds to Pasquill types A or B. [27] [39]

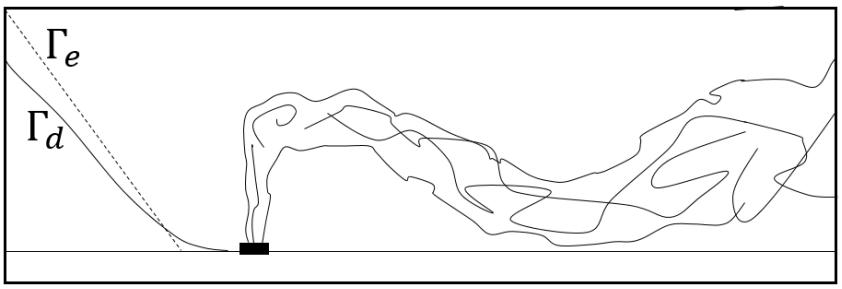

Figure 14 - Looping plume

2.3 Simulation and Modelling

When considering plume rise there are different approaches and selecting the appropriate model is important. There are four model types per [57];

- Empirical models
- Models based on dimensional analysis and similarity theory

- Models based on one-dimensional balances of mass, momentum and heat
- Computational fluid dynamics, CFD

Progressing down this list increases the amount of captured physics. This is not necessarily consistent with increased accuracy in the solution [4], but can often be seen to results in wider applicability.

2.3.1 Empirical models

Empirical models are algebraic expressions without need for space or time integration. They are developed based on measurements from field or laboratory testing, as well as statistical methods or similarity theory analyses [8]. Empirical models are easy to use, due to the simplicity of the expressions. However, these are tuned equations with small areas of application [4] (Find second source, Briggs atm or briggs handbook). They become obsolete and inaccurate outside the range at which they were fitted [7] [57] (control), but can perform well inside intended areas of application [4].

2.3.2 Dimensional analysis and similarity theory

Models based on dimensional analysis and similarity theory use dimensional arguments and integral conservation expressions. Relations are derived among characteristic global parameters, such as expressing plume rise through ambient and source conditions [58]. Typically, constants are used in the derivation of the equations, like entrainment constants. Such assumptions limit the applicability as they may not be adequate for many situations. [58].

Classical plume theory is a well-known example of models based on dimensional analysis and similarity theory. In fact, these are the most common used models [57]. Classical plume theory and common assumptions are briefly presented in the below chapter of *classical plume theory.*

2.3.3 One-dimensional balances

Models based on one-dimensional balances calculate a three-dimensional plume. However, the distance travelled by the plume is the only independent variable. One-dimensional models solve ordinary differential equations to retrieve at solutions for mass, momentum and energy. They are sometimes used when considering large buoyant sources. One-dimensional models require numerical integration and is more demanding than empirical expressions [57]. However, they offer great insight to assumptions and dynamics of plume rise.

2.3.4 Computational Fluid Dynamics, CFD

A general term used for programs developed to solve flow fields is *computational fluid dynamics*. It is defined as the set of procedures that enables numerical simulation of fluid flows by use of computers [59] [28]. A flow region is divided into a finite number of elements and differential equations describing fluid motion is applied to each element [28]. Various numerical methods can be applied to solve such a flow field, like finite difference, finite volume and finite element [59] [28].

The word *simulation* indicates that the solution to the equations of fluid motion for a system is solved numerically by computers, while modelling of physics suggests an approximation of the physical phenomena through models [59].

A simple algorithm for solving a CFD problem is now presented, followed by a further description. The purpose is introductory and the description quite general. [59]

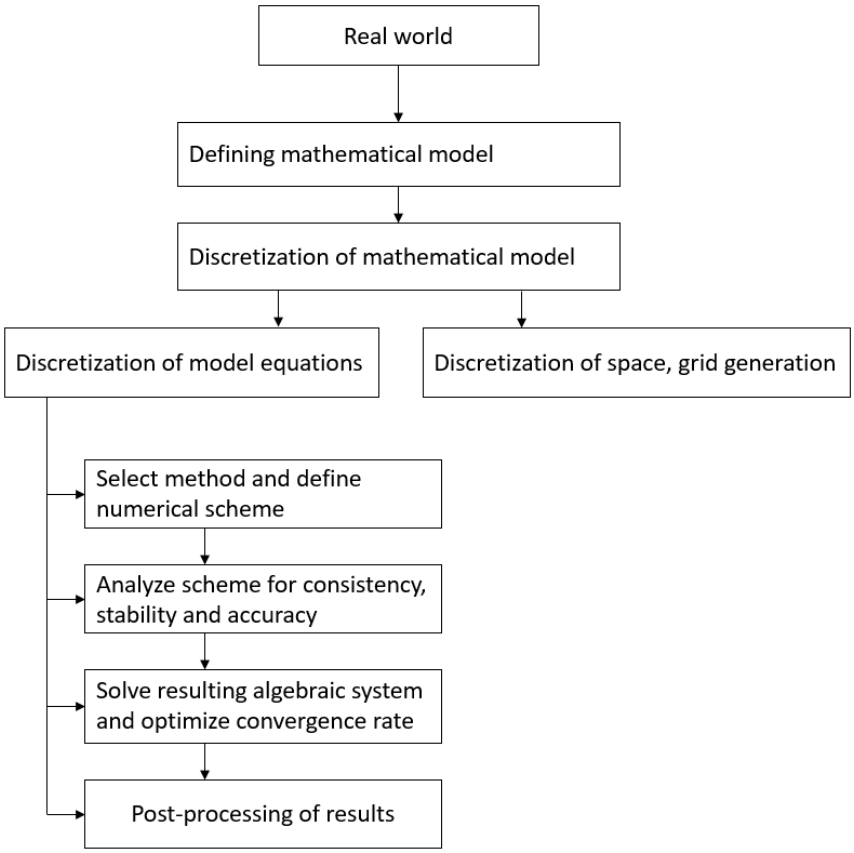

Figure 15 - Schematic procedure for use with CFD

Defining mathematical model – Define the physics intended to simulate in order to choose suited procedure and models. Modelling assumptions are associated with some level of error when compared to the real world. Discrepancies between experiments and CFD results are commonly a cause of inadequate description of real world physics, like choosing the wrong model.

Discretization of the mathematical model – Transform theoretical and mathematical model into numbers, the process of discretization. It includes the *discretization of space* which assigns the system a finite number of points which replaces the continuity of real space, grid generation. The second part is the *discretization of model equations*. It is the transformation of mathematical operators, such as partial derivatives, so that they correlate with the finite number of points in the system.

Define numerical scheme – Neighbouring grid points are assigned algebraic relations; the relations constitute a numerical scheme.

Analyse scheme for consistency, stability and accuracy – The replacement of the continuum by discrete points generate errors. The numerical scheme must satisfy certain criteria's to be accepted and level of accuracy must be established.

Solve resulting algebraic system and optimize convergence rate – The grid point values are obtained by solving the numerical scheme of the main flow variables. Solution algorithm depends on problem in question, for time-dependent flows, special attention is given to the time integration. However, all numerical schemes result in a system of algebraic equations at the end of the discretization process.

3 CONSIDERATIONS AND DISCUSSIONS ON THE MODELLING OF FIRE PLUMES AND THE ABL

This chapter focuses on the modelling of fire plumes within the ABL. It is based upon previously presented theory and it is recommended that the reader is acquainted with previous chapters upon reading this section.

The first chapter seeks to explain the basics of Fire Dynamics Simulator, FDS, the applied fire model. A short introduction to the governing equations and the turbulence model is presented. The chapter then explains the simulation setup with regards to the fire modelling. The second chapter presents simulation setup for the ABL. Considerations and discussions will be considered where they appear. The chapter serves the purpose of presenting the applied simulation setup based on performed considerations.

To get a better understanding of the following text a short description will be given here. Simulations have been performed on a section of the atmospheric boundary layer. The simulation considers plume rise from sources of different heat release rates during different environmental conditions. Figure 16 show the simulation setup that will be described below.

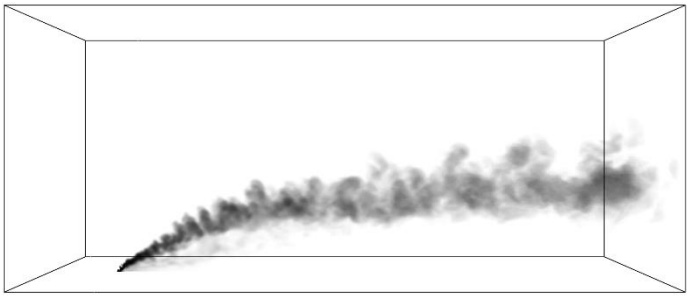

Figure 16 - Simple introductory picture of the simulated domain.

3.1 Modelling of fire

3.1.1 Fire Dynamics Simulator – The fire model

A brief introduction to Fire Dynamic Simulator, FDS, and belonging models will follow. Information is taken from the FDS user's guide [60] and technical reference guide [61].

FDS is an open source computational fluid dynamics, CFD, model of fire-driven fluid flow. It is the product of an international collaborative effort led by the National Institute of Standards and Technology, NIST, and Technical Research Centre of Finland, VTT [60] [61]. FDS is appropriate for low-speed thermally-driven flows from fires, Mach numbers below 0.3, with emphasis on heat and smoke transport. The core algorithm is a predictor-corrector scheme which is second order accurate in space and time. The default combustion model is a single-step mixing controlled reaction model. Turbulence is treated by Large Eddie Simulation, LES, with the Deardoff model as default turbulence closure.

By dividing the physical space into many rectangular cells the low Mach number equations can be solved numerically. Within each cell quantities are assumed uniform, such as temperature, velocity or concentrations, and change only with time. The accuracy depends on number of cells describing the physical space, which is limited by the available computing power [61]. The purpose of LES simulation is to calculate mean cell values for mass, momentum and energy explicitly, while accounting for subgrid transport and chemistry effects on the mean fields by use of models [60]. Being a LES model, FDS prefers uniformly spaced grid [61]. Vector components are assigned to cell faces and scalar quantities to cell centres This is referred to as staggered grid and its purpose is to reduce checker-boarding in the pressure-velocity coupling [60].

3.1.1.1 Conservation of mass and species

FDS uses a simplified approach to the chemistry of combustion. It is usually one fuel with one or two reactions, considering incomplete combustion and production of carbon monoxide and soot. This simplified approach leaves at least six gas species to be tracked, namely; Fuel, O_2, N_2, CO_2, H_2O and CO, it is also possible to track soot. The gas species are clustered together to form *lumped species,* mixtures that transport and react together. For a single-step reaction this results in two transport equations, one for the fuel and one for the products. The air is everything else, hence, it is the background species. Fuel is usually a single gas species, while air is made up of, O_2, N_2 and trace

amounts of CO and water vapor. No distinction is made between the transport of single or lumped species

The species transport equation takes the form,

$$\frac{\partial}{\partial t}(\rho Z_\alpha) + \nabla(\rho Z_\alpha \boldsymbol{u}) = \nabla(\rho D_\alpha \nabla Z_\alpha) + \dot{m}_\alpha''' + \dot{m}_{b,\alpha}''' \tag{3.1}$$

Here, Z_α is lumped species mass fraction of species α, ρ is grid cell density, $\boldsymbol{u}$ is the velocity vector, D_α is diffusion coefficient of species α, $\dot{m}_\alpha'''$ is the mean chemical mass production rate of the species per unit volume, determined from the combustion model. $\dot{m}_{b,\alpha}'''$ is the bulk subgrid source term, representing addition of mass from subgrid scale particles, such as evaporating droplets, also in need of modelling [61].

3.1.1.2 Momentum transport

Equation 3.3 presents the LES momentum equation. It is a result of applying the Favre filter to the filtered DNS equations. It is the subgrid scale stress τ_{ij}^{sgs} that needs a suitable closure by a turbulence model. All other variables are primitive or computable,

$$\frac{\partial \bar{\rho}\widetilde{u_\imath}}{\partial t} + \frac{\partial\left(\bar{\rho}\widetilde{u_\imath}\widetilde{u_\jmath}\right)}{\partial x_j} = -\frac{\partial \bar{p}}{\partial x_i} - \frac{\partial \bar{\tau}_{ij}}{\partial x_j} - \frac{\partial \tau_{ij}^{sgs}}{\partial x_j} + \bar{\rho} g_i + \bar{f}_{d,i} + \overline{\dot{m}_b'''}\widetilde{u_{b,\imath}} \tag{3.3}$$

3.1.1.3

3.1.1.4 Conservation of energy

The simplified transport equations of mass, momentum and energy, developed by Rehm and Baum, are referred to as the *low Mach number* combustion equations. The simplified equations are widely adopted in the combustion research community. They describe the motion of low speed gas under propulsion of buoyancy forces. For such conditions the spatially and temporally resolved pressure could be decomposed into a background and perturbation pressure. The background pressure, which includes the atmospheric stratification, $\bar{p}(z,t)$, is retained in the equation of state. The perturbation pressure, $\tilde{p} = (x,y,z,t)$, drives the fluid motion [61].

A consequence of this decomposition is the possibility of internal energy and enthalpy coupling through the thermodynamic background pressure, $h = e + \bar{p}/\rho$. In terms of sensible enthalpy, h_s, the conservation equation for energy can be written,

$$\frac{\partial}{\partial t}(\rho h_s) + \nabla(\rho h_s \boldsymbol{u}) = \frac{D\bar{p}}{Dt} + \dot{q}''' + \dot{q}_b''' - \nabla \cdot \dot{\boldsymbol{q}}'' \tag{3.4}$$

Where, $\dot{q}'''$ is the heat release from chemical reactions per unit volume, $\dot{q}_b'''$ is the energy transferred to the subgrid scale particles, $\dot{\boldsymbol{q}}''$ represent the radiative, conductive and diffusive heat flux. This equation is not solved directly, instead, the velocity divergence is factored out. Solving the velocity divergence, volumetric expansion rate, assures conservation of energy.

3.1.1.5 LES and Turbulence Closure

By applying a box filter to the DNS equations the filtered LES equations are retrieved. Problems arise when nonprimitive variables occur, such as the cell mean value $\overline{\rho u_i u_j}$, which cannot be calculated on the grid. It is the turbulent viscosity, μ_t, that essentially needs modelling. It occurs within the subgrid scale stress from equation 3.3. The default closure model of FDS is Deardoff's model,

$$\mu_t = \rho C_v \Delta \sqrt{k_{sgs}} \tag{3.5}$$

3.1.1.6 Combustion

Heat release rate per unit volume, $\dot{q}'''$, and the mean chemical mass production rate of species α, $\dot{m}_\alpha'''$, are determined through the combustion model. This latter quantity needs closure by modelling as the grid spacing is typically in orders of magnitude greater than the flame thickness. The heat release rate is a function of the production rates, as it is determined through the heats of formation from the produced species.

For the length and time scales associated with chemical reactions in turbulent flow, the temporally and spatially scales of a simulation may be orders of magnitude to great. When reactions are more complex, such as by generation of soot, the approach is a simple mixing environment method. The computational cells are viewed as turbulent batch reactors, where species react when mixed. The reactions are infinitely fast by default. The mixing time scale is determined by either the process of buoyant acceleration, SGS advection or diffusion, whichever is the fastest. For such infinitely fast chemistry the reacting species are converted to products within a grid cell at a rate determined by this characteristic mixing time scale.

3.1.1.7 Courant Friedrich-Lewy, CFL, constraint

Within a time step a fluid element should not travel more than one grid cell. This is restricted by the CFL constraint. Stability criteria for explicit schemes may be understood as a way to maintain physically realizable conditions. FDS applies several constraints in order to maintain stability during conditions of expansion, diffusion and advection of velocity and scalar fields.

Simply put, the CFL constraints is given by,

$$CFL = \delta t \frac{\|\boldsymbol{u}\|}{\delta x} \approx 1 \tag{3.6}$$

Where δt is the time step, δx is the length of the grid cell in direction of motion, and $\boldsymbol{u}$ is the velocity vector.

3.1.2 Characterizing the Fire

This chapter covers considerations to input parameters describing the fire plume.

3.1.2.1 Source Conditions

According to the theory presented in chapter on *Buoyant plumes,* a natural fire correspond to a certain range of $\dot{Q}^*$ values. Assessing this variable assures that the input describing the fire in FDS corresponds to a natural fire. Performed simulations have $\dot{Q}^*$ ranging from 1.4 to 2.38.

3.1.2.2 Fuel

In FDS the assigned fire is a propane gas fire releasing 46 MJ/kg of energy [62]. For the performed simulations, the actual fuel is considered to be of less importance. A soot production rate of 0.08 g/g of fuel burnt is assigned the fire, see subchapter on *gas composition*.

3.1.2.3 Heat release rates

The heat release rates chosen for these simulations are 5, 20 and 40 MW. This correspond to fires assumed reasonable in urban environments. 5 MW would be consistent with a normal sized vehicle on fire [63] [64], while the larger effects are consistent with small houses, buses or trucks.

The heat release rate is of importance as the driving force of the plume depends upon it. As can be seen from equation 2.26, the buoyancy flux depends upon the convective energy release rate. This release rate was said to typically correspond to a fraction of 0.6-0.7 of the total heat release rate, as given in the chapter on *fire and plume dynamics*. It corresponded to the part of the energy that was

not radiated away or stored within the fuel. In FDS the radiative fraction is an input parameter. It cannot be calculated in LES simulations as it depends on flame temperature and chemical composition [61], neither of which is sufficiently solved on the applied grid. Assigning propane as fuel in the input file makes FDS automatically set the radiative fraction to be 0.3. A reasonable value based on presented theory.

3.1.2.4 Combustion

For simulations in this work, combustion is performed by default settings. Special treatment of the combustion is not desired. It is the heat released per unit time that is of importance, not how it is released. Default settings will suffice.

3.1.2.5 Gas composition

The composition of combustion products are determined by the default *simple chemistry* reaction equation. For a simple hydrocarbon reaction the reactants are fuel, oxygen and nitrogen, while products are water vapour, carbon dioxide and nitrogen [61]. In addition, soot production has been specified at 0.08 g/g of fuel burnt [65].

The production of soot is rather high. It corresponds to burning of materials with a somewhat higher soot yield than typical hydrocarbons. Recall from earlier chapters that the soot production is highly case sensitive. The fires considered in this work are highly ventilated outdoor fires affected by atmospheric winds disturbing the combustion region. It is some uncertainty related to the testing conditions under which the soot yield was measured. It is unsure if it is transferable to outdoor fires. Sensitivity analysis were performed, see chapter 4. Analysis indicates that increased soot yields results in increased final rise height.

3.1.2.6 Grid resolution

The grid size of the computational domain is in general approached in chapter 4. However, a short consideration of the grid size with regards to the fire will be given here. In general, when determining the grid resolution near the fire a characteristic fire diameter is used. This parameter was noticed by NIST and Quintiere and Ma and is important if quantities are to be assessed in the vicinity of the fire, like flame height [61] [66]. For simulations performed in this thesis such quantities was assumed of less importance. The fire becomes a point source in space when considered within the atmospheric boundary layer. It is the released energy that is of importance. This energy is what drives the plume. It is assumed that the grid resolution needs to be fine enough for accurate transport of smoke and is less dependent on the grid resolution than if quantities surrounding the fire were to be considered. Again it is stressed, it is the transport of released energy that is of importance not details on how or

where this energy is released locally in space. For this reason, it is assumed sufficient to derive at a grid independent solution with regards to the transport characteristics of the plume.

3.2 Modelling of the ABL

The computational domain can be divided into three regions; the upstream region, the central region and the downstream region, see figure 17 [46].

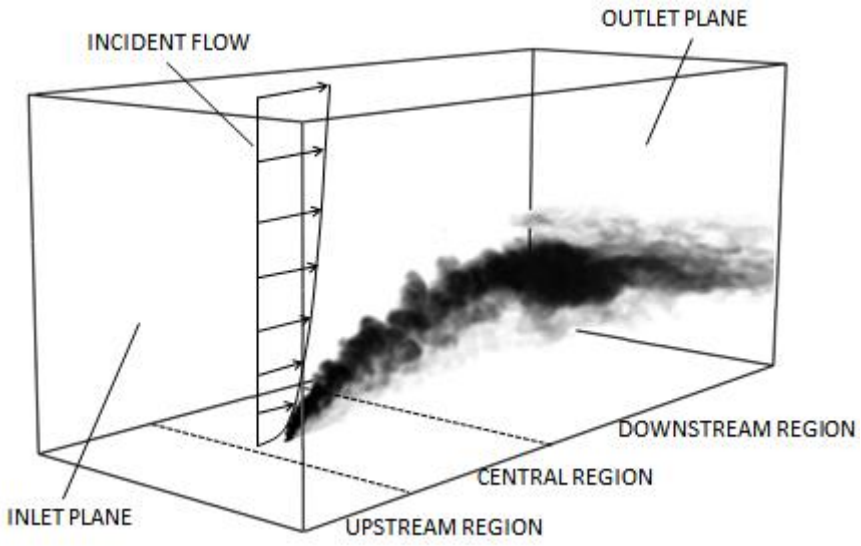

Figure 17 - Showing the different regions within the domain as well as the inlet and outlet planes

The upstream region span's from the inlet plane to the central region. Characteristic for this region is that obstacles are typically modelled implicitly, meaning that their physical shape is not included in the domain [46]. Instead, their impact is accounted for by so that surface to air interaction can be modelled by wall functions. The overall effect of the wall modelling on the flow should have the same effect, even though the actual obstacles are excluded. It is at the beginning of this region, at the inlet plane, that a specified flow is introduced to the domain.

The length of the upstream region should be of an extent so that upstream disturbances are avoided [46]. For the case of this thesis disturbances could occur if the fire is placed too close to the vent. In the initial testing of the domains the incoming wind profile was seen to attach to the lower regions of

the rising plume and flame, causing a circulation to occur, yielding high ground velocities which decreased with height within the circulation. The minimum distance for avoiding disturbances appeared to depend on the size of the vent and the size of prescribed quantities for the inlet.

In the central region interactions are modelled explicitly. For this reason the grid might be somewhat finer compared to the upstream region, so that more of the physics can be captured. It is in this region that the fire is introduced and where the initial interaction of wind and plume takes place.

The downstream region is the region from the end of the central region to the outlet plane. This is the region where the smoke plume is transported downwind. As for the upstream region, the downstream region typically applies implicit modelling.

There are several reasons why the domain is divided into different regions. Firstly, the size of the computational domain restricts the size of the largest eddies, as is also the case in the real world, where the largest turbulent structures of a flow is restricted by the physical domain [36]. If the computational domain is to represent a part of the atmospheric boundary layer it needs to be of comparable size, so that the main scales of turbulence, integral scale, present in real life can be resolved within the computational domain [22] [36]. However, this requirement would have resulted in a considerable addition to the computational cost if all flows within the domain had to be equally solved for. For this reason the domain is given sufficient dimensions, to allow for the integral scale of turbulence, while less important physics is solved implicitly. Such as wall modelling, chapter 3.2.7, where the net effects of wall flow supposedly is reproduced.

3.2.1 Generation of turbulent flow

There are different methods for generation of inflow boundary condition to LES. Considering the work of Jarrin it can be divided into *recycling methods* and *synthetic methods* [37], both which can be used to generate inlet conditions for atmospheric flows. In general, a recycling method would first create the time dependent wind data by use of a precursor simulation. Then implement the generated wind data as inlet condition to a new successor simulation, as can be seen from figure 18. This way consistency is assured as the inlet turbulence is generated by the same solver as used by the successor. The advantage of the approach is the generation of coherent structures, observed in atmospheric flow, which is typically not the case if synthetic inflow boundary conditions are used [22]. Synthetic turbulence generation methods synthetize inflow conditions by use of some stochastic procedure. Such procedures construct random velocity signals by use of a random number generator. It resembles turbulence but is a crude approximation of real turbulence. Its underlying assumption is that turbulence can be reproduced by a set of low order statistics. Velocity, Reynolds

stresses and turbulent kinetic energy can typically be reproduced, but the structure of the synthetized turbulence could differ sensibly from the real flow [37]. By use of such a model a precursor simulation is not necessary and the simulation can be run directly by applying a synthetic model to the inlet.

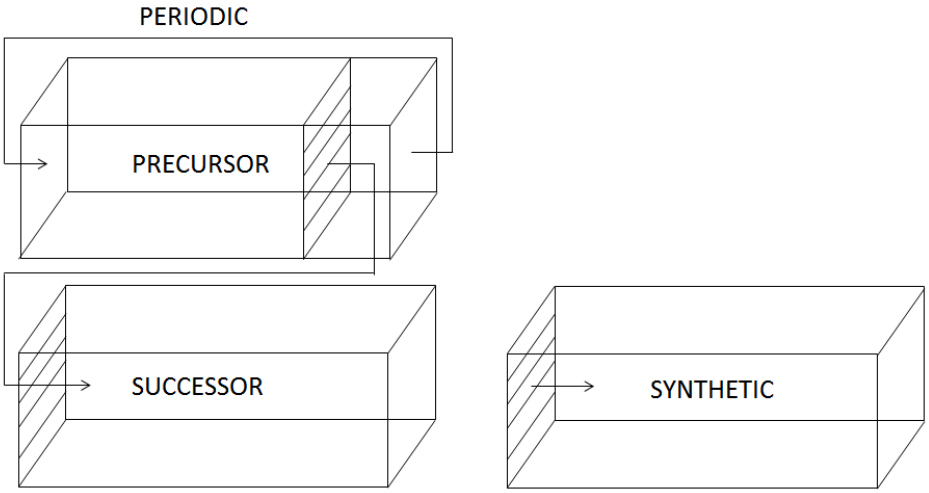

Figure 18 - Principle schematics for use of precursor simulations and synthetic eddy modelling

3.2.2 Application of isotropic turbulence

For the simulations performed in this report the synthetic eddy modelling, SEM, of Nicolas Jarrin has been applied as inlet boundary condition together with a specified power law wind profile [37] [60]. The approach of Jarrin is grounded on the presence of large coherent structures which carry most of the Reynolds stresses. The Synthetic Eddy Method constructs a stochastic velocity signal for homogenous isotropic turbulence [37]. During neutral atmospheric conditions turbulence is almost isotropic resulting in equal spread of smoke in the vertical and horizontal [21]. The use of an isotropic synthetic velocity signal is therefore a reasonable assumption for the neutral simulations, but becomes cruder during simulations of stable atmospheres. Turbulence during such stabilities become more anisotropic [21]. However, the stability used in these simulations do not deviate substantially from neutral conditions. It is therefore assumed adequate to use an isotropic turbulence approach to the stable conditions as well.

3.2.3 Synthetic Eddie Modelling

The Synthetic Eddy Method, SEM, generates a box of synthetic eddies. For each eddy in the SEM box a location and intensity vector is generated. The position of the eddies within the box, before the first time-step, are taken from a uniform distribution and is independent from each other. The

amplitudes of the signal are dependent on an independent random variable. Eddies are then convected through the box at a velocity corresponding to the specified power law wind profile ascribed at the inlet plane, the characteristic flow velocity. When an eddy convects out of the box it is immediately regenerated randomly on the inlet face of the SEM box. The time averaged of the produced signal converges towards the mean value of the flow as the interval extends in time, referred as a stationary ergodic random process. Considering Reynolds decomposing, the synthetic modelling can be understood as adding fluctuations to the mean flow. See [37] for details on the SEM modelling.

When applying the synthetic eddy modelling to the inlet plane, specification of number of eddies, N, characteristic eddy length scale, σ, and the root mean square velocity fluctuation, RMS, are required [60] [37]. This information can be retrieved from literature, RANS simulations or analytical formulas. In this work literature has been used to determine the required input values. Sensitivity studies were then performed to analyze the effect of these variables on the overall solution. Sensitivity results are presented in chapter 4. In general, the number of eddies affects the intermittency of the signal. Low values of N may result in a velocity signal with regions empty of any fluctuations, but with high energy in the sporadic occurring eddies, as the energy of the signal is independent of N. Considering the σ value, greater values results in a signal of greater length and time scales [37].

From literature, it is known that the largest vertical eddies span from the surface to the capping inversion [21] [15]. This implies that the value of σ could be close to the height of the computational domain, as the domain only considers the height up to the capping inversion. The numbers of eddies was determined from initial testing and set to be 100'000. The RMS velocity is somewhat more complicated. It can be considered by use of the friction velocity, u_*, see previous chapters. The standard deviation of the wind fluctuations for turbulence over flat terrain with uniform roughnes has been found to relate to the friction velocity by $\sigma = Au_*$, here for isotropic turbulence [23]. This is merely a rule of thumb based on extensive field measurements. The value of A for values of the roughness length $z_0 = 0.05$, is determined to be 2.5 [23]. The friction velocity is determined for neutral conditions from the formula presented in [67]

$$u_* = \kappa U_\infty \left(ln\left(\frac{C_{zn} u_*}{z_0 |f|}\right)\right)^{-1} \tag{3.7}$$

Here κ is the von-Karman constant set to be 0.41, U_∞ is set equal to the windspeeds at the boundary layer height, C_{zn} is a constant which according to Tjernstrüm and Smedman was determined to be 0.3, z_0 is the roughness length and f is the Coriolis parameter [67] calculated at 58 degrees latitude to be $0.0001233\ s^{-1}$. Above equation is solved iteratively.

A rough estimate of the standard deviation can then be computed. Based on calculations of the standard deviation a turbulence intensity of 10 % was initially applied. However, sensitivity studies for turbulence intensities of 5, 10, 15 and 20 % gave a somewhat lower final rise height for the cases of 15 and 20 % intensity. The value of the turbulence intensity for most applications is between 0.05 – 0.2 [23]. Because a higher calculated final rise height would not be beneficial with regards to people safety, the final value of the RMS velocity was set to equal a 15 % turbulence intensity.

3.2.4 Power law wind profile

The power law profile applied with the SEM at the inlet plane is considered a fully developed equilibrium profile. It represents the roughness of the upstream terrain, that is, terrain that is not included within the computational domain. Depending on ground roughness, vertical momentum flux, boundary layer height, topography and stability, the wind will have a particular variation with height [47] [24]. This is already mentioned in chapter 2. The power law exponent shall supposedly take these variables into account. It refers to the mean velocity profile for uniform level surfaces. The exponent value is normally about 0.1 to 0.2 [23]. Sensitivity studies indicate higher final rise height for low exponent values.

The exponent used in this work was set to be 0.1. Calculations according to equation 2.21 suggest a somewhat higher value. However, in order to avoid too high wind speeds aloft, it was reduced to 0.1. Too high wind speeds are not beneficial for the low Mach number solver. The reference height was set according to meteorological standard at 10 meters [42].

Wind velocities corresponding to Beaufort's scale 0 to 3 has been applied to the power law wind profiles in the performed simulations. Table 1 presents a description of the scale as well as corresponding velocities in meters per second at 10 meters height.

Beaufort's scale characterizes [27];

Table 1 - Beaufort's wind scale. Showing corresponding types, velocities and effects

Beaufort's scale	**Wind type**	**Wind velocity [m/s]**	**Effects**
0	Calm	< 0.28	
1	Light air	0.28 – 1.38	Smoke rises vertically. Wind direction shown by smoke drift, not by vanes
2	Light breeze	1.66 – 3-1	Wind felt on face, leaves rustle, moves vanes
3	Gentle breeze	3.33 – 5.28	Leaves and small twigs in constant motion
4	Fresh breeze	5.6 -7.8	Raises dust and moves paper, small branches move
5	Moderate breeze	-	Small trees begin to sway, crested wavelets form on inland water

3.2.5 Longitudinal vertical boundaries

The vertical boundaries at the sides of the computational domain can have different properties, periodic or open. A periodic vent is a vent that introduces the flow back into the domain on the opposite side from where the flow left, while an open vent is open to the free. Periodic boundary conditions are only to be applied to flows which are homogenous in the stream-wise direction, consistent with fully developed flows [37]. The indication during this work is that periodic vent traverse the domain faster than by use of open vents. This is also indicated by [22].

In the simulations performed in this work, open boundaries was applied regardless of the prolonged computational time. There were two reasons for this. For simulations with periodic vents spurious pressure fluctuations occurred frequently within the domain. This is not an unfamiliar problem when dealing with tunnel flows in FDS. The root cause is the way that the perturbation pressure is retrieved at [60]. This is an iterative process by which each iteration is bringing the old and new values of the perturbation pressure closer together. The pressure iteration solver is designed to minimize the normal component of velocity at mesh interfaces or walls [68]. The iteration stops either when the pressure tolerance criteria is reached, by default it is $20/\delta x^2$, or at the max number of iterations, by default 10. If mismatch between the old and new pressure fields are too high fluctuations could occur [60]. Technically this error can be alleviated by reducing the pressure tolerance and increasing the number of iterations, which results in increased computational time. Secondly, the periodic vents showed less consistency to the assigned wind profiles than did the open boundaries. The reason is thought to be related to the poor modelling of the wall flow at the ground.

As this wall flow does not satisfy the y^+ criteria the periodic vents seem to quickly disturb the specified profile to be become more uniform with height. Based on this, open boundaries were applied to the longitudinal sides of the domain.

3.2.6 Top horizontal boundary

The top horizontal boundary represents the height from earth's surface to the capping inversion. The capping inversion was the stable inversion layer at the end of the boundary layer. It is difficult to represent this layer within the computational domain. To model this layer a friction free wall has been applied, as was done by Andreas Bechmann [22]. Allowing winds to pass at velocities corresponding at prescribed velocities, while at the same time preventing smoke from further rise. Such a boundary will not allow fluxes to pass which might be problematic for high energy release rates. None of the simulations in this work however, consider penetration of inversion layers. The effects are not sufficient to achieve this at such heights. Further, if a plume reaches the inversion layer the momentum and temperature of the plume will be considered as to evaluate validity. It is assumed that the effect of the friction free wall for the current heat release rates are negligible.

3.2.7 Ground and wall modelling

The ground within the domain is given a roughness corresponding to that of a relatively flat grassy terrain. The value of the roughness is set to 0.02 [40].

The bottom of the atmosphere consists of different size roughness elements. A computational mesh which resolves individual elements would be impossible [22]. It is simply too computational expensive. A modelling approach is necessary. However, in order to get satisfactory modelling results grid cells adjacent to the wall should be reduced so that they fall within the log layer [60]. This can only be achieved by stretching the grid. A function that should be avoided in FDS. The technical reference guide states that it is best if a mesh consist of cubes [61]. If cells are shrinked at one location, they must be stretched somewhere else within the domain. The aspect ratio for such stretching of cells should not exceed 2-3. Further, stretching reduces efficiency [60].

For an unstretched grid, not fulfilling the y^+ wall modelling criteria, a series of windsimulations were performed. The wind field was then assessed at different downstream distances. It was found that the power law profile maintained its shape well throughout the domain. Some changes in wind speed was seen at the lower and middle heights when passing halfway through the domain. This occurs for two reasons; (1) the wind is introduced at the inlet plane as a power law profile. To have a fully established wind field, the profile needs to traverse the entire domain. This takes time, and since the air in front of the profile initially is at rest, the profile reduces at the front but builds up with time. This could have been partly solved by introducing a pressure difference across the inlet and

outlet planes, but that would rely more heavily on the wall modelling and the belonging y^+ criteria. Such a solution was not wantingly. (2) The wall flow is not sufficiently solved. This resulted in the profile becoming gradually more uniform with height, at the bottom regions, as the end of the domain was approached. This however, took considerable downwind distances to become prominent. At these distances the importance of the profile is assumed near absent. The profile is assumed to be of importance mainly in the vicinity of the fire and the first hundreds of meters downwind from the source. These are the regions where almost all of the cooling and dilution of the plume takes place. Beyond this region, the plume has risen to heights that maintain its original velocity throughout the domain. This is supported by [4]. Based on this, it appears to be unnecessary to reduce the value of the y^+ criteria. The modelling of the windfield is more than sufficient with regards to the wind profile and velocities for regions of importance, above half the domain length.

3.3 Solution procedure

This chapter presents overall solution procedure applied in the work of this thesis. All parts of the procedure are to some degree present within the report.

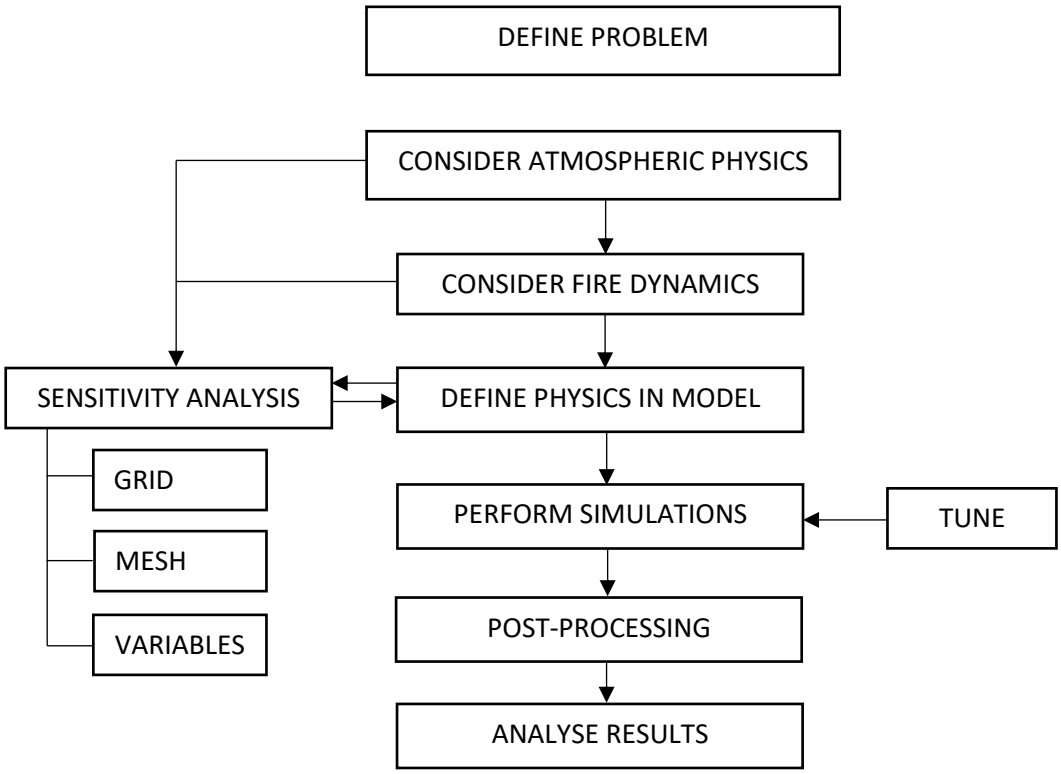

Figure 19 – Simplified overall solution procedure used in this work

3.4 Post-processing of simulations

This subchapter presents the methodology used in retrieval of the mean thermal plume lapse rate. It is the lapse rate of the plume, or the rate at which the plume temperature changes with altitude in the atmosphere.

3.4.1 Finding an interval

Turbulence and atmospheric flow can be said to be quasi-random, that is, for a certain period of time well defined mean values may be defined. When mean values for the plume lapse rate are to be retrieved, the instantaneous velocities need to be considered in order to choose a suited interval. Hence, attention is given to occurring gust in the wind field. These gusts can become highly influential. It is desired that the intervals as far as possible are equal.

3.4.2 Wind profiles

The synthetic eddy modelling is applied to induce fluctuations to the flow. Figure 20 presents mean wind velocities as a function of height from the ground. These profiles represent the incident wind profiles, as they are measured 22 meters upwind from the fire. The curves for the U and V-velocities are seen as quite straight lines at zero velocity, while the mean U-velocity can be seen to take on the prescribed power law profile. Notice is taken to the fact that the mean velocity for the interval at the height of 10 meters appears to be 5.5 m/s. Clearly, differences will exist between simulations of similar prescribed wind velocities. Such variations in the occurring winds can potentially cause for differences in seemingly equal simulations.

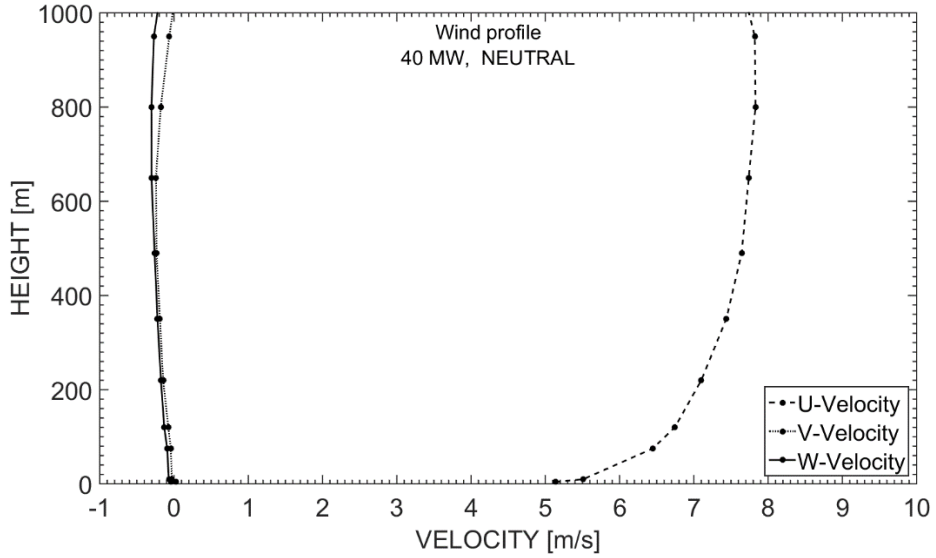

Figure 20 - Presenting incident wind profiles of U,V and W velocities. Conditions are neutral.

3.4.3 Thermal plume criteria

When considering the plume lapse rate a criterion is needed to decide whether a certain data point has sufficient temperature to be considered a part of the thermal plume. In this work a criterion based on the mean excess temperature of the plume has been applied. This excess temperature is the temperature above the ambient at the considered altitude. If this temperature is$(T_0 - T_\infty) \geq 0.5$ degrees Celsius then it is within the thermal plume.

The criterion is based upon consideration of several aspects. Firstly an area of application is decided upon. This is important as depending on the object of analysis, a conservative rise height might be either high or low altitudes. Although such considerations could be addressed through safety factors at a later stage in the calculation it is implemented here for convenience in later calculations. For this work it is considered that people safety in the vicinity of the fire would be the applicable area for the results. Hence, a conservative approach is a somewhat lower final rise height of the plume. Further sensitivity analysis presented in chapter 4.2 indicates that the final rise height is sensitive to changes in the atmospheric conditions. Such findings support the chosen criterion.

Moreover, the criterion shows good results when compared to the final rise height of plumes. The criteria further allow a more convenient consideration of the extracted slicefiles. If temperatures are set to low, then regions of higher temperatures elsewhere within the domain will appear as noise. Therefore, applying the criteria of 0.5 assures consistency and reliability in the post processing, as well as saving on computational time.

3.4.4 General description on calculation of plume temperature lapse rate

The plume temperature lapse rate is computed as the change of mean plume temperature per unit height. It is calculated by considering all data points, at a specified height, that contains sufficient excess temperature to be considered a part of the thermal plume. A mean value is then calculated by dividing the total excess temperature by the number of data points. This assumes that the data points are uniformly distributed across the thermal plume area and that each point therefore represents the same area.

The mean thermal plume temperature lapse rate is obtained by use of data from the FDS slice files. Data is dumped to these files every $\left((T_{end} - T_{begin})/nframes\right)$ seconds, which is $nframes$ times per simulation. For this work the default settings of FDS has been used, which corresponds to data being saved every two seconds.

Gas temperatures in FDS are computed at cell centres, but the data given in the slice files correspond to linearly interpolated cell corner values.

The approach is equal for horizontal and vertical slices. It is the orientation of the plume which decides which slices that will be used.

In the following description, consider a horizontal slice of data points that fully engulfs the thermal and visible plume. The mean plume temperature at the height of this slice is then found through the following steps;

1. Extract necessary data from the FDS slice files by use of the program fds2ascii

   The data extracted is; (1) a single reference slice containing the mean background distribution of atmospheric temperature and (2) DX number of slices for a specified steady state interval. It is necessary when calculating the mean temperature for a specified interval to consider near instantaneous slices of the temperature distribution, see figure 21. It is not sufficient to compute the average temperature for the interval in one setting, which is easily done in fds2ascii, as this would yield a different mean plume area and temperature.

2. Subtracting the reference slice from the instantaneous slice

   The slice data dumped by fds2ascii is stored as comma separated files. The different slices are saved as matrices in Matlab and the reference slice matrix is subtracted from the DX

instantaneous slices. The remaining matrices represent slices of excess temperature from the ambient at this height.

3. Applying criteria

The matrices of excess temperature are then exposed to a filter. All values below aforementioned temperature criteria become 0. Other values remain unchanged. The mean temperature for each slice is then calculated by use of the filtered matrices. The excess temperature is summed and divided by the number of data points. It is this excess mean data point temperature that is taken to represent the mean thermal plume temperature.

When calculating the mean excess temperature from the filtered matrices, the whole population of data points within the area of the thermal plume is considered. However, the grids that constitute the slice, in total, are of different sizes. This means that there are a different number of data points per area depending on position within the slice. This could affect the calculation if for instance the densest grid experienced the highest temperatures. This would result in more data points with high temperature and an increase in mean plume temperature. As the plume rises, the large temperature differences disappear and local peak values become less significant. At these heights, the thermal plume area falls in between different sized grids, but it seems of negligible effect as the excess temperatures has become lower and more uniform across the thermal plume area.

4. Control

Mistakes are easily made when large amounts of data are treated, especially considering that the data is divided between 4 meshes. To get a better control, some measures have been implemented. Firstly, the post-processing scripts are divided into several scripts so that errors are more easily found. Secondly, when the data has been retrieved from all 4 meshes a plotter script compiles the retrieved matrices and creates a picture of the excess temperature. This makes it easy to assess if the slices has been correctly treated. The pictures are 560 x 420 pixels.

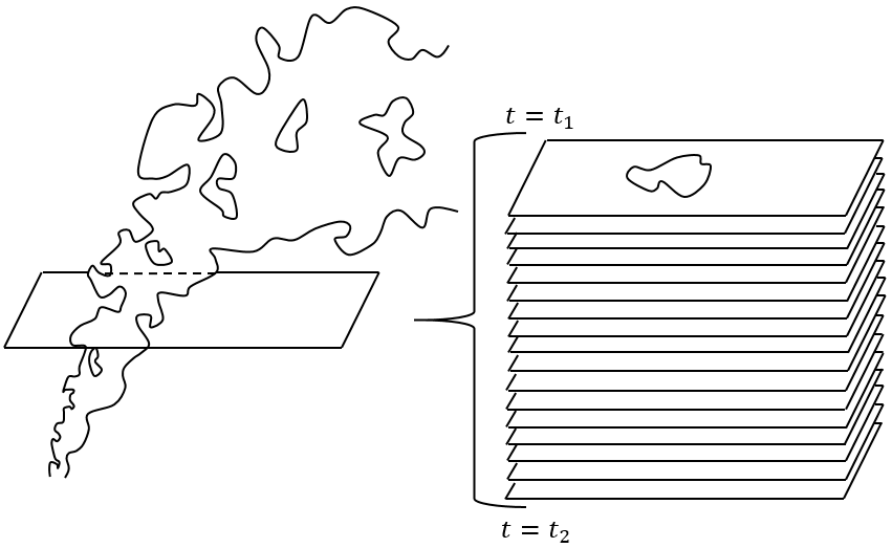

Figure 21 - Showing principle of post processing procedure at a particular height. Slices are withdrawn every 4 seconds during entire interval.

3.4.5 Retrieving plume height

Retrieving the mean excess plume temperature is similar for the horizontal and vertical cases. However finding the corresponding height is rather different. Vertically rising plumes uses horizontal slices, located at specific heights. Therefore, it is rather straight forward to plot the heights of the slices to the corresponding mean excess temperatures. The bent over plumes however uses vertical slices and the height corresponding to the calculated temperatures needs to be found by a different approach.

Finding the height of the plume in the vertical slice begins by filtering all matrices of excess temperature. The filter turns the matrices into binary matrices, by applying the temperature criteria and assigning 0's if the criteria is not fulfilled and 1's if the criteria is fulfilled. The binary matrices are then plotted and saved as binary pictures of 520 x 460 pixels. In the above chapter on calculation of the plume temperature lapse rate, step 4 involved the plotting and saving of the original matrices. These matrices can now be visually compared to the binary pictures assuring the binary picture appears to be the correct representation, see figure 22.

Figure 22 - The picture on the left is the plotting of the original subtracted matrices. While the picture on the right is the result of plotting the binary matrices. Both pictures are vertical slices showing the cross section of a bent over plume at 250 meters downstream from the source. Though not considered in this report, note the appearing counter rotating vortices [4] [58]

Then, a new Matlab script reads the binary picture and finds connected objects within. The connected objects considered are only pixels with value 1, corresponding to pixels of excess temperature. The connected objects are referred to as blobs, as they appear as blobs in the two-dimensional picture. As the fire plume cross section is not circular, as commonly assumed, the script needs to identify all blobs of a certain size on the picture. A filter that removes blobs consisting of 5 or less connected pixels from the picture is applied. These pixels get the value 0, black. A built in function in Matlab, *regionprops*, now detects the blobs and find several properties belonging to them, such as the center of area, see figure 23. This center is given in pixels coordinates. A loop then calculates the mean coordinates in the X and Y directions of the picture based on the number of blobs that were present. Usually this number is about 1-5 depending on the distance from the source. From these coordinates by converting from pixel values to meters the location of the thermal plume centerline is assessed. This approach has some steps of reduced accuracy. The main assumption however, is that the appearing blobs together always represent the centerline. Meaning, no measure is taken to account for different areas, see figure 23, right side. In general this appears to be a sufficient assumption as the blobs are never widely spread.

See appendix B for details on some of the Matlab scripts that has been used.

Figure 23 - On the left side is the binary image from figure 22 after Matlab reads the saved image and additionally converts the colours. The pixel coordinates of the two appearing blobs is saved as a temporary mean value for this specific picture. Then all temporary values from all pictures of the same slice are used to calculate the mean position of the plume at this particular downwind distance. The picture on the right is an attempt to show how three appearing blobs will be weighted the same when calculating the mean coordinates of a single picture.

3.4.6 Input parameters

The following table presents all input data used in FDS. Occurring variables are only those used in the main simulations. Sensitivity analysis data can be found in chapter 4 and appendix A.

Table 2 – Table containing input parameters. Parameters are determined from sensitivity analysis and best practices.

Variables		Small domain	Large domain
Domain			
Domain size, LxWxH	[m]	2000x800x500	2754x1200x1200
Inlet plane		Power law wind profile & SEM	Power law wind profile & SEM
Outlet plane		Open	Open
Vertical longitudinal plane		Open	Open
Top boundary		Friction free surface	Friction free surface
Ground		Roughness 0.02	Roughness 0.02
Wind			
Power law reference height	[m]	10	10
Power law exponent		0.1	0.1
Velocity		0.5/1/2/5	0.5/1/2/5

Atmosphere			
Environmental lapse rate	[℃/$\boldsymbol{m}$]	0.009/0.00649	0.009/0.00649
Integral length scale	[m]	450	1000
Turbulence intensity		15 %	15 %
Number of eddies		100’000	100’000
Ground temperature	[℃]	15	15
Fire			
Heat release rates $\dot{\boldsymbol{Q}}^*$	[MW]	5/20/40	5/20/40
Soot yield	[g/g]	0.08	0.08
Grid			
Fire mesh	[m]	1	2
Other mesh	[m]	4	6

4 SENSITIVITY ANALYSIS

This chapter first presents a grid sensitivity analysis. The analysis considers solution of different sized grids as well as the transfer between meshes. Grid sensitivity is performed for different heat releases and wind conditions. Then, sensitivity studies of input variables on the overall solution are presented. These solutions are simulated inside a domain of neutral atmosphere and 2 m/s wind. The fire produced 40 MW.

4.1 Grid analysis

A grid analysis is performed to ensure grid independency with regards to the transport of the fire plume. It has been stressed in earlier chapters that quantities in the vicinity of the fire cannot be considered sufficiently resolved due to the large grid surrounding the fire. The fire is considered a point source in space. Region of interest is located some distance away from this source and comprises the transport of buoyant products. It is the transport of the fire plume within this region that needs to be considered so that a grid independent solution can be derived at. As the domains consist of six meshes with two different grids it is necessary to assess the grids as well as the transfer between them.

Sensitivity analysis is performed for the extremities of HRR and wind speeds. Simulations are performed on two different domains. Both domains are equal to applied domains except for mesh number 6 which has been reduced in the downwind direction to save computational time. Reducing the downwind distance should not affect the sensitivity analysis. The analysis is comparative and serves only to compare the solutions between different resolutions and transfers.

Table 3 below show the different simulations performed during the sensitivity analysis.

Table 3 - Input parameters for performed grid sensitivity

Simulation:	Domain:	HRR: [MW]	Wind speed: [m/s]	Fire mesh: [m]	Other mesh: [m]	MESH to MESH
#1	Small	5	0.5	0.5	2	16
#2	Small	5	0.5	1	2	4
#3	Small	5	0.5	1	4	4
#4	Small	5	5	0.5	2	16
#5	Small	5	5	1	2	4
#6	Small	5	5	1	4	4
#7	Large	40	0.5	1.5	3	4
#8	Large	40	0.5	2	4	4
#9	Large	40	0.5	2	6	9
#10	Large	40	5	1.5	3	4
#11	Large	40	5	2	4	4
#12	Large	40	5	2	6	9

4.1.1 Small domain

Figure 24 presents the results from simulations of three different grid compositions. Compositions were as follows, given from the fire mesh to adjacent meshes; 0.5 to 2 meters, 1 to 2 meters and 1 to 4 meters. First and latter of these compositions has a 16 to 1 cell transfer ratio. Meaning that 16 cells from the fine mesh, borders to 1 cell in adjacent meshes. The 1 to 2 meters composition has a 4 to 1 ratio. All simulations are performed during a 5 MW fire and 0.5 m/s wind conditions. This corresponded to a height of 300 meters. The curves in figure 24 clearly show grid independent results for the different mesh resolutions. Further, it is evident that a 16 to 1 transfer ratio between meshes appears similarly smooth as a 4 to 1 transfer ratio.

Figure 25 consider the same simulation, but with increased winds as the only difference. Winds in simulations presented in figure 25 was 5 m/s. For these simulations winds are much more severe, and gusts appear frequently. Even though the simulations of 0.5 to 2 meters' composition and 1 to 2 meters' composition appear to coincide the most, it is believed that it is the severe winds that cause these simulations to deviate from the last one. Considering the high winds and occurring gusts it appears difficult to get any better match than what presented from this figure. Off course, had the intervals for calculations been extended substantially higher similarity would probably been achieved.

Considering the results presented from figure 24 and 25 the applied grid resolution for the small mesh was determined. A uniform cell size of 1 meter's cells in the fire mesh and 4 meters' cells in adjacent meshes were applied, all in all 14'012'000 cells.

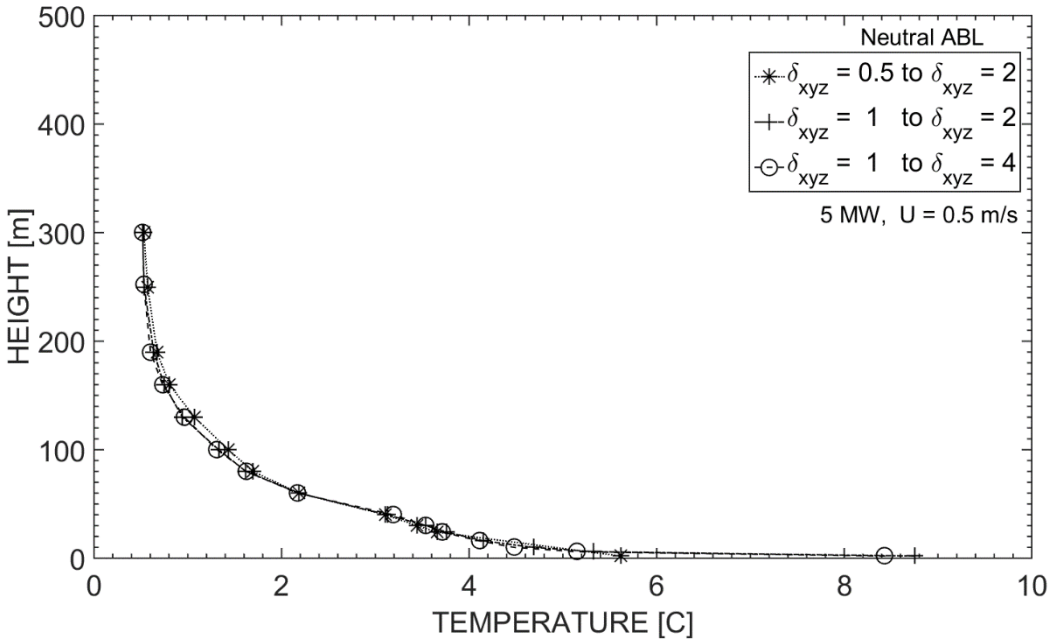

Figure 24 - Results from sensitivity of 5 MW fires in a neutral atmosphere with 0.5 m/s wind. Temperature is excess plume temperature, the temperature above ambient.

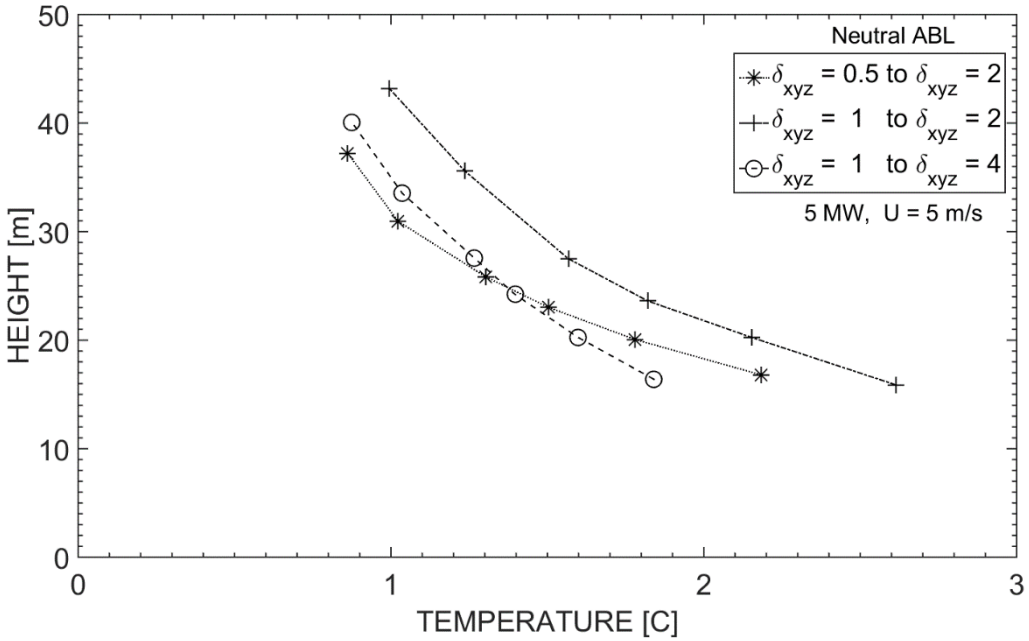

Figure 25 - Results from sensitivity of 5 MW fires in a neutral atmosphere with 5 m/s wind. Temperature is excess plume temperature, the temperature above ambient

4.1.2 Large domain

Figure 26 presents the results from simulations of three different grid compositions. Compositions were as follows, given from the fire mesh to adjacent meshes; 1.5 to 3 meters, 2 to 4 meters and 2 to 6 meters. The two first of these compositions has a 4 to 1 cell transfer ratio, while the latter has a ratio of 9 to 1. All simulations are performed during a 40 MW fire and 0.5 m/s wind conditions. Processing was ended when the outlet plane was approached, corresponding to a height about 750 meters. It is evident from the results that the solution has become grid independent. It is further clear that the 9 to 1 transfer ratio performs as well as the 4 to 1 ratios.

Figure 26 presents simulations identical to those presented in figure 25, except from the increase in wind speed from 0.5 to 5 m/s. Results can be seen to coincide somewhat better than what was observed for the 5 m/s wind case in the small domain. However, similar conclusions must be drawn. The conditions during these winds are more difficult to get alike. Occurring wind fields are randomly generated and are therefore not equal between cases. Only during the low wind conditions such as presented in figure 26, is it possible to have curves coincide to such a degree. For the high winds this appears to be difficult. As was pointed out for the small mesh, for extended intervals the curves would probably become increasingly similar. However, the curves are not too unlike and it appears to be a sufficient solution if considering results presented in figure 26 as well.

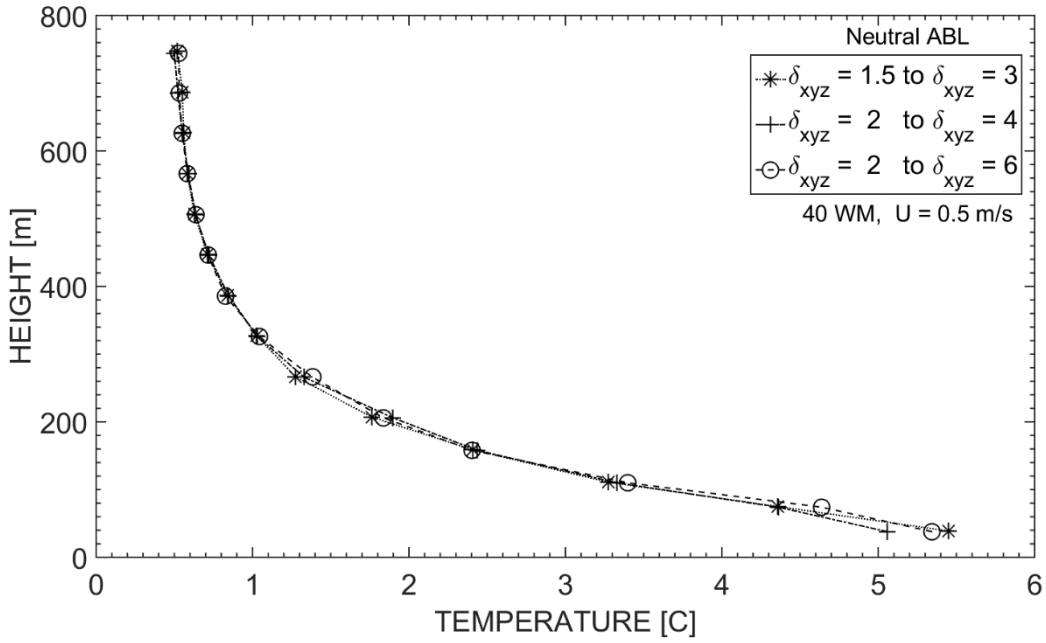

Figure 26 - Results from sensitivity of 40 MW fires in a neutral atmosphere with 0.5 m/s wind. Temperature is excess plume temperature, the temperature above ambient

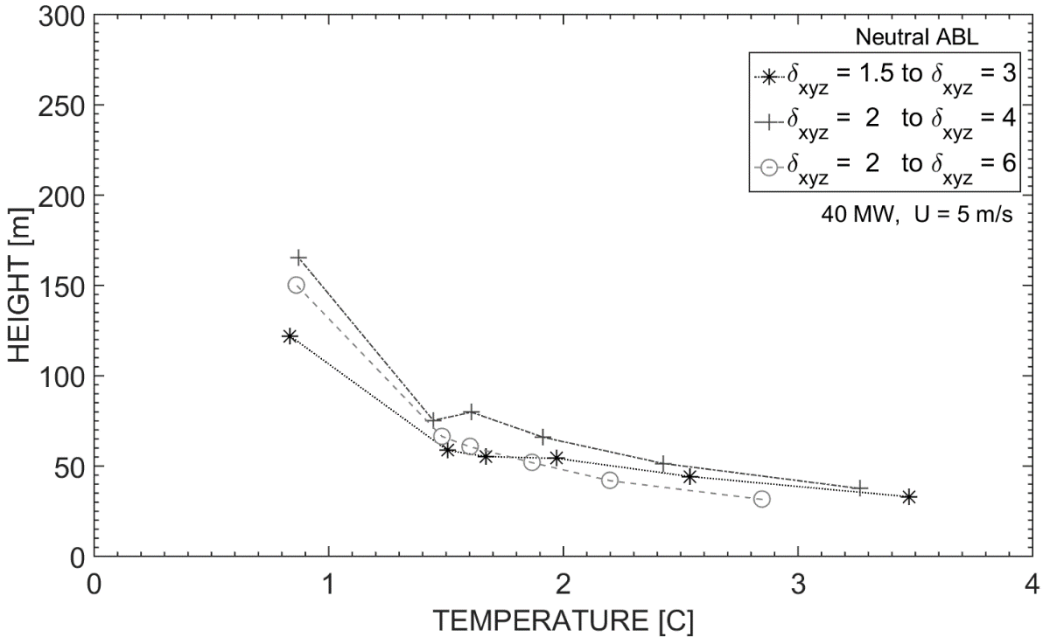

Figure 27 - Results from sensitivity of 40 MW fires in a neutral atmosphere with 5 m/s wind. Temperature is excess plume temperature, the temperature above ambient.

4.1.3 Concluding on mesh compositions

Considering the results presented in figure 24 to 27 from performed grid analysis, a grid composition has been determined for both the small and large domain. Recall that all cells are squares. The small domain is assigned a grid composition of 1 meter cells in the fire mesh and 4 meters' cells in the adjacent meshes. This is a cell transfer ratio of 16 to 1 which has been seen to be as smooth as smaller ratios. Total number of cells in the small domain is 14'012'000.

For the large mesh the grid composition has been determined to be 2 meters' cells in the fire mesh and 6 meters' cells in adjacent meshes. This corresponds to a cell transfer ratio of 9 to 1. This ratio has also appeared as smooth as transfers at lower ratios. Total number of cells in the large domain is 19'108'800.

4.2 Sensitivity of input parameters

4.2.1 Source conditions

Figure 28 presents mean excess temperature lapse rates for fire plumes originating from sources of different characteristic heat release, $\dot{Q}^*$. Sources correspond to $\dot{Q}^*$ values of 0.84, 2 and 4.75. It can be seen that it is the source with lowest initial momentum that reaches the highest altitude at 334 meters. Remaining sources of $\dot{Q}^*$ equal to 2 and 4.75 reached heights of 273 and 281 meters respectively. Considering the 2 m/s wind it is not expected to find the source of the lowest initial momentum to reach the highest altitude. Especially when all sources are by far buoyancy dominated.

When considering the wind fields of these simulations it is found that the simulation corresponding to $\dot{Q}^*$ = 2 are exposed to a heavier wind field than does $\dot{Q}^*$ =4.75. This might have impacted on the final rise height, resulting in lower heights for the $\dot{Q}^*$ = 2 case. In that case it would appear sources of lower initial momentum reached higher altitudes. Perhaps a part of an explanation could be related to the break-up of the plume. For higher $\dot{Q}^*$ values the initial momentum near the source is greater. A rising parcel with increased momentum should experience increased resistance. This resistance could be involved in an earlier break-up of the thermal plume compared to plumes from lower $\dot{Q}^*$ sources. Eventually causing plumes that have higher initial momentum to break apart and become dispersed at lower heights.

On the contrary, if the $\dot{Q}^*$ value decreases the area of the source increases. Recall that these are all 40 MW fires. If the fire area increases, then classic plume theory suggests that the surface area of the plume through which entrainment takes place also increases. Clearly such an approach leads to increased entrainment and dilution. Hence, fire plumes originating from low $\dot{Q}^*$ sources should reach lower altitudes. However, if the plume is categorized as a lazy plume [6] it might contract a certain distance above the source [4]. Such contraction could perhaps alter the theory on enlarged surface area of the plume.

In general, it is difficult to assess the effect of the source condition. As will be evident throughout the report, the observed differences are likely to be caused by the synthetic eddy modelling. This model applies a random number generator as explained in chapter 3.2.3. It is thought that produced conditions are highly influential on the plume. Rendering the source conditions for the tested range, 0.84 – 4.75, as insensitive parameters.

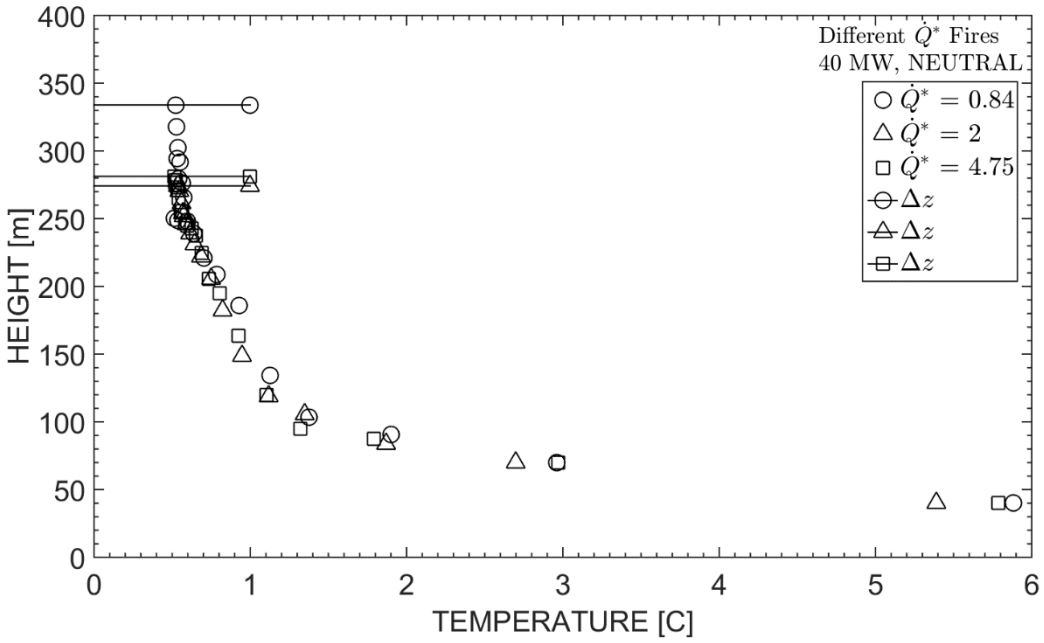

Figure 28 - Mean excess plume temperature, above ambient, as a function of altitude. Figure show results from simulation of different source conditions, $\dot{Q}^*$. Horizontal lines are plotted for convenience indicating height of maximum rise.

4.2.2 Soot yields

Figure 29 presents mean excess temperature lapse rates for fire plumes originating from fires with different soot yields. The curves represent fires of equal HRR, but with a soot production corresponding to 0.01, 0.08 and 0.2 g/g. It can be seen that the plumes with higher soot yields reaches higher altitudes. The fire plume corresponding to a soot fraction of 0.01 reaches a height of 253 meters. Fire plumes of higher yields reaches 274 and 302 meters respectively for yields of 0.08 and 0.2 g/g. Outer limits of the soot yields correspond to 50 meters rise height. It is believed that the synthetic turbulence is the prime cause for observed differences.

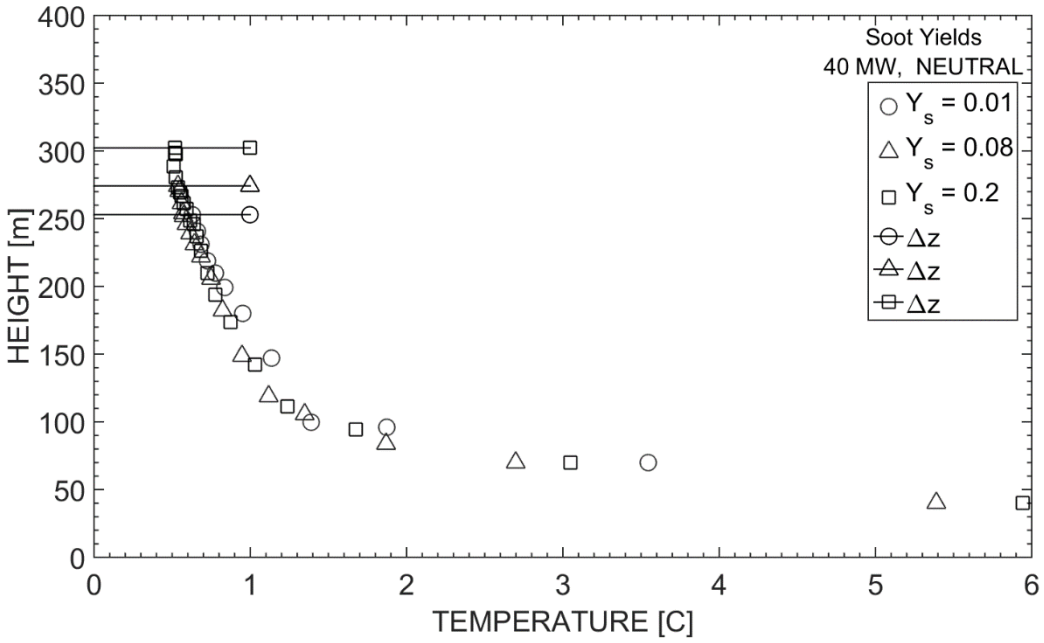

Figure 29 - Mean excess plume temperature, above ambient, as a function of altitude. Figure show results from simulation of different soot yields, Y_s. Horizontal lines are plotted for convenience indicating height of maximum rise.

4.2.3 Atmospheric turbulence length scales

Figure 30 presents mean excess temperature lapse rates for fire plumes rising during conditions of different integral turbulence length scales. Length scales of 500, 800, 1000 and 1100 meters was applied to the 1200 meters high boundary layer. It can be seen that for smaller turbulent scales the fire plume reaches higher altitudes. Final rise height was 319, 307, 274 and 265 meters respectively for the 500, 800, 1000 and 1100 meters cases. Greatest difference can be seen between the 500 meters and 1100 meters case, where it is about 54 meters. The results are consistent with theory presented in chapter on *Neutral conditions*. Large length scale eddies are capable of pushing the entire plume towards lower altitudes. When the wind fields are given attention, this is further supported. It is the 500 and 800 meters cases that experience the most gusts of winds, and still they rise higher.

Further, in chapter 2.1.6 the Reynolds number was presented in equation 2.10. If consideration is made to the turbulent Reynolds number. Then, a reduction in the length scale for constant velocity fluctuations results in reduced turbulence. Assuming that external conditions affect the entrainment, then reduced length scales should result in higher final rise height. Consistent with simulations.

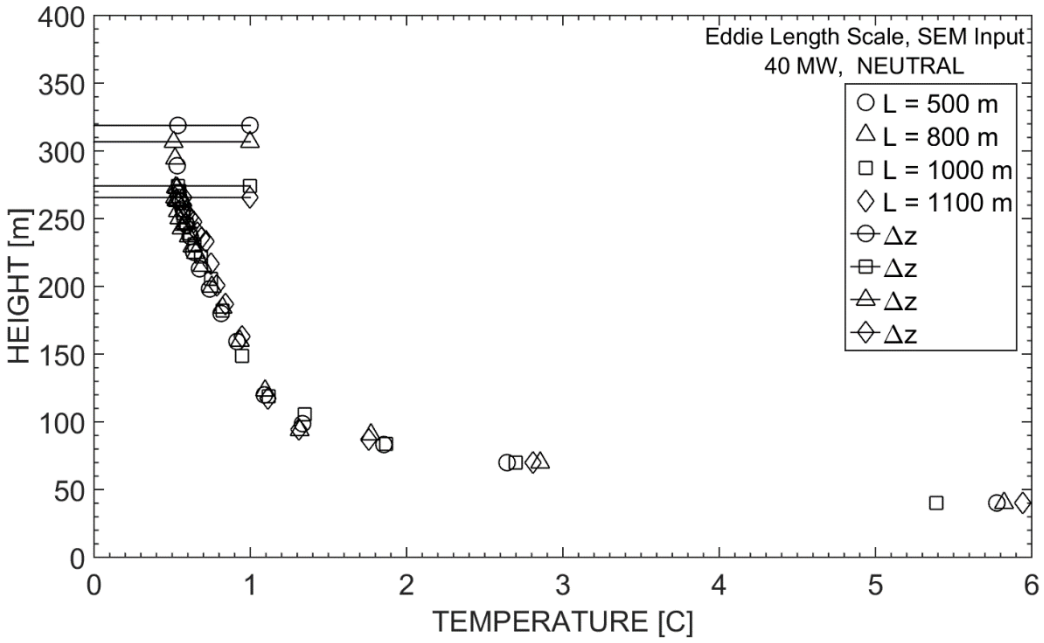

Figure 30 - Mean excess plume temperature, above ambient, as a function of altitude. Figure show results from simulation of plume rise during conditions of different atmospheric turbulence length scale. These scales are applied as input to the synthetic eddy modelling. Horizontal lines are plotted for convenience indicating height of maximum rise.

4.2.4 Number of eddies, N

Figure 31 presents mean excess temperature lapse rates for fire plumes rising at the presence of a different number of eddies, see chapter on *Synthetic eddy modelling*. Simulations with 1'000, 10'000 and 100'000 eddies were performed in order to evaluate the effect of velocity fluctuation intermittency on the final rise height. As can be seen there is no apparent tendency with regards to final rise heights. It is t

he case with N = 10'000 that reach the highest altitude at 311 meters. The two remaining cases of N = 1'000 and N = 100'00 reach heights of 281 and 273 respectively. It appears that the simulation is rather insensitive to the number of eddies. This is not surprisingly. It is the largest eddies that will affect the plume trajectory the most. This was partly evident through the above consideration of the eddy length scales in figure 30. A number of 1'000 eddies appears then to enough for a consistent number of large scale structures. The fact that the velocity signal may experience some intermittency for these low values of N does not become apparent on the results. It appears that a number of 1'000 eddies manage the same results as N = 100'000. Occurring deviation on the N = 10'000 case is ascribed different wind conditions.

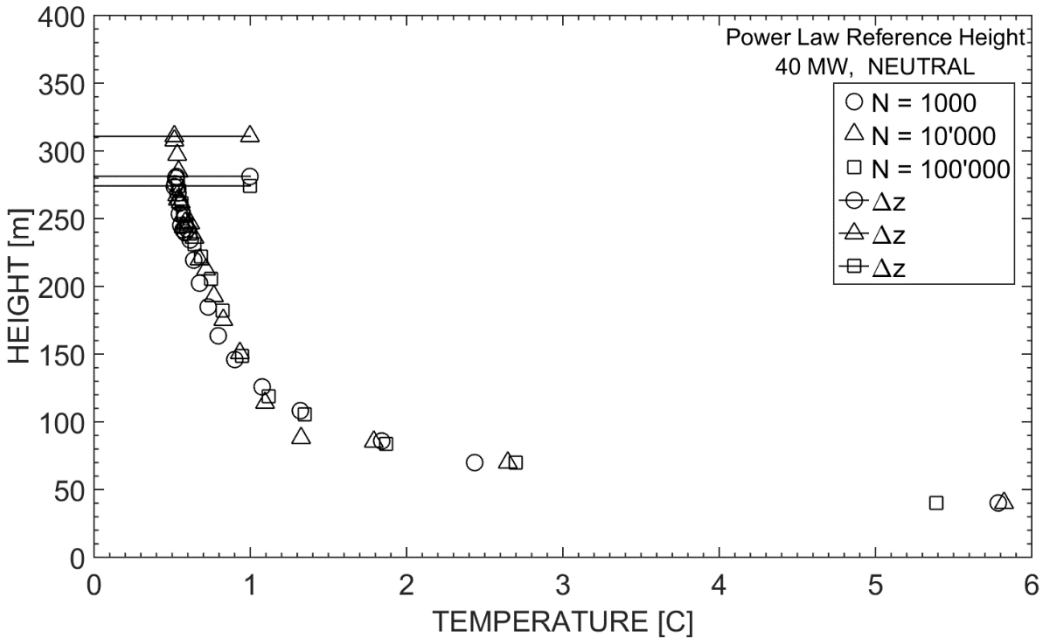

Figure 31 - Mean excess plume temperature, above ambient, as a function of altitude. The figure show result from simulations of plume rise with different numbers of eddies in the synthetic eddy box. This parameter is an input to the synthetic eddy modelling. Horizontal lines are plotted for convenience indicating height of maximum rise.

4.2.5 Power law exponent

Figure 32 presents mean excess temperature lapse rates for fire plumes rising during power law profiles of different exponents. Exponents of 0.1, 0.2 and 0.3 were used in the simulations. For higher values of the exponent the wind increases faster with height. Thus, exposing the fire plume for greater wind speeds at lower altitudes compared to lower values of the exponent. It can be seen from the figure that the curve representing the highest exponent reach lower altitudes compared to the others. For the plume exposed to winds with a power law profile of 0.3 the final rise height was 221 meters. Exponents of 0.1 and 0.2 reached 274 meters and 299 meters respectively. This is not consistent with expectations. It was thought that lower exponents should have plumes reaching farther heights. However, when consideration is taken to the occurring winds, it is found that the two situations that are most alike are the cases of 0.1 and 0.3. The simulation with exponent of 0.2 experiences somewhat different conditions. If comparison is made between the two extremities of 0.1 and 0.3, a difference of 53 meters is seen. Here, with the 0.1 exponent case reaching farther up into the atmosphere due to lower winds during the rise.

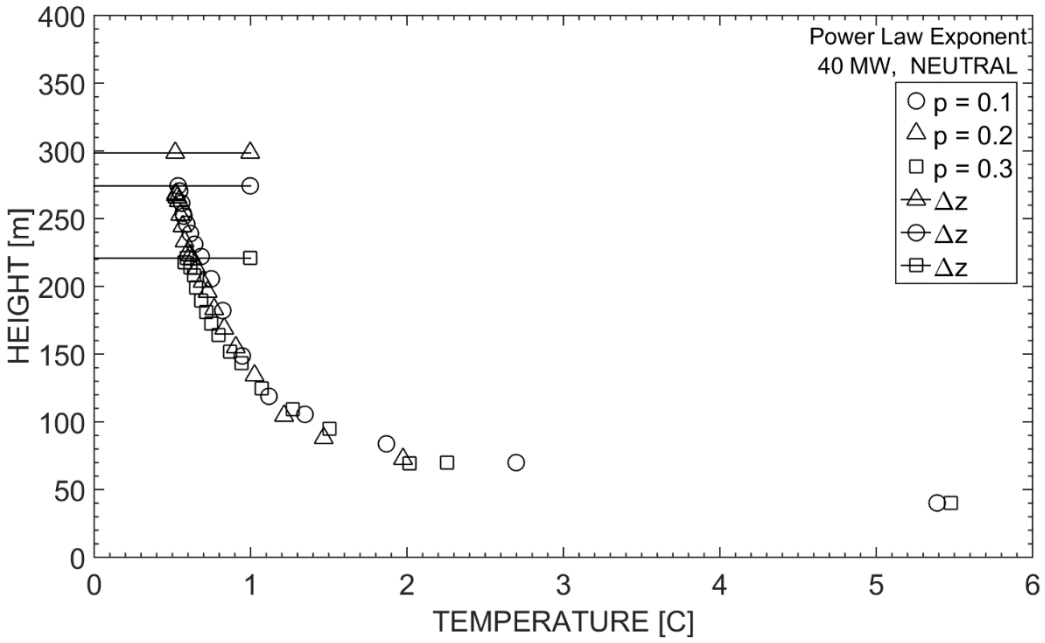

Figure 32 - Mean excess plume temperature, above ambient, as a function of altitude. The figure show result from simulations of plume rise during wind profiles of different exponents. This parameter is an input to the applied power law profile. Horizontal lines are plotted for convenience indicating height of maximum rise.

4.2.6 Power law reference height

Figure 33 presents mean excess temperature lapse rates for fire plumes rising during power law profiles of different reference heights. Heights of 5, 10, 20 and 30 meters was applied to the simulations. The reference height affects the wind profile by changing the altitude at which the profile should reach its reference velocity. If the reference velocity is constant an increase to the reference height results in lower wind speeds. It is evident through the curves in figure 33 that increasing the reference heights results in increased final rise heights. Results show a final rise height corresponding to 309 and 311 meters respectively for the cases of 20 and 30 meters reference heights. For reference heights of 5 and 10 meters the final rise height is seen to coincide at 273 meters. Results are consistent with theory. When the plume rises through regions of lower wind speeds it reaches higher altitudes

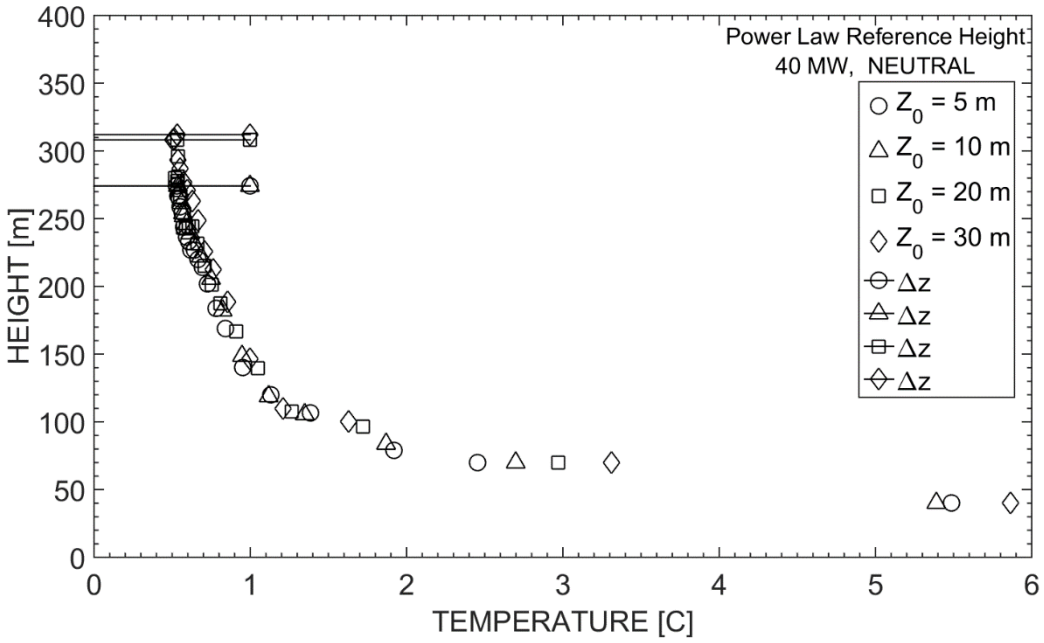

Figure 33 - Mean excess plume temperature, above ambient, as a function of altitude. The figure show result from simulations of plume rise during wind profiles with different reference heights. This parameter is an input to the applied power law profile. Horizontal lines are plotted for convenience indicating height of maximum rise.

4.2.7 Concluding on sensitivity studies

In general, it appears difficult to assess results from the sensitivity study as the synthetic eddy modelling appears highly influential. Clearly, many variables are rendered insensitive as the synthetic eddy modelling appears to dominate the flow. As the turbulence model applies a random number generator to induce turbulence, simulations are never equal. It appears that except for variables that influence the wind field, the final rise height near randomly floats in between 250 and 325. Possibly, this is only the result of the synthetic eddy modelling and does not necessarily reflect the effect of the different variables.

5 COMPARISON WITH PLUME RISE EQUATIONS

This chapter compares FDS results with common plume rise formulas. Applied equations are presented in the chapter *Plume* . These are empirical and analytical solutions to final rise height. Note that the formulas were initially intended for stack plumes. A somewhat different approach is therfore needed for application to fires.

Figure 34 to 39- presents common plume rise equations, dashed lines, and FDS simualtion, solid lines. Plots show final rise height as a function of wind speeds and heat release rates. Note that the FDS results represents the thermal plume. It is known that the thermal plume for the 5 m/s case is transported far downwind. This plume enters regions where the wind profile is seen to have lost some of its characteristic shape. It is the poor wall modelling that cause for these effects, see chapter 3.2.7. Therefore, there are some uncertainty related to the simulation results of the 5 m/s cases.

Figure 34 presents neutral conditions 5 MW heat release. Clearly, the FDS solution appear among the bulk of the plume rise equations. It can be seen to follow the same development except from the 5 m/s case. This case appear among the variety of solutions from the plume equations. However, it deviates from the development of the bulk which it initially followed. It can be seen that the lower wind speed cases are somewhat lower than the plume rise equations.

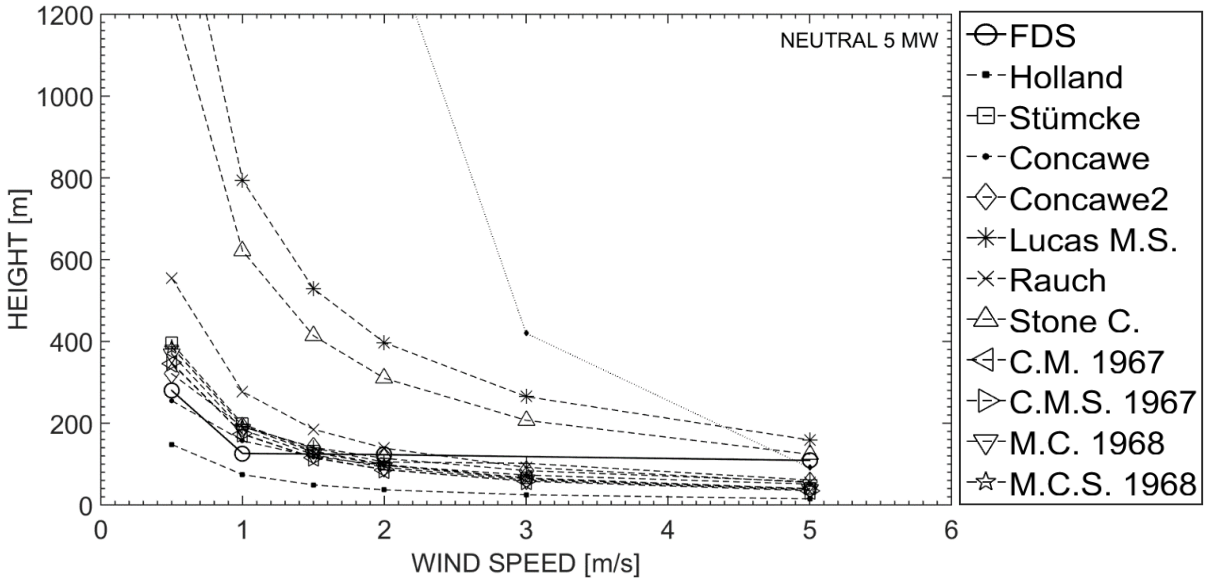

Figure 34 – Presenting comparison of FDS and common plume rise equations for a neutral atmosphere and 5 MW fire. FDS results are presented as a solid line, while plume rise equations are dashed lines.

Figure 35 presents results for the same cases as figure 34. However, the plume rise equations has been corrected based on the work of Carson and Moses [56]. A wider spread is seen among the plume equations. Clearly, the results of FDS appear to correlate reasonably. The 5 and 2 m/s cases are seen to deviate from the development of th plume rise equations. Notice the wide range of final rise heights at lower wind speeds.

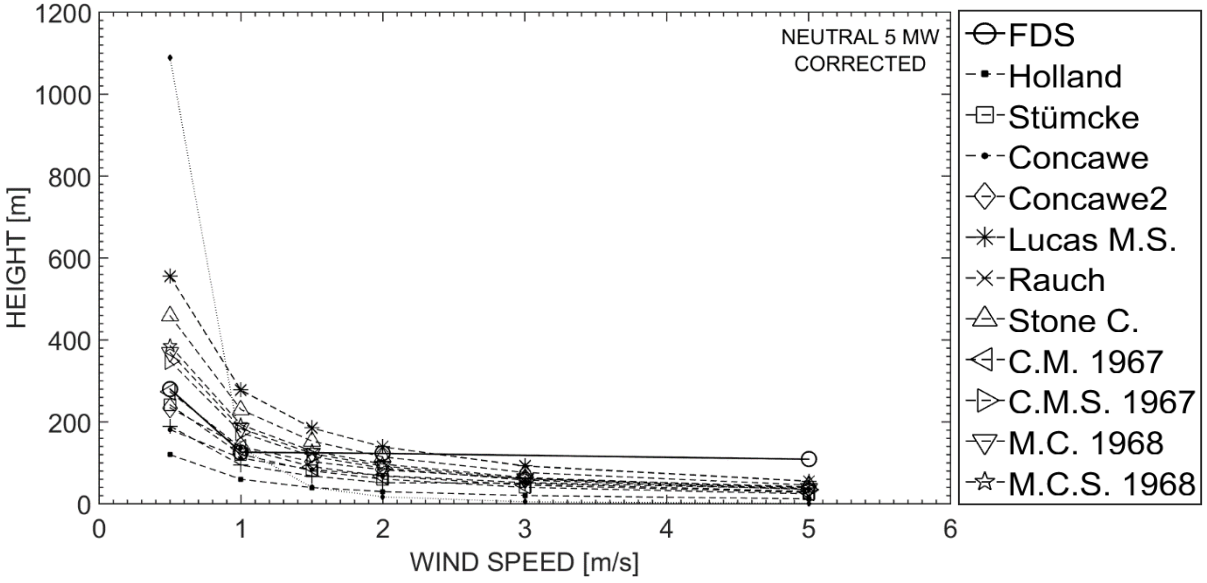

Figure 35 - Presenting comparison of FDS and common plume rise equations for a neutral atmosphere and 5 MW fire. These are the corrected equations by Moses and Carson [56]. FDS results are presented as a solid line, while plume rise equations are dashed lines.

Figure 36 presents final rise heights during 40 MW heat release. Obviously, the FDS solution corresponds nicely to the plume equations at 0.5, 2 and 2 m/s wind. Again, it is the 5 m/s case that deviates from the slope seen by the plume rise equations. The 5 m/s case remains within the range of solutions at this velocity.

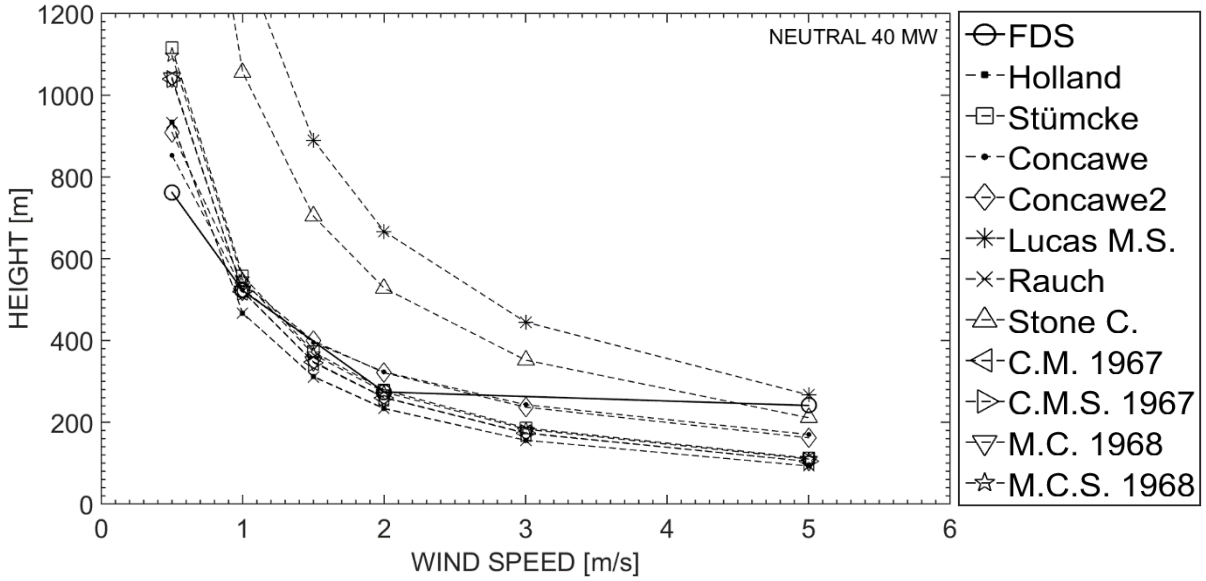

Figure 36 - Presenting comparison of FDS and common plume rise equations for a neutral atmosphere and 40 MW fire. FDS results are presented as a solid line, while plume rise equations are dashed lines.

Figure 37 presents final rise heights during 40 MW conditions. Plume equations have been corrected by the suggested factors of Carson and Moses [56]. Results show that FDS still have a general good agreement.

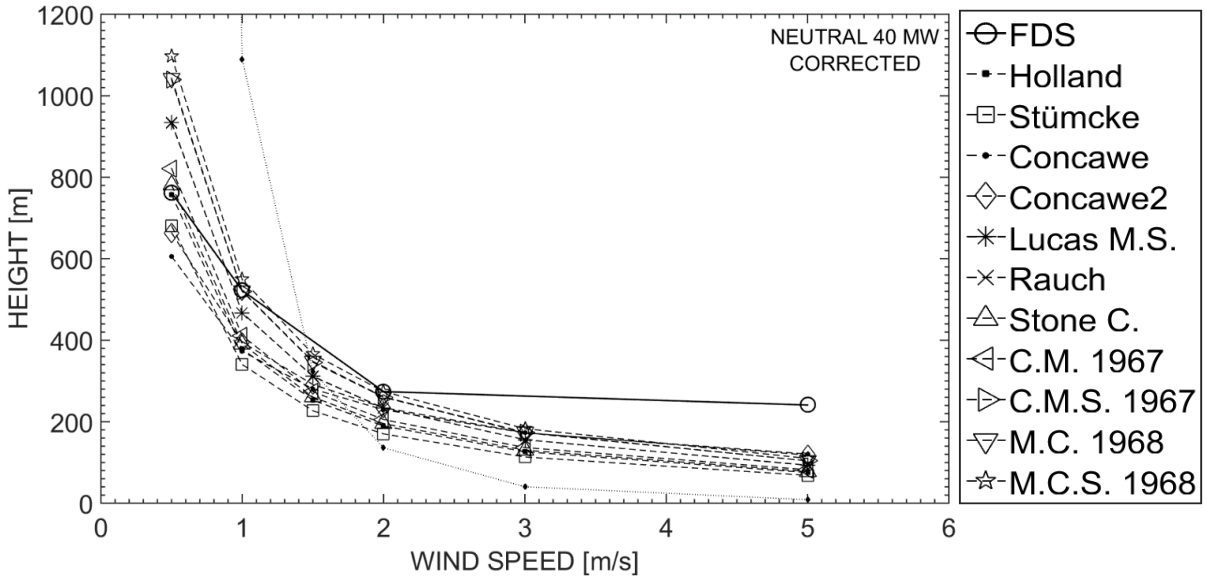

Figure 37 - Presenting comparison of FDS and common plume rise equations for a neutral atmosphere and 40 MW fire. These are the corrected equations of Moses and Carson [56]. FDS results are presented as a solid line, while plume rise equations are dashed lines.

Figure 38 presents results from a 5 MW fire during stable conditions. Results can be seen to correlate well.

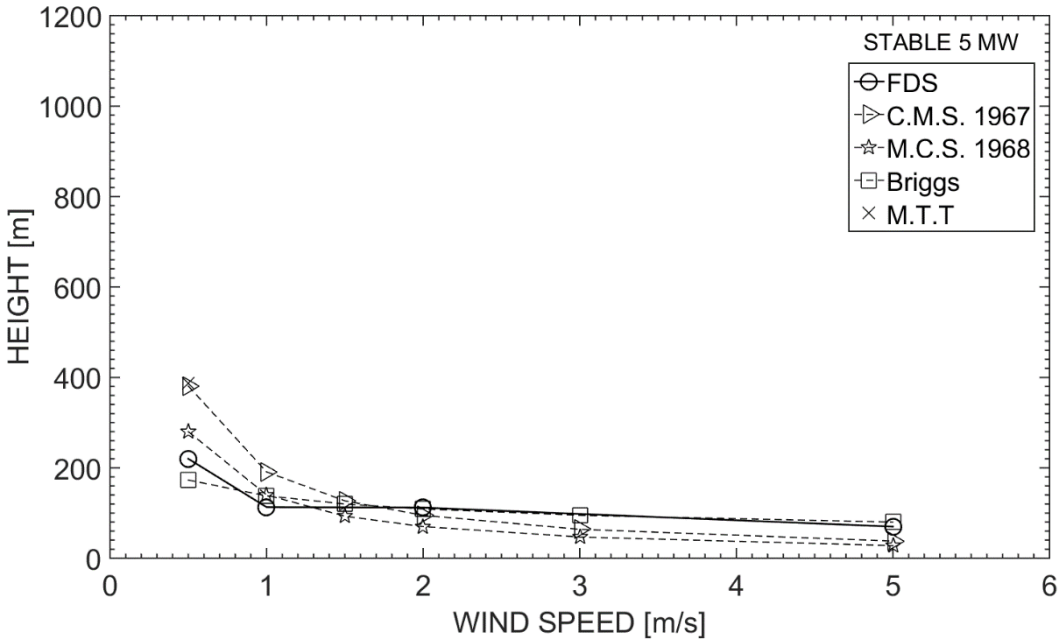

Figure 38 - Presenting comparison of FDS and common plume rise equations for a stable atmosphere and 5 MW fire. FDS results are presented as a solid line, while plume rise equations are dashed lines.

Figure 39 presents results from 40 MW simulations during stable conditions. As for the 5 MW stable case relatively good consitency is found.

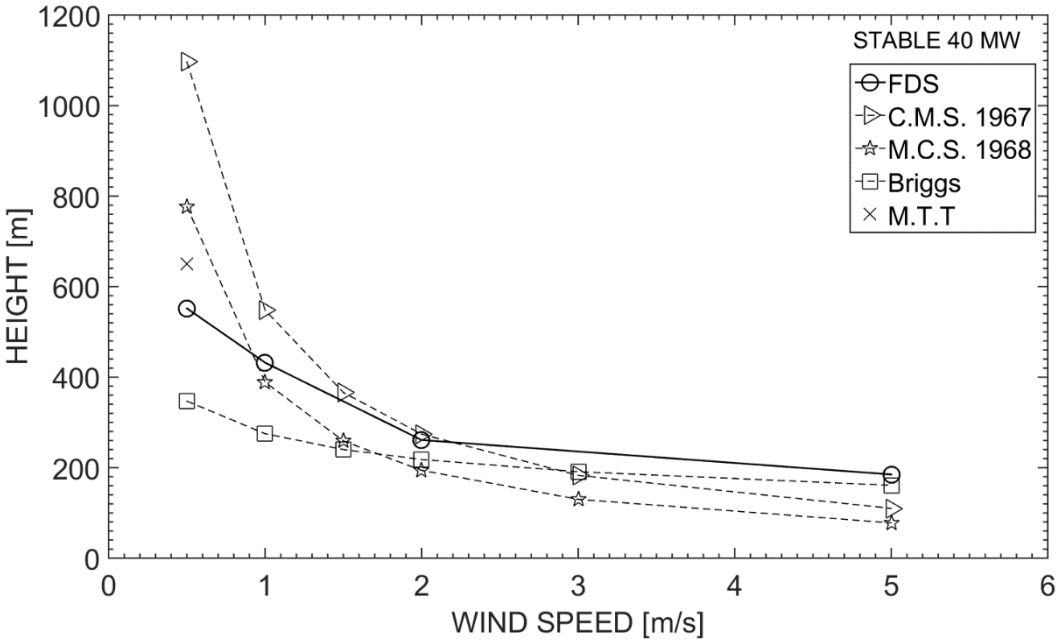

Figure 39 - Presenting comparison of FDS and common plume rise equations for a neutral atmosphere and 5 MW fire. FDS results are presented as a solid line, while plume rise equations are dashed lines.

5.1 Consideration of comparisons

Clearly, good agreement was seen for the cases 0.5, 1 and 2 m/s winds. However, the 5 m/s winds are seen to over predict the final rise height compared to the plume rise equations. In general, the comparison has strengthened the reliability of the results. Simulations of 0.5, 1 and 2 m/s winds are considered to be good approximations. The 5 m/s case is less reliable as predictions and comparisons indicate this solution to deviate from the common plume equations. Even though, the 5 m/s case will be included for completeness.

6 PLUME LAPSE RATES

The following figures 40 to 45 presents plume lapse rates of excess temperature. The x-axis shows smoke plume temperature above the ambient, in degrees Celsius. The y-axis shows height above ground level in meters. The origin represents ambient temperature at ground level.

The lapse rates are presented in two types of constant axis frames. This is done to allow for direct comparison of results. The two different types of frames represent the two different sizes of boundary layers used. The 5 MW cases were simulated within a smaller atmospheric section, with lower boundary layer height, length and width. While the 20- and 40 MW cases were simulated within a boundary layer of greater dimensions. Consequently, the conditions are not equal. However, it is the development of the plume lapse rates during different conditions that is interesting.

The individual plots show the development of plume lapse rates for equal heat release rates with alternating wind speeds. Although the technique for measuring the average thermal plume temperature can vary, the spacing of the measurements is near constant. A rough interpretation between neighbouring markers is a 40 metre jump along the theoretical plume centreline. Further, the vertical and horizontal spacing between the markers indicate how fast the height and mean temperatures are changing.

Depending on the peak heat release rate the different plots may be observed to start at different heights. This is done to avoid measurements within any region of flames. The curves are plotted from this height until the temperature criteria is no longer fulfilled. The lapse rates are thus only defined for heights above the mean flame height, L, and below heights, H, of plume temperature less than 0.5℃ above ambient, $D_{\Gamma_p} = \langle L, H(\bar{T})], \bar{T} \geq 0.5$. The last plotted marker for a specific wind speed, therefore represents the last measured height at which the temperature criteria was fulfilled. This height represents the final rise height of the thermal plume. Limited plume rise is thought to exist

beyond this height, see chapter on *General Description of Plume in Quiescent Stratified Environment* and *Thermal plume criteria.*

The figures present plume temperature lapse rates for 5, 20 and 40 MW cases during conditions of 0.5, 1.0, 2.0 and 5 m/s winds. Each plot represents either stable or neutral environmental lapse rates. Recall, that a lapse rate is the change of a variable with height. Upcoming plume lapse rates are for excess temperature.

6.1 Neutral atmosphere

Figure 40 show plume lapse rates for a neutral atmosphere and 5 MW heat release rates. It can be seen that the curves takes on the shape of a power function. The 0.5 m/s wind curve is seen to loose temperature rapidly with height to about 70 meters altitude. At this point it appears to be an increase in the curves slope, corresponding to a decreasing rate of change in excess temperature with height. Hence, the lapse rate decreases. The lapse rate reduces even further at a height of 180 meters, where the temperature becomes almost constant with height. The final rise height of the thermal plume is observed at about 285 meters.

The curve representing the 1 m/s wind case, triangle, appears to develop in between curves of higher and lower wind speeds. The curve show similar rapid decrease in excess temperature as for the neutral 0.5 m/s wind case. However, it can be observed that at the height of 70 meters two markers appear to be plotted at nearly the same height, but with a temperature difference of 0.7 degrees Celsius. This is due to the plot being discontinuous at this point. It is caused by the different approaches when calculating the mean plume temperature. The calculation of the mean thermal plume temperature is performed by use of either vertical or horizontal slices, see chapter *General description on calculation of plume temperature lapse rate*. When the different approaches are brought together at a height depending on wind speed, plume momentum and buoyancy, such discontinuity could occur for the worst of cases. Though, it is not as evident in the other plots. This error decreases with the distance from the point of discontinuity in both directions. In general, the error has disappeared at neighboring markers.

The final rise height of the thermal plumes at 1, 2 and 5 m/s wind speeds can be seen to merge at nearly the same heights. The 1 m/s wind case is the highest of the three, at about 125 meters. Closely followed by the 2 m/s wind case at about 122 meters and 5 m/s wind case at 110 meters.

Clearly the lapse rates for the 5 MW fire change much faster for the high wind speed cases compared to the low case of 0.5 m/s wind. Note that the curves appear similar in shape even though the wind speeds change.

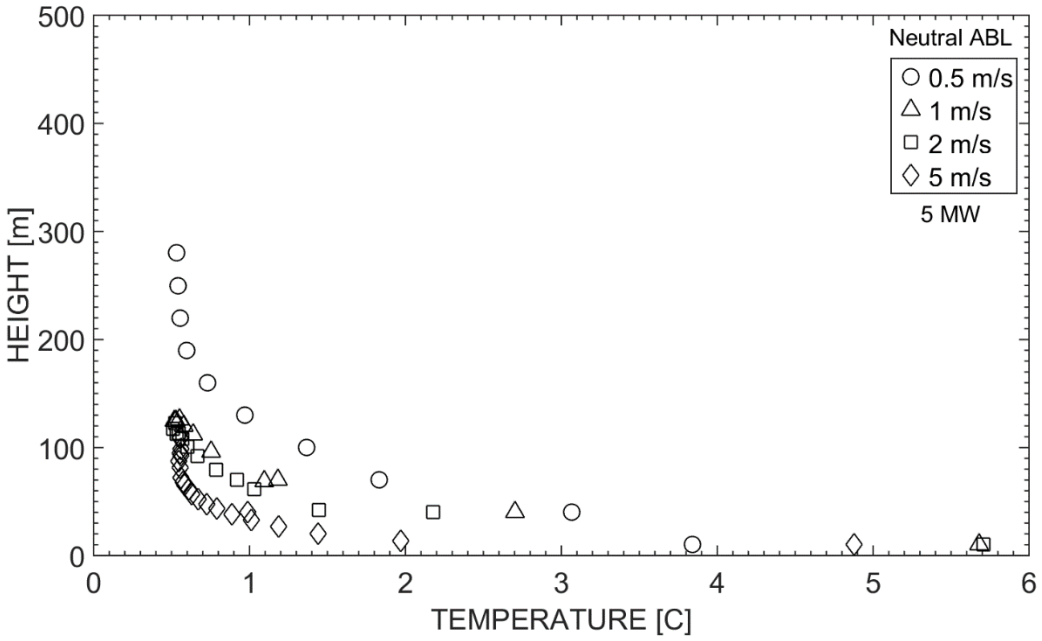

Figure 40 - Plume lapse rates of excess temperature at corresponding height within the atmosphere. All curves represent a 5 MW fire and neutral conditions. Wind speeds are represented by the curves. Curves cease at about $0.5\,℃$ above the ambient temperature at that height. This is in accordance with applied criteria. The highest occurring marker for a curve represents the final rise height of the thermal plume.

Figure 41 appears similar as the 5 MW cases with regards to lapse rate development. The differing distance between spacing of the markers is attributed to the scales on the y-axis, recall that the 5 MW case is simulated in a smaller atmospheric segment. When comparing the curves from the two figures the heat release rate has significant impact on the final rise height. This is no surprise as it is of major importance to the buoyancy flux, the driving force of the rising plume. Curves in figure 41 have 4 times the heat release rate as the curves in the plot from figure 40. Comparing the case of 0.5 m/s winds, a difference in final thermal plume height is observed to near 300 meters. This si a near doubling, and appears to be the case for the final heights of the thermal plumes in all the curves.

Notice the very dense plots of the 5 m/s curves. Occurring markers are very close. This indicates that the rise of the thermal plume is greatly reduced. However, the thermal plume is still present for considerably downwind distances. Recall that each marker can roughly be interpreted as a 40 meter jump along the trajectory of the plume. Plumes rising in 5 m/s winds are greatly bent over and so

each marker closely represents a 40 meters downwind transport. Hence, the thermal plume is transported great distances downwind but plume rise appears to be prevented by ambient winds.

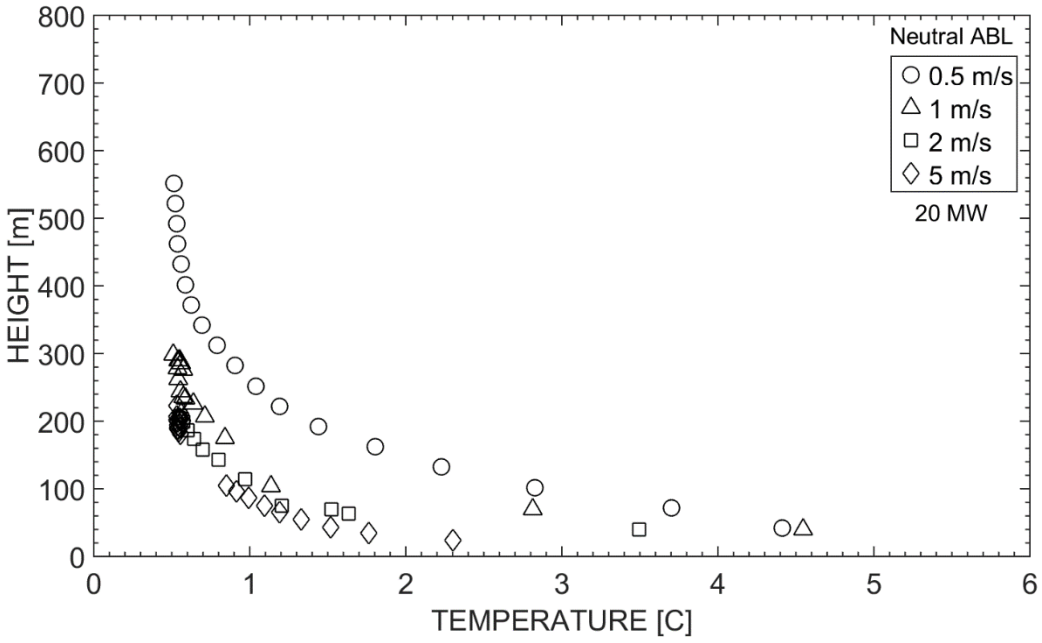

Figure 41 - Plume lapse rates of excess temperature at corresponding height within the atmosphere. All curves represent a 20 MW fire and neutral conditions. Wind speeds are represented by the curves. Curves cease at about 0.5 ℃ above the ambient temperature at that height. This is in accordance with applied criteria. The highest occurring marker for a curve represents the final rise height of the thermal plume.

Figure 42 shows plume lapse rates from a 40 MW fire during neutral conditions for different wind speeds. For all curves it is observed a rapid rate of change in the plume lapse rates for the lower regions of the atmosphere. For the cases of 0.5 and 1 m/s wind speeds the lapse rates trail off and becomes almost constant with height. For these cases, the plume rises during conditions of near constant lapse rates. The case of 1 m/s wind rises about 200 meters from 350 meters height to 550 meters height, with the temperature changing only about 0.1 degree Celsius. For the 0.5 m/s case the plume rises about 400 meters with the temperature changing only from 0.87 degrees at 400 meters to just above 0.5 degrees at almost 800 meters at the final rise height. The near constant temperature rise is not the case for the higher wind speeds. Both the 2 m/s and 5 m/s cases appear to reach their final heights at 274 and 211 meters respectively, without such near-isothermal rise. Obviously this is related to the ambient turbulence, which is discussed further in chapters below.

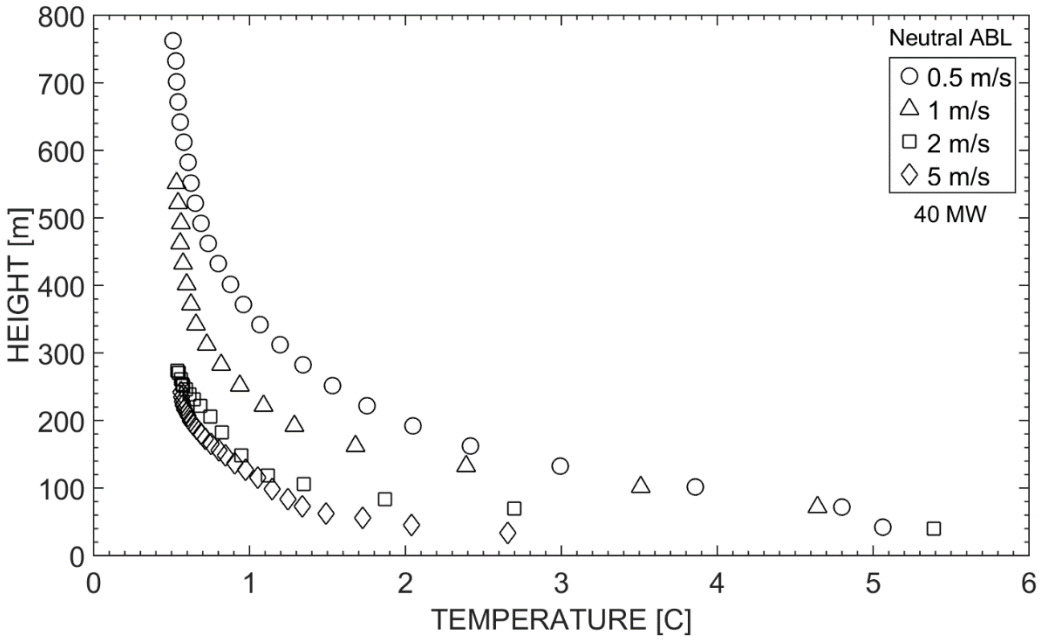

Figure 42 - Plume lapse rates of excess temperature at corresponding height within the atmosphere. All curves represent a 40 MW fire and neutral conditions. Wind speeds are represented by the curves. Curves cease at about 0.5 ℃ above the ambient temperature at that height. This is in accordance with applied criteria. The highest occurring marker for a curve represents the final rise height of the thermal plume.

6.1.1 Initial rise and shape

Evidently for all the curves shown in the figures 40 -42, the temperature is seen to decrease substantially in the lower regions. This is due to the large instabilities and temperature differences that are present here. The fire induces turbulence as energy is released and hot gases rises, entraining ambient air, diluting and cooling the thermal plume. From turbulence theory it is known that for increasing mean flow velocity, the eddy velocity increases. As the domain remains unchanged the fire induced entrainment must be at its greatest in the low regions of high temperature differences. Clearly, these are the regions of high plume velocities. Consequently, the thermal plume temperature reduces substantially in the lower regions of plume rise. Such decrease would further explain the power function shape of the thermal plume lapse rate. As vertical plume velocities decreases due to entrainment, the entrainment itself decreases as it depends on the temperature difference. Hence, the lapse rates decreases rapidly when temperatures become low, and are therefore seen to rise.

Furthermore the shape of the curves and differences between heat releases could be explained through classical plume theory. According to this theory the temperature scales on the heat release rate to the power of 2/3, which corresponds to increasing temperatures with increasing heat release.

Clearly increased heat release should result in higher altitudes being reached by the thermal plume. Rearranging the classical equations result in velocity to scale on the square root of the centerline temperature. This relationship indicates that the velocity of the plume decreases faster when temperatures are low. Hence, entrainment decreases faster. Such correlations could explain the changing slope of the lapse rate.

6.1.2 Final rise heights

Clearly all the plots for higher wind velocities results in lower final rise heights for the thermal plume. Only the curves representing 0.5 m/s winds and 1 m/s for the 40 MW case is seen to rise at nearly constant temperatures. As already mentioned these large differences in the development of the thermal plume can partly be ascribed the ambient external conditions. At low altitudes the wind speeds are less than aloft due to surface drag, but depending on the vertical momentum flux it quickly increases with height. The power law exponent chosen in these simulations represents a high vertical momentum flux and so wind speeds increases rapidly with height in the lower regions. The increasing wind speeds are causing for increased turbulence intensity, and could result in the break–up of the thermal plume at high winds. Consequently, the small excess temperatures that could increase final rise during low wind conditions quickly becomes dispersed and diluted. Hence the plume rise is limited by the ambient conditions.

In general, is the criteria set at 0.5 degrees Celsius above ambient that cause the curves to be cut off at respective heights. The development of the higher wind speed curves beyond this criterion could be equal to the lower wind speed cases. However, the plume break-up, suggest that a near constant temperature rise for the higher wind speeds are unlikely to occur. The fact that the plume envelope will stay intact during high wind speeds and low temperature differences seems unlikely. It would be a paradox to the assumption of Hoult, stating that ambient turbulence can be ignored as the plume internal turbulence intensity exceeds the atmospheric intensity [54]. During low mean thermal plume temperatures, the temperature distribution within the plume is not assumed to contain very large local differences, and therefore the turbulence intensity within the plume is not considered substantial.

Even though, if attention is given to figure 40 and the case of 5 m/s wind, it is seen that near constant temperature rise is possible even during high wind conditions. Apparently, by considerations of the wind field, this rise is possible as wind conditions are different. Occurring field of wind are randomly generated by the synthetic eddy modelling. Consequently, overall effects of the wind may affect plumes differently. For the case of the high wind in figure 40, the plume never experienced the gusts that impacted the other cases. Hence, it could develop similarly to the lower

wind cases. In general the synthetic eddy modelling is seen to affect results heavily. It makes it challenging to distinguish external and internal effects of plume rise.

6.1.2.1 Critical winds

For the lower wind speeds the differences in final rise height is substantial. Comparing the cases of 0.5 m/s to the cases of 1 m/s, the resulting differences is at its lowest for the 5 MW case at 150 meters. For the cases of 20 and 40 MW, it exceeds 200 meters. Such great differences for relatively small changes in ambient wind velocities imply that small changes to the atmospheric conditions may cause severe changes to the experienced plume conditions. Consequently, a situation involving fire plumes could quickly turn for the worse, with plumes changing radically in an instant. Moreover, the impact of the wind on the final rise height decreases as the wind velocities increases. Even though the increase in wind velocity is greater when going from 2 m/s to 5 m/s wind, compared to going from 0.5 m/s to 1 m/s, the difference in final rise height is far greater when the wind increases in the lower range. This indicates a critical velocity for the final rise height of the thermal plume as it appears to become less dependent upon the velocities.

6.1.3 Thermal plumes during high winds

Note that even though thermal plumes during higher atmospheric winds are seen to disperse rather quickly. It is not as simple as solely ascribing it to plume break-up and the cease of temperature. As was pointed out earlier the higher wind curves was seen to be denser than the lower wind speed curves. This indicated a far downwind transport. Clearly the plume rise is inhibited by the ambient turbulence, but it does not rise and immediately dissolves. It becomes transported downwind while rising very slowly with distance from the source. A reason for the thermal plume to stay intact for such wind conditions so far downstream is due to the bending over. As the plume is transported horizontally entrainment conditions change. It is believed that longitudinal shear becomes the main mechanism for turbulence generation at the plume edge. Intuitively this entrainment is less than transverse as velocity differences should be smaller. This is supported by bent over plume equations where the longitudinal entrainment coefficient is less than transverse coefficients [4]. As the plume initially rises in the vertical, the initially dilution of the plume is substantial as can be seen from all curves and plots during high winds. Keep in mind however, that the comparison performed in chapter *COMPARISON WITH PLUME RISE EQUATIONS* indicated a slight mismatch between empirical equations for the 5 m/s cases. As predicted in advance due to poor wall modelling and gradually loss

of the power law wind profile with downstream distance. The 5 m/s case reaches significant downwind distances and so results could be affected.

The development of the plume lapse rate in general appears quite similar in shape for the different velocities.

6.2 Stable atmosphere

The simulations during stable environmental lapse rates are shown in the figures 43-45. The curve for the 5 MW and 0.5 m/s wind case, figure 43, experiences a rapid change in temperature during its low altitude rise, as is the common denominator for all cases independent of wind speeds, heat release rate or stability. The 5 MW curve, similar to the 5MW curve for neutral conditions, has a changing slope. At about 75 meters' height there is a slight decrease in the lapse rate, before going through a quite constant change for the last parts of its rise. Initially it appears to develop similarly to the neutral case of equal effect, but there is one difference. Contrary to the neutral case which reached a final plume height at 285 meters, the stable case is seen to level off at about 225 meters.

The curves for 1 m/s and 2 m/s winds appears similar to what described for the neutral cases. A small bend in the lapse rate may be ascribed the curves at an elevation of about 50 meters, a small distance below what appeared for the neutral condition. The final rise height is almost equal. Regarding the 5 m/s wind case it seems to experience a lower final rise height during stable conditions. The excess temperature quite linearly decays until it settles at a final height at about 60 meters, 50 meters lower than for the equal case during neutral conditions. Clearly the stable conditions have a reduced final rise height for the thermal plume, as expected. For stable conditions the environmental temperature decreases with height at a lower rate than the adiabatic rate. Causing the plume to rise into gradually warmer regions. Further, air entrained along the way does not have the same potential temperature as air aloft. Causing the buoyancy flux to reduce, relative to the ambient, as the entrained air are denser than air aloft.

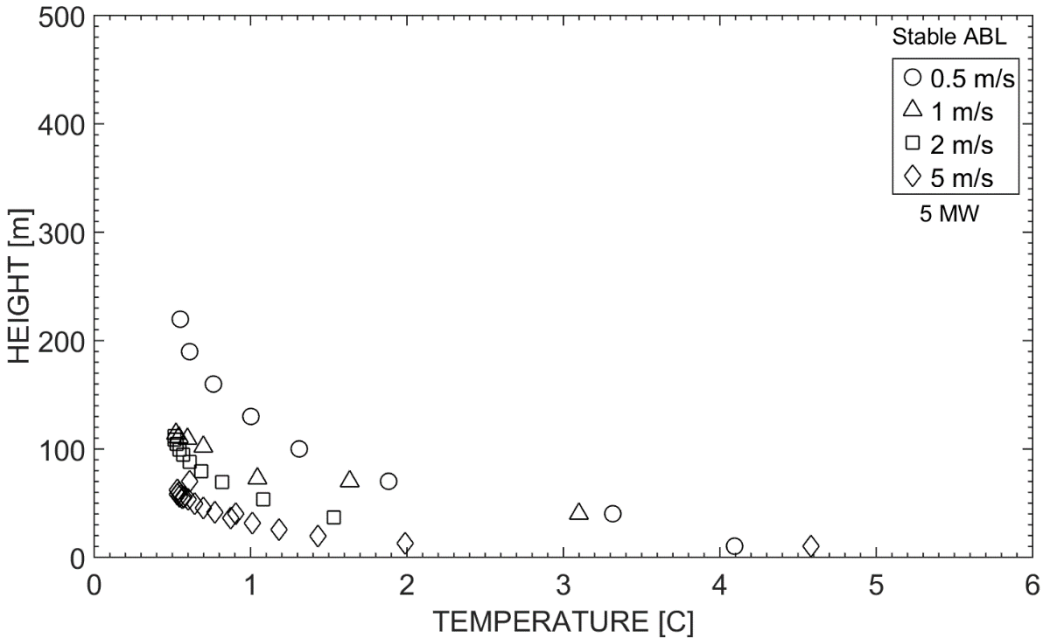

Figure 43 - Plume lapse rates of excess temperature at corresponding height within the atmosphere. All curves represent a 5 MW fire and stable conditions. Wind speeds are represented by the curves. Curves cease at about $0.5\,℃$ above the ambient temperature at that height. This is in accordance with applied criteria. The highest occurring marker for a curve represents the final rise height of the thermal plume.

Considering figure 44 it is seen that the lapse rate represented by the 0.5 m/s curve does not undergo the same distinct changes in the slope. It rises with nearly constant temperature dilution before the lapse rates gets significantly reduced at a height of 250 meters. It then continues to rise during constant lapse rate until final rise height is reached at 450 meters. The final rise height for the similar neutral case was 565 meters.

When considering the curves representing the remaining wind speeds, the lapse rate also appears different from the neutral conditions. The lapse rate appears quite linear in the lower regions, temperature is decreasing at what seems to be a constant rate. The final rise heights however is not too different. The stable cases of 1 m/s and 2 m/s settles at 250 and 180 meters height, respectively, compared to the neutral case where the heights were 300 and 200 meters. For the last curve of the stable 20 MW plot, the 5 m/s wind case, similar behavior is seen as for the other plume lapse rates during stable conditions.

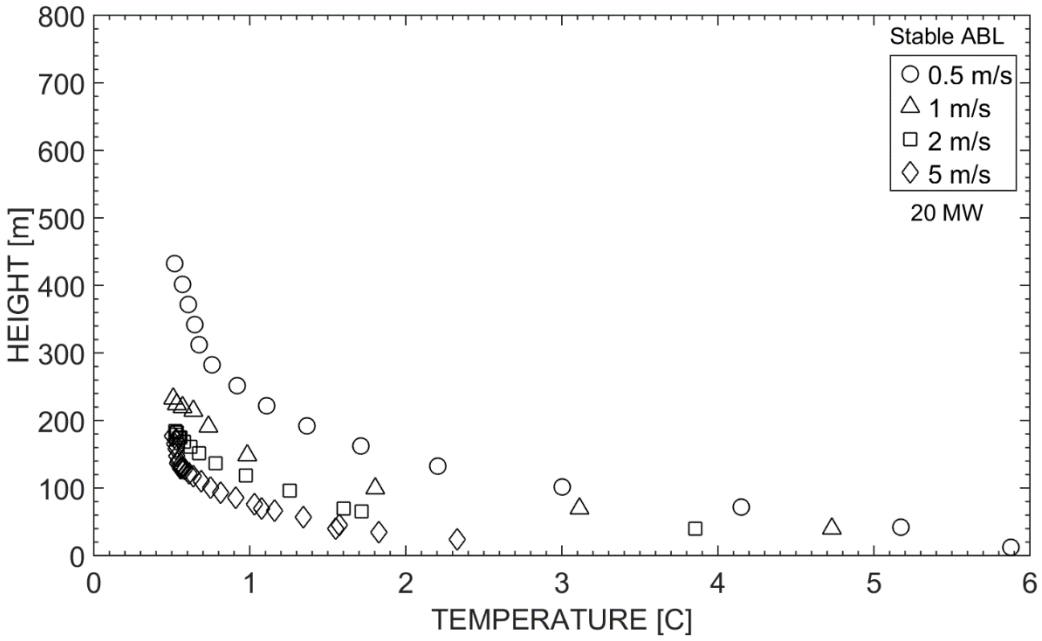

Figure 44 - Plume lapse rates of excess temperature at corresponding height within the atmosphere. All curves represent a 20 MW fire and stable conditions. Wind speeds are represented by the curves. Curves cease at about 0.5 ℃ above the ambient temperature at that height. This is in accordance with applied criteria. The highest occurring marker for a curve represents the final rise height of the thermal plume.

Considering figure 45, the plume lapse rates develop similar to what observed for the other stable cases of 5 and 20 MW. The 40 MW fire plumes reach higher altitudes, as can be seen for the lapse rate given by the 1 m/s curve. A final rise height of 450 meters is reached compared to 250 and 115 meters for the stable 1 m/s wind cases of 20 MW and 5 MW respectively.

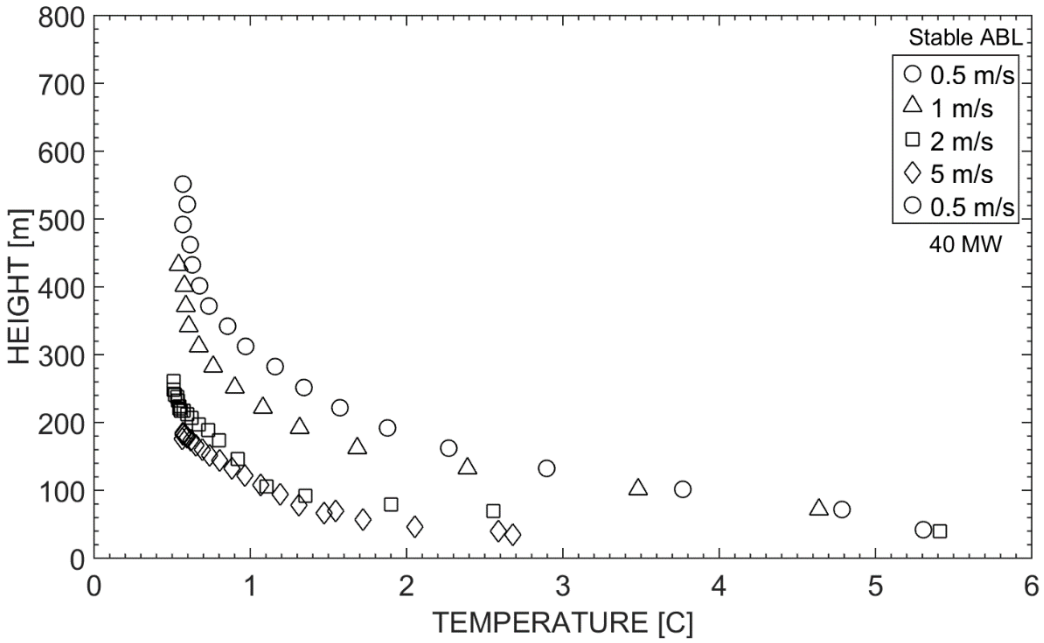

Figure 45 - Plume lapse rates of excess temperature at corresponding height within the atmosphere. All curves represent a 40 MW fire and stable conditions. Wind speeds are represented by the curves. Curves cease at about $0.5\,℃$ above the ambient temperature at that height. This is in accordance with applied criteria. The highest occurring marker for a curve represents the final rise height of the thermal plume.

In general, the plume lapse rate during stable conditions decreases significantly at lower altitudes of plume rise. Increasing heat release rate results in increased final rise heights and increased wind velocities reduces the height. In general, the development appears equal to neutral conditions. However, the final rise height of the thermal plume occurs at somewhat lower altitudes. Clearly this is as expected and is consistent with theory. It becomes more evident at lower wind speeds because the external effects of ambient turbulence are almost absent. Causing the final rise height to depend more on stability. Consequently the stable simulations highlight the effect of ambient turbulence with regards to atmospheric temperature stratification. Indicating that stability becomes of less importance as atmospheric winds increases. Further studies is needed on this topic, but it could point towards two different approaches in estimating plume rise; (1) in which final rise height of the thermal plume should be based on a stability and (2) another in which final rise height should be calculated from the mean wind.

7 FIRE PLUME LAPSE RATES IN THE ATMOSPHERE

The upcoming plots given in the figures 46-51 presents plume temperature lapse rates of calculated average temperatures. These plume lapse rates are plotted at their actual calculated temperatures to allow for comparison with the adiabatic- and environmental lapse rates. The x-axis shows temperature in degrees Celsius at a corresponding height, y-axis, within the atmosphere. Depending on which curve that is considered the plots give temperatures with height for different thermal fire plumes, the environment and the theoretical adiabatic rise. The markers constituting the different plume lapse rates are equal to the markers presented in figures 40-45, so that any movement towards a neighboring point can roughly be interpreted as a 40 meter jump along the plume centerline.

Each plot show plume lapse rates for 0.5, 1 and 5 m/s winds divided on plots of effects 5, 20 and 40 MW. The stabilities are neutral or stable. The plots are presented in two different constant axis frames dependent on their respective boundary layer dimensions.

The development of the excess temperature plume lapse rates is commented in chapter 6. This section considers the plume lapse rates compared to the environmental and adiabatic lapse rates. The two latter lapse rates are presented as dashed and continuous lines respectively. Occurring difference between these lines indicate the stability of the atmosphere, as described in chapter 2.1.5.

Recall from previous chapters that the thermal plume will reach its final rise height when it is surrounded by equal density fluid. A typical simplification in plume theory is assuming the smoke to consist of air, which is mostly the case. Hence, the density differences can be considered through temperatures, consequently, lapse rates. If the lapse rate of a thermal plume is known together with the surrounding environmental lapse rate. Then, the final rise height of the thermal plume could be assessed through the intersection between these lapse rates. This intersection corresponds to the altitude where the plume has cooled to temperatures equal to the surrounding ambient fluid.

The figures 46-48 presents the neutral atmospheres. Consequently, in these plots it can be seen that the environmental and adiabatic lapse rates coincide to a high degree. Figures 49-51 have more differing lapse rates. These are stable conditions, the environmental lapse rate is observed less than the adiabatic.

In general, when considering all the plots the different plume lapse rates are observed to coincide surprisingly well with the adiabatic rise for certain intervals of the plume rise. This is especially evident through the lower wind speeds and neutral conditions, as seen in figure 46-48. During these conditions the plume reaches higher altitudes and it becomes clear that the adiabatic rise take place after some distance.

7.1 The adiabatic rise

Results presented in figures 46-51 show surprisingly good agreement between the thermal plume lapse rate and the theoretical adiabatic rate of cooling. Note that it is the slope of the adiabatic curve that is to be compared with the plume lapse rates, not the overlap. Presented lapse rates are seen to cool adiabatically for certain intervals of the rise depending on the wind speed, heat release and stability. It is the lower regions of the rise that appear to clearly deviate from this simplified approach. Clearly this region is shaped by the intense mixing taking place.

Considering the dominating physics in the lower regions leads to the suggestion that adiabatic rise occurs when the change in temperature caused by the change in pressure exceeds the temperature change caused by mixing. This appears to occur some distance above the ground where the thermal plume has cooled sufficiently. This height of transition between mixing and adiabatically cooling will throughout be referred to as the *height of adiabatic cooling.* It is the height at which cooling by pressure changes dominates cooling by entrainment within a rising fire plume.

Figure 46 is seen to follow the previously mentioned power function at lower altitudes. The 0.5 m/s curve is seen to rise adiabatically from a height of about 100 meters to its final rise height of 285 meters. Increasing wind speeds is seen to increase the lower altitude mixing and cooling of the plume, resulting in a shorter height of adiabatic cooling. This is especially evident in figure 48 and 51.

Except from the significant increase on the final rise height of the plume figure 46, 5 MW, is seen to have similar shaped curves as figure 47, 20 MW. Notice is taken on the impact of wind speed on the height of adiabatic cooling. For the 20 MW plot it is seen that the adiabatic rise starts at about 100, 150 and 200 meters respectively for the cases of 5, 1 and 0.5 m/s wind. When comparing to the

height of adiabatic cooling during stable conditions, figure 50, the heights appear unchanged. It would be expected that the stable case would have a lower height compared to the neutral case. This would be consistent with theory as the lower region mixing is considered a function of lower altitude velocities, and hence, temperatures. During stable conditions the environmental lapse rate change less with height than for neutral conditions, bringing the plume and environmental temperatures closer together with height than for neutral conditions. When the plume buoyancy flux is diluted with height, velocities trails off followed by entrainment. Theory therefore suggests the height of adiabatic cooling to decrease with increased static stability. However, the difference in the simulated stabilities is not substantial. Values for the mean atmospheric stability is assigned the stable environmental lapse rate in the performed simulations, recall the atmosphere is stable on average. While the neutral lapse rate value is close to the adiabatic, but approaches the adiabatic lapse rate from below, meaning it is slightly stable. It is the difference between the considered stabilities that will give rise to differences in initial adiabatic rise height. The fact that the thermal plume is diluted so quickly, cause for the different stabilities to impact at low altitudes. If the stabilities are not too unlike, then their difference at low altitudes is not significant and the initial adiabatic rise height appears constant.

Note that the development of the plume lapse rates indicates insignificant heat loss by radiation. Clearly this is supported by the low occurring temperatures.

7.1.1 High wind speeds

Notice from figures 48-51 how the curves for the higher wind speeds appear to cool adiabatically at some point during rise. This is interesting as the lapse rates during high wind speeds are expected to be affected by external entrainment. Seemingly, the greater wind conditions still allow for adiabatic cooling. Perhaps indicating that cooling by external entrainment is not as obvious as expected. Instead, it might be more influential with regards to the break-up of the plume. This would be in conjunction with the assumption of Hoult [54], mentioned earlier. Stating that external conditions can be ignored as long as internal turbulence intensity is greater than external intensity. During these conditions the plume can be thought to dominate its own cooling until ambient turbulence becomes dominant. The plume then breaks apart and is quickly dispersed. However this can only be a part of the cause, as plume temperatures get very low compared to the ambient temperature and would not be consistent with high internal turbulence intensities. Another reason is thought to be the bending of the plume. Which should reduce entrainment, as mentioned earlier. Great uncertainty is related to the results of the high wind speed cases of 5 m/s, as these are beyond downwind distances of reliable wind field simulations. A detailed analysis of these simulations therefore seems unnecessary.

7.2 Final rise height

Clearly, when the curves are used to assess the final rise height of the thermal plume, it can be seen that the final rise height does not correspond to the intersection between the environmental lapse rate and the plume lapse rate. The reason for this is simply the applied criterion. Obviously, it would never allow the plume lapse rate to pass the environmental lapse rate, as it in the best of cases will deviate from the environmental lapse rate by $0.5\,℃$, corresponding to the temperature criteria. However, the general idea, which needs further investigation, is that the plume rise from the height of adiabatic cooling can be approached by the theoretical adiabatic line.

If it is in interest to simulate the actual intersection then consequently the accuracy or approach of the criteria must be improved. Clearly many different approaches are available like coupling to soot concentrations. Soot concentrations has the benefit of not being a part of the general atmosphere.

Curves that do not intersect with the environmental lapse rate are likely to have a potential for further rise at the altitudes at which they cease. Which is consistent with theory, due to momentum.

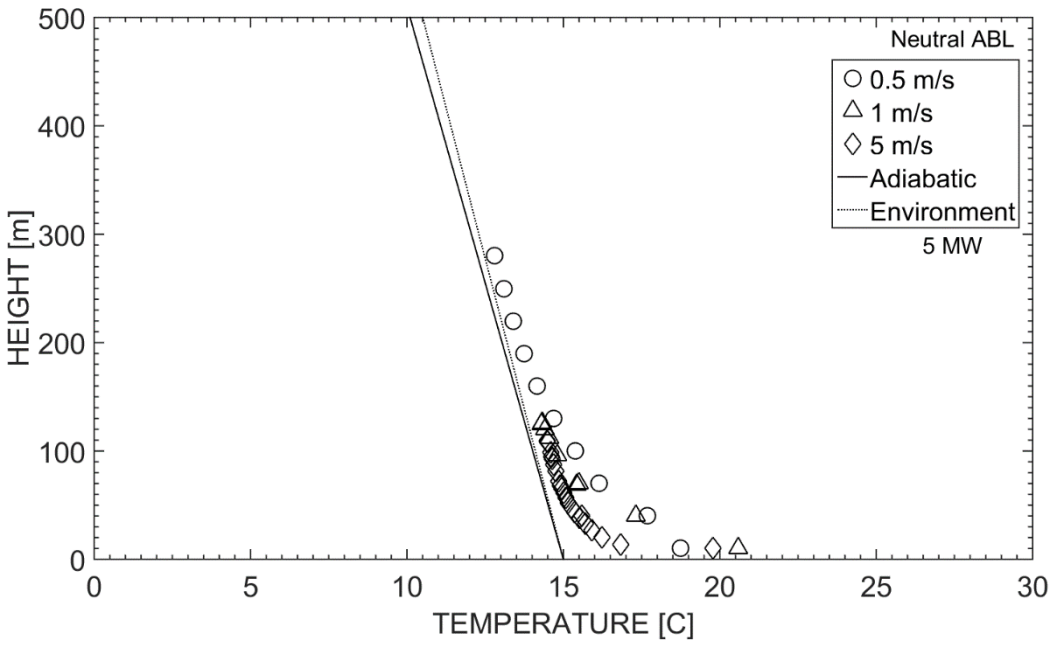

Figure 46 - The figure present the calculated mean plume temperature as a function of height in a neutral atmosphere. Curves in the plot are 5 MW cases. Wind speeds are 0.5 m/s, 1 m/s and 5 m/s. Occurring solid line are the theoretical adiabatic line, indicating the rate of change of an air parcel that cools adiabatically. Dotted lines represent the actual environmental lapse rate.

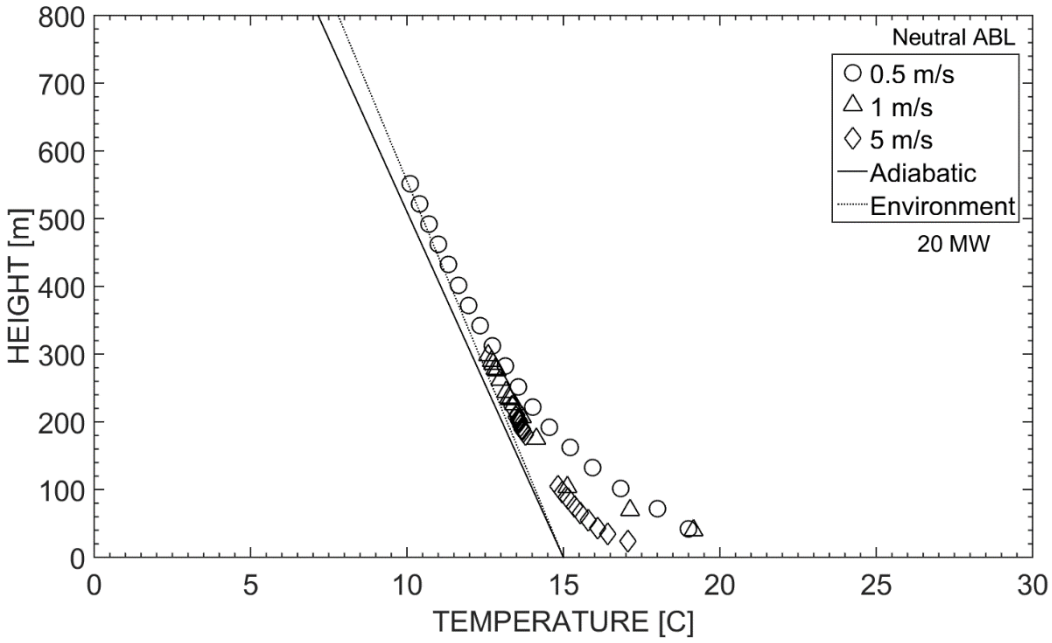

Figure 47 - The figure present the calculated mean plume temperature as a function of height in a neutral atmosphere. Curves in the plot are 20 MW cases. Wind speeds are 0.5 m/s, 1 m/s and 5 m/s. Occurring solid line are the theoretical adiabatic line, indicating the rate of change of an air parcel that cools adiabatically. Dotted lines represent the actual environmental lapse rate.

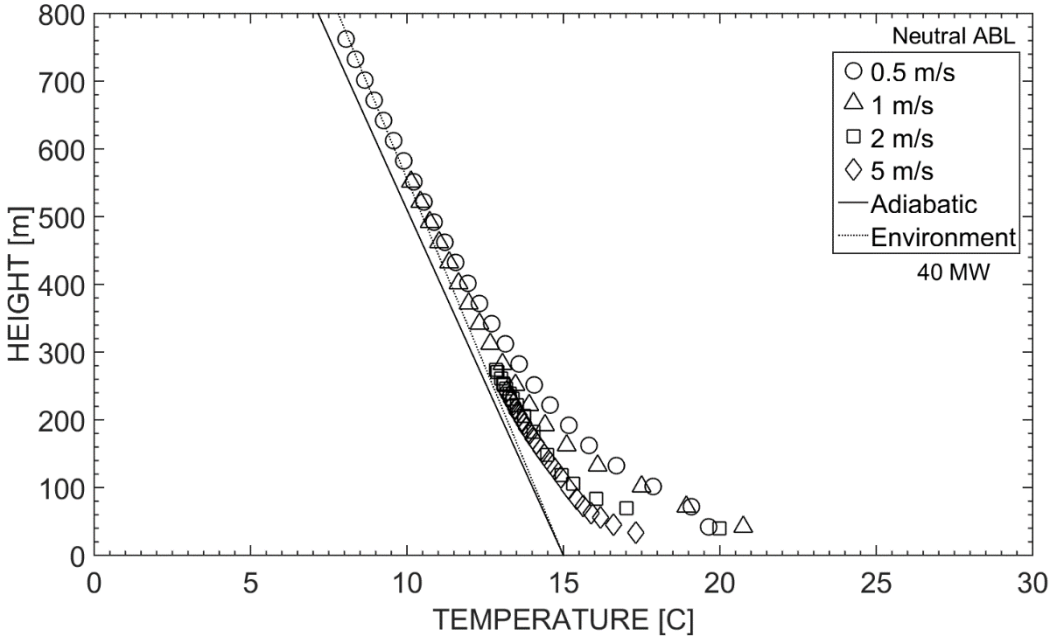

Figure 48 - The figure present the calculated mean plume temperature as a function of height in a neutral atmosphere. Curves in the plot are 40 MW cases. Wind speeds are 0.5 m/s, 1 m/s and 5 m/s. Occurring solid line are the theoretical adiabatic line, indicating the rate of change of an air parcel that cools adiabatically. Dotted lines represent the actual environmental lapse rate.

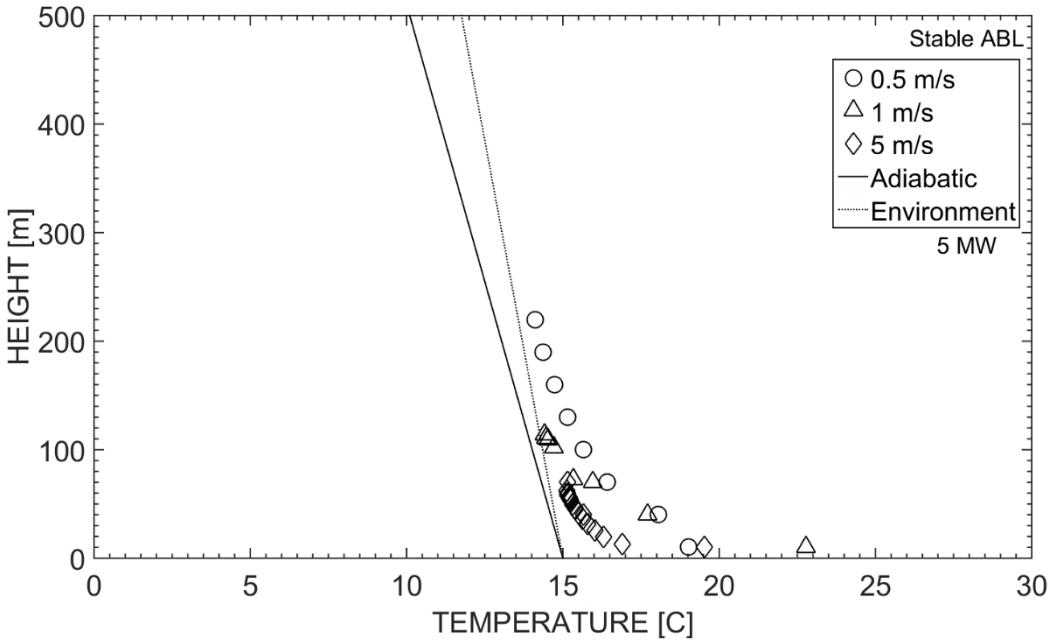

Figure 49 - The figure present the calculated mean plume temperature as a function of height in a stable atmosphere. Curves in the plot are 5 MW cases. Wind speeds are 0.5 m/s, 1 m/s and 5 m/s. Occurring solid line are the theoretical adiabatic line, indicating the rate of change of an air parcel that cools adiabatically. Dotted lines represent the actual environmental lapse rate

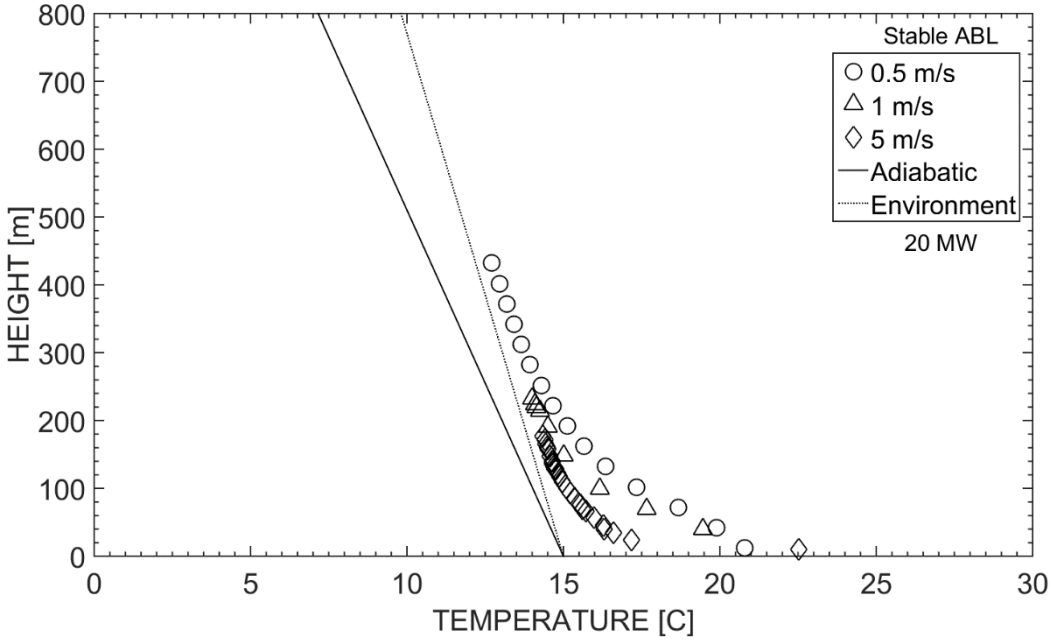

Figure 50 - The figure presents the calculated mean plume temperature as a function of height in a stable atmosphere. Curves in the plot are 20 MW cases. Wind speeds are 0.5 m/s, 1 m/s and 5 m/s. Occurring solid line are the theoretical adiabatic line, indicating the rate of change of an air parcel that cools adiabatically. Dotted lines represent the actual environmental lapse rate

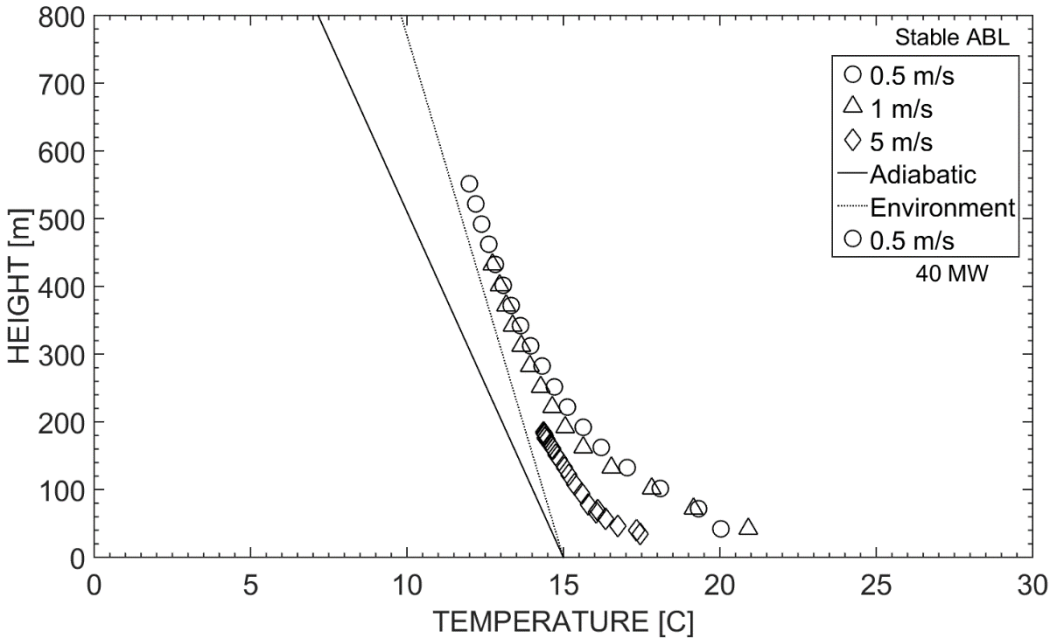

Figure 51 - The figure presents the calculated mean plume temperature as a function of height in a stable atmosphere. Curves in the plot are 40 MW cases. Wind speeds are 0.5 m/s, 1 m/s and 5 m/s. Occurring solid line are the theoretical adiabatic line, indicating the rate of change of an air parcel that cools adiabatically. Dotted lines represent the actual environmental lapse rate

8 CONCLUSION

This thesis has investigated fire plume lapse rates in an environment of synthetic turbulence. A relatively simple method for assessing plume temperatures was developed. Sensitivity studies were then performed to assess input variables. Fire plume lapse rates were considered during equal wind conditions for slight changes in stability. Results of final plume rise height were compared with common plume rise equations as an indication of validity. Fire plume lapse rates were compared with the theoretical adiabatic rate of cooling. The main application of interest is regarded to the description of plume lapse rates, to be used in assessing final rise height of fire plumes.

8.1 Sensitivity studies and synthetic eddy modelling

Results from sensitivity studies turned out difficult to interpret. The synthetic eddy modelling was found to be the prime cause. It applies a random number generator to induce turbulence on the field. Disturbances appeared to greatly overcome the effect of variables such as the characteristic heat release rate. In general, insensitive parameters could not be sufficiently assessed. Occurring differences could not be distinguished from whether they originated from the specific variable or the synthetic eddy modelling. This was mostly variables related to the fire. However, variables related to the wind field could be assessed. Such as increased integral scales, which caused for lower final rise height of the thermal plume. Similar results were found for the decrease of power law reference height or increase of power law exponent. Number of eddies in the synthetic eddy modelling was found to be insignificant above the lower limit of 1000. It was thought to depend on the size of the inlet vent. Rather, it appeared to depend on the length scales. These structures are present in the synthetic eddy model for low values of N. From the work of Jarrin [37] low values are known to affect the intermittency of the velocity signal.

In general, it is found that the synthetic turbulence reduces many of the problems related to fire simulations of smaller scales. As the atmospheric conditions easily dominate insensitive parameters it appears that the fire problem reduces in number of dependent variables. Clearly, the sensitivity analysis indicates the strong influence of atmospheric conditions on plume rise.

It is recommended for future investigations that sensitivity studies are simulated during quiescent environments or by use of precursor simulations. Clearly, these approaches will guarantee equal inlet conditions. Sufficient intervals for calculation of mean values are important

8.2 Fire plume lapse rates

From considerations of plume lapse rates and final rise heights of the thermal plume it was found;

- Increased heat release rates results in increased final rise height of the thermal plume. Less obvious however was that increased heat release rates, for lower wind speeds, resulted in greater distances of constant rate of change in temperature. Increased winds, $\geq 2\ m/s$, were seen to inhibit or reduce these constant changes.
- Wind speeds greatly affect the final rise height and lapse rate development. Final rise height of the thermal plume decreases substantially with increased winds. Of particular importance is the large differences observed when the wind speed increases above the lower range 0.5 m/s – 1 m/s. Rough calculations indicates that changes in the wind speeds above this range, from 2 m/s and above, could reduce the final rise height by 50 %. Obviously, this is problematic with regards to people and environmental safety.
- For a specific heat release it appears that a critical velocity exists. A velocity that renders the fire plume unable to reach higher altitudes. Knowledge on such velocities would be beneficial in the calculation of plume rise.
- The stability was simulated during equal wind conditions. Results were to indicate effect of not being able to accurately determine the stability. Clearly, during low wind speeds the difference in final rise height can become substantial even for relatively small changes in the stability. Interestingly the effect of stability reduces with increasing wind speeds. Consequently, it suggests that plume rise calculations might need to depend on either wind speed or stratification. This could simplify calculations. Further, the critical velocity is the very same velocity as indicated above.
- Bent over plumes appears to be trapped to some degree. Plumes that are bent over are seen to rise very slowly and stay at low altitudes. However, the thermal plume is present for considerable downwind distances. This latter observation indicates that the thermal plume does not break up immediately due to the high occurring winds. It is necessary to highlight that the 5 m/s wind cases are the most uncertain with regards to intact wind profiles.
- Lapse rates are seen to be very similar in shape for the different wind and stability conditions.
- Finally, it appears that descriptions of a plume lapse rate for use in final rise height assessments is possible. Such lapse rates could form a new simple approach in assessing plume rise. An approach allowing for visual interpretations However, far more research is needed. In the end, it must be highlighted that final rise height cannot be pinpointed and that a plume occupies a volume of different concentrations in space.

8.3 Adiabatic rise

Considerations of plume lapse rates during neutral atmospheres indicated adiabatic cooling. Initiation of this cooling occurred at a certain height above ground which was referred to as the *height of adiabatic cooling.* It represents the height at which cooling by pressure changes dominates cooling by entrainment. Stable conditions appeared to cool close to the adiabatic rate. Small differences occurred due to the ambient temperature stratification. Potential temperature is not constant for a stable atmosphere, which affects the buoyancy flux. Adiabatic cooling therefore appears to be limited to within a certain range of environmental lapse rates in the vicinity of the adiabatic rate.

8.4 Simulations and plume rise equations

Validity of performed FDS simulations was strengthened through comparisons with common plume rise equations. The 5 m/s wind simulation was found to be of questionable reliability.

8.5 Future directions

This has been a rather rough approach to a complicated problem. It was in the interest of this thesis to highlight areas in need of further study. Therefore, the conclusion itself contains the elements in need of further investigation

9 References

[1] D. Drysdale, An Inroduction to Fire Dynamics, West sussex: John Wiley & Sons Ltd., 2011.

[2] J. Zhu, M. Y. Chol, G. W. Mulholland, S. L. Manzello, L. A. Gritzo and J. Suo-Antilla, "Measurements of Visible And Near-IR Optical Properies of Soot Produced From Laminar Flames," *Proceedings of the Combustion Institute,* pp. 2367-2374, 2002.

[3] G. A. Briggs, "Plume Rise and Buoyancy Effects," in *Atmospheric Science and Power Production*, Springfield, Virginia, Office of Scientific and Technical Information United States Department of Energy, 1984, pp. 327-366.

[4] A. Tohidi and N. B. Kaye, "Highly Buoyant Bent-over Plumes in a Boundary Layer," Elsevier, Clemson, 2015.

[5] J. Hübner, "Buoyant plumes in a turbulent environment," Wolfson College, 2004.

[6] C. A. N. and S. S. S. Cardoso, "Turbulent Plumes with Internal Generation of Buoyancy by Chemical Reaction," Department of Chemical Engineering and Biotechnology, University of Cambridge, Cambridge.

[7] G. A. Briggs, "Plume Rise Predictions," in *Lectures On Air Pollution And Environmental Impact Analyses*, Boston, Massachusetts, American Meteorological Society, 1975, pp. 59 -.

[8] W. E. Heilman, L. Yongqiang, S. Urbanski, V. Kovalev and R. Mickler, "Wildland fire emissions, carbon, and climate; Plume rise, atmospheric transport, and chemistry processes," Elsevier, 2013.

[9] K. B. McGrattan, H. R. Baum and R. G. Rehm, "Numerical Simulation of Smoke PLumes From Large Oil Fires," Pergamon, Gaithersburg, 1996.

[10] R. Paugam, M. Wooster, S. Freitas and M. V. Martin, "A review of approaches to estimate wildfire plume injection height within large-scale atmospheric transport models," *Atmospheric Chemistry and Physics,* pp. 907-925, 26 January 2016.

[11] R. A. Anthenien, S. D. Tse and A. C. Fernandez-Pello, "On the Trajectories of Embers Initially Elevated Or Lofted By Small Scale Ground Fire Plumes In High Winds," Elsevier, 2006.

[12] B. R. Morton, S. G. Taylor and J. S. Turner, "Turbulent Gravitational Convection From Maintained And Instantaneous sources," JSTOR, 1955.

[13] F. A. Gifford, in *Lectures On Air Pollution And Environmental Impact Analyses*, Boston Massachusetts, American Meteorological Society, 1975.

[14] G. I. Taylor, "Dynamic of a mass of hot gas rising in air," United States Atomic Energy Commission, 1945.

[15] B. Cushman-Roisin, Environmental Fluid Mechanics, Hanover, New Hampshire: John Wiley & Sons Inc., 2014.

[16] X. Zhang and A. F. Ghoniem, "A Computational Model For The Rise And Dispersion Of Wind-Blown Buoyancy-Driven Plumes-I. Neutrally Stratified Atmosphere," *Atmospheric Environment,* pp. 2295-2311, 1993.

[17] S. R. Hanna, G. A. Briggs and R. P. Hosker, jr, Handbook on Atmospheric Diffusion, Technical Information Center U.S Department of Energy, 1982.

[18] D. P. Hoult and J. C. Weil, "Turbulent plume in a laminar cross flow," *Atmospheric Environment,* pp. 513-531, Vol. 6 1972.

[19] C. Hirsch, Numerical Computation of Internal and External Flows, Burlington: Elsevier, 2007.

[20] Z. Xiaodong, "CFD Simulation of Neutral ABL Flows," Technical University of Denmark, Roskilde, 2009.

[21] R. Stull, in *Atmospheric Science: An Introductory Survey*, California, Elsevier, Inc, 2006.

[22] A. Bechmann, "Large-Eddy Simulation of Atmospheric Flow over Complex Terrain," Risø National Laboratory, Roskilde, 2006.

[23] B. Jacob, J. Mann and M. Nielsen, "Introduction to Micro Meteorology for Wind Energy," Technical University of Denmark, Roskilde, 2013.

[24] H. W. Tieleman, "Strong Wind Observations in The Atmospheric Surface Layer," Elsevier, Blacksburg, 2007.

[25] R. Geiger, R. H. Aron and P. Todhunter, The climate near the ground, Lanham: Rowman & Littlefield Publishers, INC, 2003.

[26] J. A. Young, "Static Stability," in *Encyclopedia of Atmospheric Sciences*, 2003.

[27] J. Mudakavi, Principles And Practices of Air Pollution Control And Analysis, New Delhi: I. K. International Publishing House Pvt. Ltd., 2010.

[28] E. J. Finnemore and J. B. Franzini, Fluid Mechanics with Engineering Application, New York: McGraw-Hill, 2002.

[29] American Meteorological Society, "http://glossary.ametsoc.org/wiki/Main_Page," 26 January 2012. [Online]. Available: http://glossary.ametsoc.org/wiki/Lapse_rate. [Accessed 21 March 2017].

[30] MetEd, Comet, "www.meted.ucar.edu/," University Corporation for Atmospheric Research, 2014. [Online]. Available: http://www.meted.ucar.edu/mesoprim/skewt/navmenu.php?tab=3&page=2.5.2&type=flash.. [Accessed 20 march 2017].

[31] MetEd, Comet, "https://www.meted.ucar.edu," University Corporation for Atmospheric Research, 2010. [Online]. Available: https://www.meted.ucar.edu/fire/s290/unit6/print.htm. [Accessed 20 march 2017].

[32] International Civil Aviation Organization, "Manual Of The ICAO Standard Atmosphere," ICAO, Montreal, Canada, 1993.

[33] American Meteorological Society, "http://glossary.ametsoc.org/wiki/Main_Page," 26 January 2012. [Online]. Available: http://glossary.ametsoc.org/wiki/Virtual_potential_temperature. [Accessed 21 March 2017].

[34] American Meteorological Society, "http://glossary.ametsoc.org/wiki/Main_Page," 25 April 2012. [Online]. Available: http://glossary.ametsoc.org/wiki/Equivalent_potential_temperature. [Accessed 21 March 2017].

[35] U. Gaitonde, "Quality Criteria For Large Eddy Simulation," School of MACe Univeristy of Manchester, Manchester, 2008.

[36] J. H. Ferziger and M. Peric, Computational Methods for Fluid Dynamics, New York: Springer-Verlag, 2002.

[37] N. Jarrin, "Synthetic Inflow Boundary Conditions For The Numerical Simulation of Turbulence,"

School of Mechanical, Aerospace and Civil Engineering, The University of Manchester, Manchester, 2008.

[38] I. S. Ertesvåg, Turbulent strøyming og forbrenning, Trondheim: Tapir akademisk forlag Trondheim, 2000.

[39] MetEd, Comet, "www.meted.ucar.edu/," University Corporation for Atmospheric Research, 2015. [Online]. Available: https://www.meted.ucar.edu/dispersion/hysplit_v2/st4.php. [Accessed 27 Januar 2017].

[40] S. E. Larsen, "Lectures in Micro Meteorology," Technical University of Denmark, Roskilde, 2015.

[41] K. Moon, T. J. Duff and K. G. Tolhurst, "Sub-canopy forest winds: understanding wind profiles for fire behaviour simulation," Elsevier, 2016.

[42] F. V. Brock and S. J. Richardson, Meteorological Measurements Systems, New York: Oxford University Press, 2001.

[43] H. Tennekes, "The Logarithmic Wind Profile," Journal Of The Atmospheric Sciences, Pennsylvania, 1972.

[44] J. Erbrink, B. Fisher, S. Finardi, P. Jeannet, S. Joffre, M. Morselli, U. Pechinger, P. Seibert and D. Thomson, "COST Action 710; Harmonisation of the pre-processing of meteorological data for atmospheric dispersion models," Eropean commission, Luxembourg, 1998.

[45] G. Crasto, "Numerical Simulation of the Atmospheric Boundary Layer," Università degli Studi di Cagliari, Cagliari, 2007.

[46] B. Blocken, T. Stathopoulos and J. Carmeliet, "CFD Simulation of The Atmospheric Boundary Layer Wall Function Problems," Elsevier, Eindhoven, Montreal, Leuven, 2007.

[47] N. M. Zoumakis, "The Dependence of The Power-law Exponent on Surface Roughness And Stability in a Neutrally an Stably Stratified Surface Boundary Layer," *Atmósfera 1993 6(1),* pp. 79-83, 1992.

[48] B. Karlsson and J. G. Quintiere, Enclosure Fire Dynamics, CRC Press, 2000.

[49] A. S. Rangwala, "Diffusion Flames," in *SFPE Handbook of Fire Protection Engineering*, Society of Fire Protection Engineers, 2016, pp. 350-372.

[50] L.-G. Bengtsson, Enclosure fires, NRS Tryckeri, Huskvarna, Sweden, 2001.

[51] G. Heskestad, "Fire Plumes, Flame Height and Air Entrainment," in *SFPE Handbook of Fire Protection Engineering*, Society of Fire Protection Engineers, 2016, pp. 396-428.

[52] T. Log and G. Heskestad, "Temperatures of restricted turbulent fire plumes," *Fire Safety Journal,* pp. 101-115, 1997 October 1997.

[53] J. R. Garratt, The atmospheric boundary layer, Cambridge New York: Cambridge university press, 1992.

[54] D. P. Hoult, J. A. Fay and L. J. Forney, "A Theory of Plume Rise Compared with Field Observations," *Journal of the Air Pollution Control Association,* pp. 585-590, 1969.

[55] COMET program, "https://www.meted.ucar.edu/dispersion/basics/index.htm," University Corporation for Atmospheric Research, 2002. [Online]. Available: https://www.meted.ucar.edu/dispersion/basics/print.htm. [Accessed 15 May 2017].

[56] J. E. Carson and H. Moses, "The validity of several plume rise formulas," *Journal of the Air Pollution Control Association,* pp. 862-866, 1969.

[57] A. D. Visscher, Air Dispersion Modelling, New Jersey: Wiley & Sons, 2014.

[58] A. F. Ghoniem, X. Zhang, O. Knio, H. R. Baum and R. G. Rehm, "Dispersion and deposition of smoke plumes generated in massive fires," *Journal of Hazardous Materials,* pp. 275-293, 1993.

[59] C. Hirsch, Numerical Computation Of Internal & External Flows, Oxford: Butterworth-Heinemann, 2007.

[60] K. McGrattan, S. Hostikka, R. McDermott, J. Floyd, C. Weinschenk and K. Overholt, "Fire Dynamics Simulator, User's Guide, Sixth Edition," National Institue of Standards and Technology, Maryland, August 24, 2016.

[61] K. McGrattan, S. Hostikka, R. McDermott, J. Floyd, C. Weinschenk and K. Overholt, "Fire Dynamics Simulator Technical Reference Guide Volume 1: Mathematical Model," National Institute of Standards and Technology, Maryland, August 24, 2016.

[62] M. J. Hurley, "Appendix 2: Thermophysical properties," in *SFPE Handbook of Fire Protection Engineers*, Society of Fire Protection Engineers, 2016, pp. 3425-3436.

[63] A. Lecocq, M. Bertana, B. Truchot and G. Marlair, "Comparison of the Fire Consequences of an Electric Vehicle and an Internal Combustion Engine Vehicle," HAL, 2014.

[64] C. Mayfield and D. Hopkin, "Design Fires for Use in Fire Safety Engineering," bre press, Watford, 2011.

[65] M. J. Hurley, "Appendix A," in *SFPE Handbook of Fire Protection Engineering*, Society of Fire Protection Engineers, 2016, pp. 3397-3424.

[66] T. G. Ma and J. G. Quintiere, "Numerical simulation of axi-symmetric fire plumes: accuracy and limitations," *Fire Safety Journal,* pp. 467-492, 2003.

[67] J. L. Argaín, P. M. A. Miranda and M. A. C. Teixeira, "Estimation of the Friction Velocity in Stably Stratified Boundary-Layer Flows Over Hills," Springer, 2008.

[68] K. McGratta, S. Hostikka, R. McDermott, J. Floyd, C. Weinschenk and K. Overholt, "Fire Dynamics Simulator, User's Guide, Sixth Edition," National Institute of Standards and Technology, Maryland, November 26, 2013.

[69] NASA, "www.nasa.gov," 31 July 2015. [Online]. Available: http://www.nasa.gov/mission_pages/sunearth/science/atmosphere-layers2.html.

[70] M. Schatzmann and A. J. Policastro, "Effects of the Boussinesq Approximation on the Results of Strongly-Buoyant Plume Calculations," Journal of Climate and Applied Meteorology, 1983.

[71] M. B.R., "Forced Plumes," *Journal of Fluid Mechanics,* no. 5, pp. 151-163, 1959.

[72] H. G.R. and N. G. Kaye, "Virtual origin correction for lazy turbulent plumes," *Journal of Fluid Mechanics,* no. 435, pp. 377-396, 2001.

[73] K. McGrattan and S. Miles, "Modelig Enclosure Fires Using Computational Fluid Dynamics," in *SFPE Handbook of fire protection engineering*, Bethesda, National Fire Protection Association, 2008, pp. 3-229 - 3-246.

[74] J. E. Pieterse, "CFD Investigation of the Atmospheric Boundary Layer under Different Thermal Stability Conditions," Stellenbosch Univresity, Stellenbosch, 2013.

[75] B. R. Morton, "Mode," *Symposium on Combustion,* pp. 973-982, 1965.

[76] S. A. G. Gary L. Achtemeier, Y. Liu, F. G. Mendez, Y. Hu and M. T. Odman, "Modelling Smoke

Plume-Rise adn Dispersion from Southern United States Prescribed Burns with Daysmoke," *Atmosphere,* pp. 358-388, 2011.

[77] K. Anderson, A. Pankratz and C. Mooney, "A thermodynamic approach to estimating smoke plume heights," Northern Forestry Centre, 2011.

Appendix A

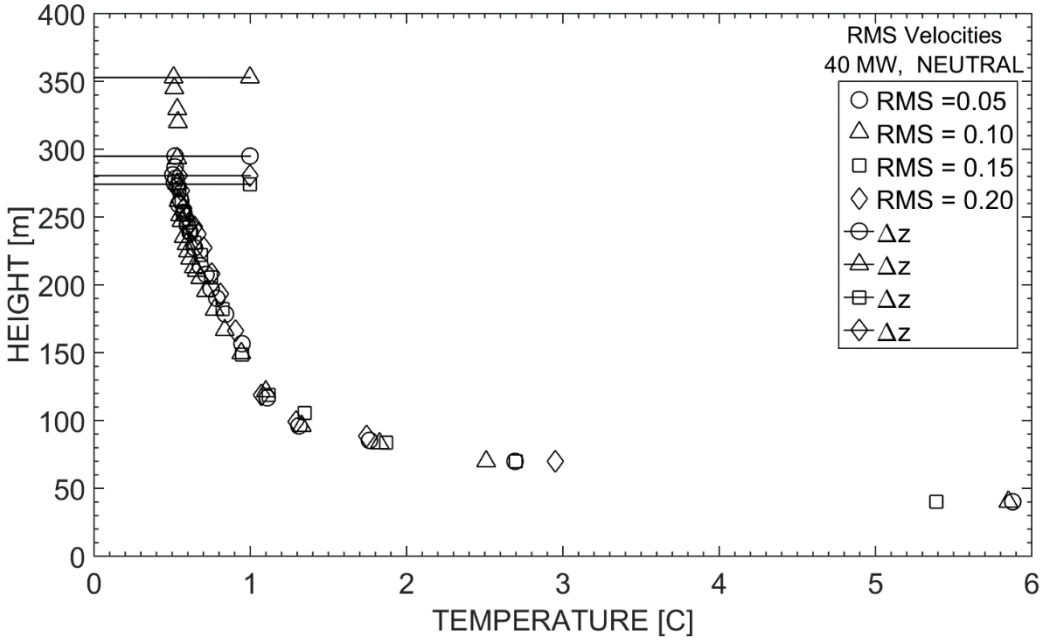
RMS Velocities
40 MW, NEUTRAL
RMS =0.05
RMS = 0.10
RMS = 0.15
RMS = 0.20
Δz
Δz
Δz
Δz
HEIGHT [m]
TEMPERATURE [C]
0
50
100
150
200
250
300
350
400
0
1
2
3
4
5
6

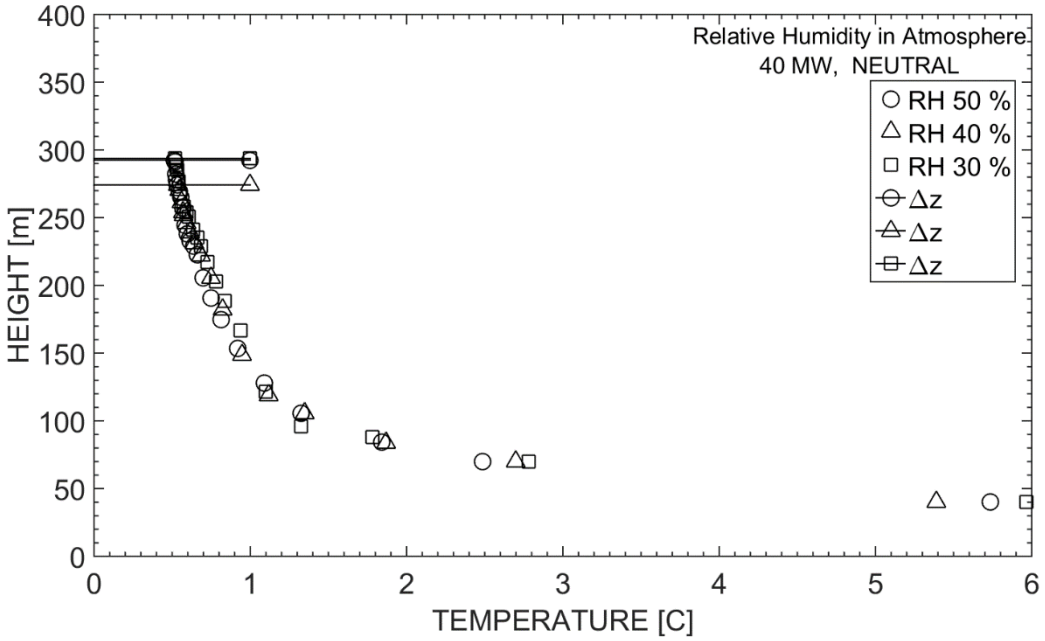
Relative Humidity in Atmosphere
40 MW, NEUTRAL
RH 50 %
RH 40 %
RH 30 %
Δz
Δz
Δz
HEIGHT [m]
TEMPERATURE [C]
0
50
100
150
200
250
300
350
400
0
1
2
3
4
5
6

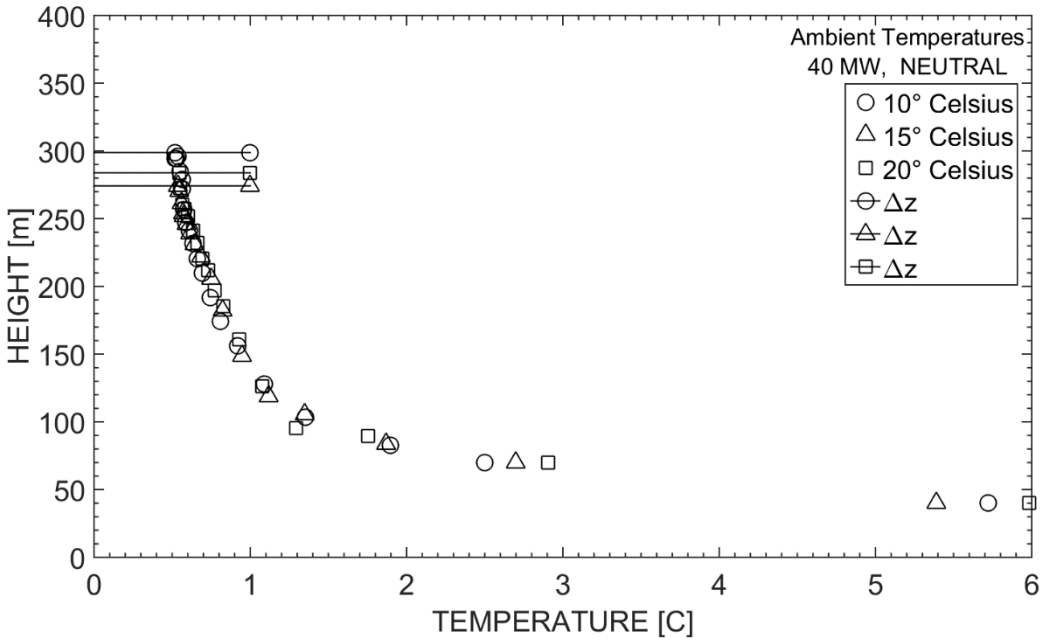
Ambient Temperatures
40 MW, NEUTRAL
10° Celsius
15° Celsius
20° Celsius
Δz
Δz
Δz
HEIGHT [m]
TEMPERATURE [C]
0
50
100
150
200
250
300
350
400
0
1
2
3
4
5
6

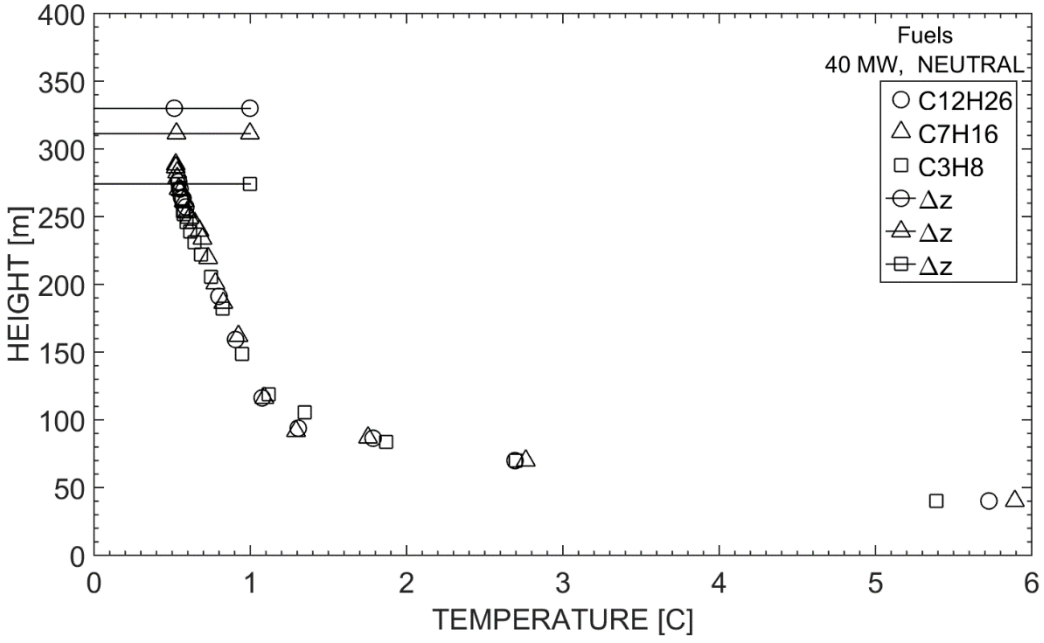
Fuels
40 MW, NEUTRAL
C12H26
C7H16
C3H8
Δz
Δz
Δz
HEIGHT [m]
TEMPERATURE [C]
0
50
100
150
200
250
300
350
400
0
1
2
3
4
5
6

Appendix B

This appendix contains the Matlab scripts required to retrieve a plume lapse rate of temperature. It consists of seven steps.

9.1.1.1 STEP 1

```
%THIS SIMPLE CODE RUNS FDS2ASCII MULTIPLE TIMES AND ENABLES FAST RETRIEVAL
%OF MULTIPLE SLICEFILES FOR USER SPECIFIED PERIODS OF TIME.

%IT IS NOT STRAIGHT FORWARD TO RUN FDS2ASCII FROM MATLAB, AS THE .BAT FILES
%WHICH RUNS FDS2ASCII NEEDS SEPARATE INPUTFILES. THIS SCRIPT THEREFORE
%CREATES .TXT INPUTFILES, BUT DELETES THEM DURING THE RUN. IN TOTAL THE
%SCRIPT CREATES ONE .TXT FILE PER SLICE BUT DELETES ALL TEMPORARY FILES
%INCLUDING THE .BAT COMMAND FILE. THE ONLY RESULT AFTER THIS SCRIPT IS .CSV
%FILES, ONE FILE PER SLICE. REMEBER TO SET YOUR EXCEL SETTINGS TO ENGLISH
%VERSION SO THAT THE .CSV FILES WILL BE AUTOMATICALLY SEPARATED.


%%%%%%%%%%%%%%%%%%%%%%% INPUTS %%%%%%%%%%%%%%%%%%%%%%%%%%%%%

%THE SCRIPTS RETRTRIEVE TWO TYPES OF SLICES. ONE REFERENCE SLICE, AVERAGED
%OVER A SPECIFIED PERIOD OF TIME, T1REF - T2REF, AND ONE MULTIPLE SLICES
%FROM THE PERIOD T1MEAN - T2MEAN. FOR THE LATTER CASE THE AVERAGEING IS
%TAKEN TO BE THE VARIABLE (T1MEAN - T2 MEAN) /DX SO THAT FOR EXAMPLE A
%PERIOD OF 100 SECONDS WITH A DX 0F 10 WOULD PRODUCE 10 SLICES PER SLICE
%GIVEN IN THE INDEX VECTOR. THIS ALLOWS MORE INSTANTANEOUS VALUES.

%GENERAL INFROMATION
index=[46:1:90]; %the indices of the slices that you want exported, THE BIG
DOMAIN HAS VALUES FROM 46 TO 107
CHID='SN153-S402_big_temperature'; %Name of the .smv file that you want
fds2ascii to access

%REFERENCE VALUES
T1REF=5; %Starting time of sample in seconds
T2REF=15; %Ending time of sample in seconds

%INSTANTANEOUS VALUES - MEAN - (REFFERRED TO AS MEAN DUE TO THE ACTUAL USE
OF THE MANY SLICES)
T1MEAN=1400; %Starting time of sample in seconds
T2MEAN=1820; %Ending time of sample in seconds
DX=105;%Number of subslice dividings per interval
N=length(index);%Length of the index vector
%%%%%%%%%%%%%%%%%%%%%%%%%%%%%%%%%%%%%%%%%%%%%%%%%%%%%%%%%%%%%%%%%%%%%%%
%%%%%%%%%%%%%%%%%%%%%%%%%%%%%%%%%%%%%%%%%%%%%%%%%%%%%%%%%%%%%%%%%%%%%%%
%%%%%%%%%%%%%%%%%%%%%%%%%%%%%%%%%%%%%%%%%%%%%%%%%%%%%%%%%%%%%%%%%%%%%%%
%%%%%%%%%%%%%%%%%%%%%%%%%%%%%%%%%%%%%%%%%%%%%%%%%%%%%%%%%%%%%%%%%%%%%%%
```

```
filename='retrieveslices.bat'; %The name of the .command file



%%%%%%%%%%%%%%%%%%REFERENCE SLICES%%%%%%%%%%%%%%%%%%%%%%%%%%%%%%%%%%%%%%%%%%%

      fileID=fopen(filename,'a+');%fopen opens file, but the permission a+
tells fopen to open or create the file for reading and writing, and to
append data to the end of the file.
      fprintf(fileID,'%s\r\n','@echo on');%Write data to text file given by
      %the file identifier, fileID. The formatting operator,%,together with
      %the conversion character, s, is used due to the string array "Echo
on".
      %This text printed in a .bat file allows input text to appear in the
      %command window(as far as I remeber)


for i=1:N %Looping for different indeces

      inputname = ['InputREF' sprintf('%d',i) '.txt'];%Name of temporary
.bat inputfile. sprintf formats data into string. Inputname is a string,
but uses data from the loop to rename the files. The d conversion appearing
after the formatting operator is used for integers, in which "i" is this
integer.
      outputname = ['REFT' sprintf('%d',i) '.csv'];%Name of created .csv
file
      fileID=fopen(filename,'a+');%Opens "filename" with reading and
writing permission, see text further above.
      formatspec='\r\n fds2ascii<%s \r\n';%Allows charactervectors and
formatting operators.\r\n is line change in txt files.
      fprintf(fileID,formatspec,inputname);%writes to document spcified by
fileID, it writes the characters from formatspec and for every formatting
operator it assigns the value of the variables given, in this case
"inputname".
      formatspec='\r\n del %s \r\n'; %The formatspec giving the delete
command string that is printed in the inputfile
      fprintf(fileID,formatspec,inputname);%Prints the above string that
cause the deletion of the inputfile.


      file=fopen(inputname,'w+'); %Open or create new file for writing.
Discards existing contents, if any. The first file takes the name
inputname(i). Inputname changes per loop.
        fprintf(file,'%s\r\n',CHID);%Printing chid
        fprintf(file,'%s\r\n','2'); %2 for slicefile
        fprintf(file,'%s\r\n','1'); %Sampling Rate: 1 for all data
        fprintf(file,'%s\r\n','n'); %No domain limits
        fprintf(file,'%s  %s\r\n',num2str(T1REF),num2str(T2REF));  %starting
& ending time for averaging (s)
        fprintf(file,'%s\r\n','1'); %Only read 1 variable
        fprintf(file,'%s\r\n',num2str(index(i))); %Variable index
        fprintf(file,'%s\r\n',outputname);%Name of desired file

        fclose('all');%close all open files.
```

```
end

%%%%%%%%%%%%%%%%%%%%DISREGARD THIS INFROMATION%%%%%%%%%%%%%%%%%%%%%%%%%%%%%%%%

%fileID=fopen(filename,'a+');
%These(two first below) are only put to use if runed outside matlab, the
%latter two are for control of successfull run. without a PAUSE in the bat
%file it closes immediately after finish. this immediate closing allows the
%status function to return the needed value of 0.
%formatspec='\r\n del %s \r\n';
%fprintf(fileID,formatspec,filename);
%fprintf(fileID,'%s\r\n','echo COMPLETED SUCCESSFULLY');
%fprintf(fileID,'%s\r\n','PAUSE');

%%%%%%%%%%%%%%%%%%%%%%%%%%%%%%%%%%%%%%%%%%%%%%%%%%%%%%%%%%%%%%%%%%%%%%%%%%%%%%%

dos('retrieveslices.bat');%Executes the creted .bat file and returns the
output. The bat file is a DOS comand file.

fclose('all');%Assure all files closed
delete('retrieveslices.bat');%Make matlab delete the .bat file. (leave no
traces)



%%%%%%%%%%%%%%INSTANTANEOUS SLICE - MEAN SLICES - %%%%%%%%%%%%%%%%%%%%%%%%%%

DXT=(T2MEAN-T1MEAN)/DX;%Time per subslice
filename='retrieveslices2.bat'; %The name of the .command file

      fileID=fopen(filename,'a+');
      fprintf(fileID,'%s\r\n','@echo on');

%This loop is equal to the one above, except that it has an extra loop. The
%extra loop accounts for the number of subslices in the period of slice
%retrieval. Notice that the name of these more "instantaneous" slices are
%also store the time from which the mean was calculated. The input and
%output name; will both be of the form NAMEi_T1MEAN_T2MEAN.txt where i
%refers to the number of the slice in index vector and T1MEAN and T2MEAN
%are starting and ending time of the period respectively.

T2MEAN=T2MEAN-DXT;
for i=1:N %Looping for different indeces

    for k=T1MEAN:DXT:T2MEAN
        k2=k+DXT;
      inputname  =  ['InputMEAN'  sprintf('%d',i)  '_'  sprintf('%d',k)  '_'
sprintf('%d',k2)  '.txt'];
      outputname  =  ['MEANT'  sprintf('%d',i)  '_'  sprintf('%d',k)  '_'
sprintf('%d',k2)  '.csv'];
      fileID=fopen(filename,'a+');
      formatspec='\r\n fds2ascii<%s \r\n';
      fprintf(fileID,formatspec,inputname);
      formatspec='\r\n del %s \r\n';
      fprintf(fileID,formatspec,inputname);

      file=fopen(inputname,'w+');
```

```
        fprintf(file,'%s\r\n',CHID);
        fprintf(file,'%s\r\n','2'); %2 for slicefile
        fprintf(file,'%s\r\n','1'); %Sampling Rate: 1 for all data
        fprintf(file,'%s\r\n','n'); %No domain limits
        fprintf(file,'%s  %s\r\n',num2str(k),num2str(k2));  %starting  time
for averaging (s)
        fprintf(file,'%s\r\n','1'); %Only read 1 variable
        fprintf(file,'%s\r\n',num2str(index(i))); %Variable index
        fprintf(file,'%s\r\n',outputname);
        fclose(file);
        fclose(fileID);
    end

end

%%%%%%%%%%%%%%%%%%%DISREGARD THIS INFROMATION%%%%%%%%%%%%%%%%%%%%%%%%%%%%%%%

%fileID=fopen(filename,'a+');
%These(two first below) are only put to use if runed outside matlab, the
%latter two are for control of successfull run. without a PAUSE in the bat
%file it closes immediately after finish. this immediate closing allows the
%status function to return the needed value of 0.
%formatspec='\r\n del %s \r\n';
%fprintf(fileID,formatspec,filename);
%fprintf(fileID,'%s\r\n','echo COMPLETED SUCCESSFULLY');
%fprintf(fileID,'%s\r\n','PAUSE');

%%%%%%%%%%%%%%%%%%%%%%%%%%%%%%%%%%%%%%%%%%%%%%%%%%%%%%%%%%%%%%%%%%%%%%%%%%%%

dos('retrieveslices2.bat');

fclose('all');
delete('retrieveslices2.bat');
```

9.1.1.2 STEP 2

```
%REFERENCE DENSITY READ%

%THIS SCRIPT IS USED TO SUBTRACT THE REFERENCE FIELD FROM THE MEAN FIELD
%AND SAVE THE DATA TO CELL ARRAY CALLED C1



STATUS = 'CREATING MATRICES' %SIMPLE STATUS PRINTED IN THE MATLAB COMMAND
WINDOW

%%%%%%%%%%%%%%%%%%%%%%%% - INPUTS - %%%%%%%%%%%%%%%%%%%%%%%%%%%%%%%%%%%%

index=[46:1:90];%INDECES OF THE WANTED SLICE
N=length(index);%Integer value for the length of index vector
```

```
%-------------------
N=20;%MANUAL SET N VALUE
%-------------------

T1MEAN=1400;%Starting time for averaging
T2MEAN=1820;%Ending time for averaging
DX=105;%Number of slices per interval per slice


%%%%%%%%%%%%%%% - INPUTS FOR CHANGE OF GRIDSIZE ETC - %%%%%%%%%%%%%%%%%%%%

hy=1200;%End coordinate y-direction
hz=1200;%End coordinate z-direction
gridsize=6;%Gridsize

Vektory=0:gridsize:hy;%Gridvector containing all points from first given
value , with spacing of gridsize, to the x end value(hx1)
Vektorz=0:gridsize:hz;%Gridvector containing all points from first given
value , with spacing of gridsize, to the y end value(hy1)

[X1,Y1]=meshgrid(Vektory,Vektorz);%Returns 2-D grid coordinates. X1 is
matrix where each row is a copy of vektorx1, while Y1 is a matrix where
each column is a copy of vektory1
%The grid represented by X1, Y1 has length vektorx1 columns and length
%vektory1 rows.


%%%%%%%%%%%%%%%%%%%
% REF DENSITY READ
%%%%%%%%%%%%%%%%%%%

STATUS = 'LOOPING REFS'

for i=1:N %Looping for different indeces
      refval = ['REFT' sprintf('%d',i) '.csv'];%Filename that changes on
every loop and that coincides with the filenames written from the "retrieve
slicefiles" script
      REFERENCEVAL=xlsread(refval,'C3:C40403');%A row-vector containing all
values from the slicefile
t=0;%Initial values
R=0;%Initial values

for k=1:201;%Number of cells in y-direction

    for k2=1:201;%Number of cells in x-direction
        t=t+1;%Make t increase by one each step
        R(k,k2)=REFERENCEVAL(t);%Saves content from REFERENCEVAL row-vector
to the matrix R. Matrix R change location corresponding to the order data
is stored in the inputfile.
    end
end
A1{i}=R;%Stores matrices as cells.
end
```

```
%%%%%%%%%%%%%%%%%%%
%MEAN DENSITY READ%
%%%%%%%%%%%%%%%%%%%
STATUS = 'LOOPING MEAN'

DXT=(T2MEAN-T1MEAN)/DX;%Time per subslice

T2M_D=T2MEAN-DXT;

for i=1:N %Looping for different indeces
    s=0;%Assure s = 0
   for l=T1MEAN:DXT:T2M_D %Run loop from T1MEAN to T2M_D (T2MEAN-DXT). It
is run from n to n-1 to assure right number of loops
        l2=l+DXT;% Assign the variable l2 the value of l+DXT so that the
name of the file that shall be read changes according to the "retrieve
slices" script
      meanval   =   ['MEANT'   sprintf('%d',i)   '_'   sprintf('%d',l)   '_'
sprintf('%d',l2) '.csv'];%Assigning the filename MEANi_T1MEAN_T2MEAN.txt to
meanval string
      MEANVAL=xlsread(meanval,'C3:C40403');%Assigning the values from the
.csv file called meanval to the MEANVAL vactor

%the following assures script not to crash as excel runs multiple times
[~, computer] = system('hostname');

[~, user] = system('whoami');

[~, alltask] = system(['tasklist /S ', computer, ' /U ', user]);

excelPID = regexp(alltask, 'EXCEL.EXE\s*(\d+)\s', 'tokens');

for j = 1 : length(excelPID)

      killPID = cell2mat(excelPID{j});

      system(['taskkill /f /pid ', killPID]);
end




t=0;%Assure initial values
M=0;%Assure initial values

for k=1:201;%Number of cells in the y-direction

    for k2=1:201;%Number of cells in the x-direction
        t=t+1;%Make t increase by one each step
        M(k,k2)=MEANVAL(t);%Saves content from MEANVAL row-vector to the
matrix M. Matrix M change location corresponding to the order data is
stored in the inputfile.
    end
end
s=s+1;%Second variable for the storing of the M matrice is introduced, due
to possibility of matrices to increase above i.
M1{s}=M;%Stores the M matrice for the same slice but for different times as
cells in M1. M1 contains DX number of cells.
   end
```

```
   B1{i}=M1;%Stores the M1 matrice containning DX number of cells, each
cell being a M matrice from the same slice. Each cell in B1 therefore
represents all the data for a particualr slice.
end



%%%%%%%%%%%%%%%%%%%%%%%%%%%%%%%%%%%%%%%%%%%%%%%%%%%%%%%%%%%%%%%%%%%%%%%
%%%%%%%%%%%%%%%%%%SUBTRACTING FIELDS%%%%%%%%%%%%%%%%%%%%
%%%%%%%%%%%%%%%%%%%%%%%%%%%%%%%%%%%%%%%%%%%%%%%%%%%%%%%%%%%%%%%%%%%%%%%

%At this step the referenceslice are subtracted from the instantaneous
slice
%Leaving behind a slice that represents only the excess from the ambient of
%the quantity in question.


    sliceperinterval=DX;

for i=1:N

    R=A1{i};%R is assigned the value of the first matrice stored in A1.
Remeber that the reference read only stored matrices directly as cells into
A1, so that any retrieval of a cell within A1 becomes the matrice, at least
if one uses curlebrace{}
    MB=B1{i};%MB is assigned the cell from the first cell of B1. MB now
contains all the matrices, equal to DX matrices, for the first slice in the
mesh number 1

    for l=1:1:sliceperinterval %Due to the way data is stored it is now
neccessary to loop through MB, retrieving the values stored within the
cells
        M=MB{l};%M is assigned the the first matrix within MB

        for k=1:201;%number of cells in the y-direction

            for k2=1:201;%number of cells in the x-direction

                CV1(k,k2)=M(k,k2)-R(k,k2);%CV1 is the name of the name of
the matrix after the referenceslice has been subtracted to leave the excess
or at least the difference from the ambient.
            end

        end
        CF{l}=CV1;%Each subtracted slice is now stored at CF. This is just
what was explained in the "MEAN SLICE" but here the background is
subtracted. CF stores all the CV1 matrices.



    end
    C1{i}=CF;%When the internal loop is finished for a value of i, the CF
matrix containing the CV1 matrices, stored as cells, is saved to C1 as
cells. C1 then contains i number of cells, each cell containing DX number
of cells (or matrices)


end
```

9.1.1.3 STEP 3

```
%NORMAL PLOTTING AND .PNG SAVE


STATUS = 'PLOTTING:'
for i=1:N


    V1=C1{i};


    for w=1:1:sliceperinterval

    VV1=V1{w};


surf(X1,Y1,VV1,'edgecolor','none','facecolor','interp')
set(gca,'position',[0 0 1 1],'units','normalized')
view(2)% setting the view for the displayed figure
hold on


set(gcf,'PaperPositionMode','auto');  %assure the save to be the size
displayed on screen
figname  =  ['figname'  sprintf('%d',i)  '_'  sprintf('%d',w)];%assigning
figname per loop
print(figname,'-dpng','-r0');%Saves  figname  as  png  and  with  screen
resolution

hold off

    end

end
```

9.1.1.4 STEP 4

```
%THIS SCRIPT USES THE SUBTRACTED MATRICES FROM THE "SUBTRACTFIELD" SCRIPT
%AND APPLIES A CRITERIA FOR THE PROPERTY IN QUESTION. EXAMPLE A DENSITY OR
%TEMPERATURE CRITERIA. BY USE OF THE CRITERIA THE MATRICES ARE TRANSFORMED
%TO BINARY MATRICES. IT IS THEN PLOTTED AS BINARY PICTURES SAVED AS 561x420
%PIXEL .PNG PICTURE.




%%%%%%%%%%%%%%%%%%%%%%%% - INPUTS - %%%%%%%%%%%%%%%%%%%%%%%%%%

CRITERIA = 0.5;%Set value of criteria


%CRITERIA is assigned to the variables low and high. Its done this way to
%easily allow for custom changes to the criterias throughout the script.
high=CRITERIA;
low=CRITERIA;

STATUS = 'PLOTTING:'
for i=1:N
    STATUS = i * (100/N)%Printing stauts to matlab command window


 %Assigning V1 the first cell of the subtracted field cells of
 %C. The V variable now contains all matrices from the i'th cell of C.

    V1=C1{i};


    for w=1:1:sliceperinterval

 %Assigning VV1w'th matrice from V.
    VV1=V1{w};


%Transforming the VVx matrices into matrices containing only 1' and 0's.
VV1(VV1>high)=1;%All values greater than high becomes 1
VV1(VV1<low)=0;%All values less than low becomes 0



%In the end there is
%a picture that isaved to the folder containing this matlab script. The
%pictures can be used for retrieval of area and other blob properties.
```

```
surf(X1,Y1,VV1,'edgecolor','none','facecolor','flat')%Creates a surface where coordinates are values correpsonding to the same i'th and j'th position within X1 Y1 and where the value at his point is VV1.
set(gca,'position',[0 0 1 1],'units','normalized')%setting position to start at lower left corner (0.0) and span the whole screen (1.1)
view(2)% setting the view for the displayed figure to view two, top view.
hold on %hold on to plot in current axes, so that new plots can be added without deleting existing plots.


set(gcf,'PaperPositionMode','auto'); %assure the save to be the size displayed on screen
figname = ['figname' sprintf('%d',i) '_' sprintf('%d',w) 'B'];%assigning figname per loop
print(figname,'-dpng','-r0');%Saves figname as png and with screen resolution


hold off

    end

end
```

9.1.1.5 STEP 5

```
%This script reads the binary .pg files created by the "plotting binary"
%script. It reads these pictures and creates matrices. These matrices can
%be used for a replotting, bu this time as a single picture. Different
%matlab functions are then used to retrieve wanted sizs such as number of
%pixels occupied by the excess quantities. The script at last can compute
%area of plume and calculate plume centre.

%%%%%%%%%%%%%%%%%%%%%%%%%% - INPUTS - %%%%%%%%%%%%%%%%%%%%%%%%%%%%%%%%%%

limit = 70;%Set a logiacal limit for the conversion of grayscale image to binary. One may need to tune this parameter.


for i=1:N

    for k = 1:DX
    cla
set(gca,'position',[0 0 1 1],'units','normalized')%assure pictures occupies the displayed area
figname=['figname' sprintf('%d',i) '_' sprintf('%d',k) 'B' '.png'];%Name of the stored png pictures corresponding to earlier scripts.
```

```
IMG1=imread(figname);%assign the picture "figname" to IMG1
IMG1=rgb2gray(IMG1);%Convert the binary picture, which may be displayed in
colors, to a gray scale image

binaryimage = IMG1 > limit;%Creates a binary image from the grayscale image
by use of the logical limit. The limit may need adjustments
binaryimage_filtered = bwareaopen(binaryimage,5); %Removing any object less
than the given number of pixels

set(gcf,'PaperPositionMode','auto'); %assure the save to be the size
displayed on screen
figname = ['figname' sprintf('%d',i) '_' sprintf('%d',k) 'C'];%assigning
figname per loop
print(figname,'-dpng','-r0');%Saves figname as png and with screen
resolution

binaryimage_label = bwlabel(binaryimage_filtered, 8);%Labels blobs of 8
connected objects. (Connectivity)

blobmeasure = regionprops(binaryimage_label, 'all');%Measures properties of
image regions, the specification of "all" makes matlab compute all shape
measurements
numberofblobs = size(blobmeasure, 1);%Counts total number of separate blobs
in the picture by taking the number of calculated areas. Area being the
number 1. listed regionprop.

areaofslice=0;%initial value
heightofslice=0;%initil slice height

for y = 1:numberofblobs
    %Sums the total area of excess quantity in the picture, in case of
    %multiple separate blobs.
        blobarea = blobmeasure(y).Area;
        blobcentroid = blobmeasure(y).Centroid;

        if blobarea>120000
            blobarea=0;
            blobcentroid=[0,0];
            areaofslice=areaofslice+blobarea;


        else
        areaofslice = blobarea + areaofslice;
        heightofslice= heightofslice + (420 - blobcentroid(2));

        end
   imshow(binaryimage_filtered)%Show the filtered binary image
   hold on
   plot(blobcentroid(1), blobcentroid(2), 'r.', 'MarkerSize', 2,
'LineWidth', 1);
set(gcf,'PaperPositionMode','auto'); %assure the save to be the size
displayed on screen
figname = ['figname' sprintf('%d',i) '_' sprintf('%d',k) 'C'];%assigning
figname per loop
print(figname,'-dpng','-r0');%Saves figname as png and with screen
resolution

end
```

```
meanheightofslice=heightofslice/(numberofblobs);

areaofslices(k)=areaofslice;%The sum vector of the areas of the quantity in
question. this vector contains DX number of areas, and each vector only
contains values for the same slice so it can be used to compute a mean
later on
heightofslices(k)=meanheightofslice;%This is a vector containing the mean
height of the plume per slice. it contains DX number of heights.

    end

    AreaOfSlices_TotalInstant{i}=areaofslices;%Each areaofslices vector are
saved as cells to this array.
    HeightOfSlice{i}=heightofslices;

end
hold off



%%%%%%%%%%%%%%%%%% - CALCULATING MEAN VALUES - %%%%%%%%%%%%%%%%%%%%%%%%%%

for o=1:N
    areavector=0;
    heightvector=0;

    areavector = AreaOfSlices_TotalInstant{o};%Assigning cell number o to
the areavector, the areavector then becomes a vector containing all the
areas calculated for a specified slice
    heightvector = HeightOfSlice{o};%HeightOfSlice array may contain
vectors of values of zero, not to be a part of calculation



    Area51=sum(areavector); %Area51 becomes the sum of all areas in the
areavector
    Height51=sum(heightvector);

    if Area51==0
    numarea=1;
    Height51=0;
    numheight=1;

    else
    numberofareas=areavector>0;
    numarea=sum(numberofareas);

    numberofheight=heightvector>0;
    numheight=sum(numberofheight);

    end
    MeanArea = Area51/numarea;%The mean area per slice is found by dividing
the totarea by the number of slices.
    MeanAreaPerHeight2(o)=MeanArea*6.1225;%(for 560x420 pixels it is
6.1225, for 561x420 it is 6.1154) Mean area per height is then found by
multiplying the pixel area with the corresponding area per pixel. The area
in Square meters is stored to the mean area per height vector
```

```
    MeanHeight = Height51/numheight;
    FinalMeanHeight2(o) = MeanHeight*2.857;%(always 2.857)


end

MeanAreaPerHeight=MeanAreaPerHeight2(MeanAreaPerHeight2~=0);%remove     zero
from the vectors to avoid them being plotted
FinalMeanHeight=FinalMeanHeight2(FinalMeanHeight2~=0);

plot(MeanAreaPerHeight,FinalMeanHeight,'r+', 'MarkerSize', 10, 'LineWidth',
2)
xlim([0,3000])
ylim([0,300])
```

9.1.1.6 STEP 6

```
%THIS SCRIPT USES THE SUBTRACTED MATRICES FROM THE SCRIPT "SUBTRACTFIELDS"
%IT USES THE MATRICES TO CALCULATE A MEAN VALUE BASED ON THE INSTANTANEOUS
%SLICES. IT THEN TAKE THESE MEAN VALUES AND PLOTS THE CHANGE OF TEMPERATURE
%WITH HEIGHT. THE RESULTING GRAPH IS THEN THE CHANGE OF THE MEAN
%TEMPERATURE FOR THE THERMAL PLUME WITH HEIGHT

%%%%%%%%%%%%%%%%%%%%%%%%%%%% - I N P U T S - %%%%%%%%%%%%%%%%%%%%%%%%%%%%%%
%%%%%%%%%%%%%%%%%%%%%%%%%%%%%%%%%%%%%%%%%%%%%%%%%%%%%%%%%%%%%%%%%%%%%%%%%%

CRITERIA = 0.5;%Criteria for the property in question
Plotheight=FinalMeanHeight;%This  is  the  different  heights  were  the  plume
has been found to be present
N=length(Plotheight);

STATUS = 'PLOTTING:'
for i=1:N


 %Assigning V1,V2,..V5 the first cell of the subtracted field cells of
 %C-. The V- variables now contains all matrices from the i'th cell of C-.
 %The values 1, 2, 3, 4 and 5 refers to the different meshes., as mentioned
 %before. Remeber that mesh 3 is given together with mesh 1, 4 and 5 in a
 %loop further below.
    V1=C1{i};


    for w=1:1:DX %runs loop from 1 to number of subintervals per interval
```

```
 %Assigning VV1,VV2,..VV5 the w'th matrice from V-.
    VV1=V1{w};
%Applying the criteria to the matrices. All values below the criteria
%becomes zero, and all values above stays the same.
VV1(VV1<CRITERIA)=0;

%TEMP TOTAL and POINTS IN TOTAL
SumTempVV1=sum(VV1);%Creates a rowvetor that contains the sum of all values
per column in a each column
SumTempVV1=sum(SumTempVV1);%Adds all values from above rowvector to a
single number which represents the sum all values above the criteria.
SumValVV1=sum(VV1>0);%Ceats a rowvector, containing the sum of all numbers
above 0 in each column. So this is not the added sum of the values, but the
number of values above 0.
SumValVV1=sum(SumValVV1);%Adds all values from above rowvector to a single
number which represents the number of values above the value 0 (which
actually is all values above specified criteria)

SumTempTot=SumTempVV1;%The total sum, per interval, of appx. excess
property, it does not need to be temperature.
SumValTot=SumValVV1;%Total number of points that constitute the sum of the
total temperatures

if SumValTot == 0;%If there are no valus above 0, meaning that there are no
points with excess property, then;

    MeanTempTemp=0;%Meantemp is equal to 0, this is done to avoid dividng
by zero which would give NaN

    MeanTemp(w)=MeanTempTemp;%Assigning the value 0 to the MeanTemp
location w. MeanTemp becomes a vector of mean values. It contains DX number
of values per vector, each vector representing the same slice.

end

if SumValTot > 0;%If there are any values above 0, then;

    MeanTempTemp=  SumTempTot/SumValTot;%Mean value of specified property
per point in space is equal to the total sum of the property divided by
number of points.

    MeanTemp(w)=MeanTempTemp;%Assigning the value of MeanTempTemp to the
MeanTemp location w. MeanTemp becomes a vector of mean values. It contains
DX number of values per vector, each vector representing the same slice.

end

    end

MeanTempTot{i}=MeanTemp;%For each loop of i a MeanTemp vector, containing
the mean values for DX number of smal intervals for the same slice, is
saved to MeanTempTot. MeanTempTot now contains i cells, where each cell
represent a vector containing mean values.

end
%%%%%%%%%%%%%%%%%%%%%%%%%%%%%%%%%%%%%%%%%%%%%%%%%%%%%%%%%%%%%%%%%%%%%%%%%%%
%%%%%%%%%%%%%% - CALCULATE MEAN TEMP FROM MEAN VECTORS - %%%%%%%%%%%%%%%%%%

TEMP_TOT=0;
```

```
for i=1:N

    MEAN_TEMP_Vector=MeanTempTot{i};%MEAN_TEMP_Vector is assigned the i'th
vector of MeanTempTot.

    TEMP_TOT=sum(MEAN_TEMP_Vector);%TEMP_TOT becomes the sum of all values
in MEAN_TEMP_Vector

    if TEMP_TOT == 0;%If TEMP_TOT = 0, then;

    MEAN_TEMP_TOT=0;%MEAN_TEMP_TOT becomes 0

    end

    if TEMP_TOT > 0;%If TEMP_TOT > 0, then;

    MEAN_TEMP_TOT=TEMP_TOT/(sum(MEAN_TEMP_Vector>0));%The  MEAN_TEMP_TOT  is
assigned the overall mean value from the DX number of  matrices within the
interval of T1MEAN to T2MEAN. This is the final mean value, the mean value
at a particular height.

    end


        MEAN_TEMPERATURE(i)=MEAN_TEMP_TOT;%The  mean  value  per  slice  and
height is stored as in the the MEAN_TEMPERATURE vector. This value is what
becomes the temperature lapse rate.

end

%%%%%%%%%%%%%%%%%%%%%%%%%%%%%%%%%%%%%%%%%%%%%%%%%%%%%%%%%%%%%%%%%%%%%%%%%%%
%%%%%%%%%%%%%%%%%%%% - P L O T T I N G - %%%%%%%%%%%%%%%%%%%%%%%%%%%%%%%%%%


plot(MEAN_TEMPERATURE,Plotheight,'b+', 'MarkerSize', 10, 'LineWidth', 2)
xlim([0,30])
ylim([0,500])

hold on
```